The role of LONP1 in the mammalian mitochondrial gene expression

Inaugural-Dissertation

Zur
Erlangung des Doktorgrades
der Mathematisch-Naturwissenschaftlichen Fakultät
der Universität zu Köln



vorgelegt von

Dieu Hien Rozsivalova

aus Dillenburg, Deutschland

Köln 2023

Berichterstatter: Prof. Dr. Aleksandra Trifunovic

Prof. Dr. Matteo Bergami

Tag der mündlichen Prüfung: 30.05.2023

Let this be a testimony of the parental sacrifice
to give their children a chance for a better future.

To my most loved mum and dad,
to my brother, to my Šimon,
and to our children.

Table of Contents

List of Figures ..... *vi*

List of tables ..... *viii*

Abbreviations ..... *ix*

Abstract ..... *xii*

1 Introduction *1*

1.1 Mitochondria **1**

1.2 OXPHOS **2**

1.3 Mitochondrial gene expression in mammals **5**

1.3.1 Replication of mtDNA 6
1.3.2 Transcription of mtDNA 7
1.3.3 Processing of the primary transcript 8
1.3.4 tRNA maturation 9
1.3.5 rRNA maturation 10
1.3.6 mRNA maturation 10
1.3.7 DNA and RNA degradation 11
1.3.8 Mitoribosomal biogenesis 11
1.3.9 Mitochondrial translation 12

1.4 Protein quality control in mitochondria **13**

1.5 Lon proteases **14**

1.5.1 Structure 15
1.5.2 Function 16
1.5.3 Lon in bacteria 16
1.5.4 Lon in yeasts 18
1.5.5 LONP1 in mammals 20
1.5.6 LONP1 in disease 23

1.6 Objectives **23**

2 Materials and Methods *25*

2.1 Materials **25**

2.2 Cell culture **28**

2.3 Mouse experiments **28**

2.3.1 Animal care 28
2.3.2 Experimental mouse models 28
2.3.3 Isolation of crude DNA 29
2.3.4 Genotyping 29
2.3.5 Agarose gel electrophoresis 30

2.4 Transmission electron microscopy **31**

2.5 Molecular biology **31**

2.5.1 Transformation of chemically competent *Escherichia coli* 31
2.5.2 Isolation of plasmid DNA 31
2.5.3 Isolation of RNA 31
2.5.4 Quantification of the nucleic acid concentration 32
2.5.5 mRNA quantification with Quantitative PCR (qPCR) 32

2.5.6 Quantitative PCR (qPCR) 33
2.5.7 mtDNA quantification via qPCR 33
2.5.8 mtDNA quantification via Southern blot 34
2.6 Biochemistry 35
2.6.1 Protein isolation from cells 35
2.6.2 Protein isolation from tissues 35
2.6.3 Isolation of mitochondria 35
2.6.4 SDS polyacrylamide gel electrophoresis (SDS-PAGE) and western blot 36
2.6.5 Blue native PAGE (BN-PAGE) and *in gel* activity 38
2.6.6 Sucrose density gradient 38
2.6.7 *In organello* transcription 39
2.6.8 *In organello* translation 40
2.6.9 High resolution respirometry 40
2.7 Omics analysis 41
2.8 Image processing and data analyses 43
3 Results 44
3.1 Generation of the mouse model 44
3.2 LONP1 deficiency causes a profound OXPHOS dysfunction 50
3.3 Whole heart proteomic analysis revealed a wide-scale change in the LONP1 KO heart proteome 53
3.4 Loss of LONP1 led to an accumulation of mitoribosomal proteins 57
3.5 LONP1 deficiency altered the *de novo* synthesis of mtRNA and mt proteins, but not mtDNA levels 59
3.5.1 A cell model with siRNA-mediated knockdown of *Lonp1* does not phenocopy LONP1 deficiency *in vivo* 63
3.5.3 RNAseq analysis revealed a transcriptional regulation of the observed changes on the protein level 66
3.6 Investigating the insoluble proteins in LONP1 KO 72
4 Discussion 76
4.1 LONP1 in OXPHOS 77
4.2 LONP1 in mt gene expression 79
4.2.1 LONP1 in mitoribosomal biogenesis 79
4.2.2 LONP1 in RNA processing 81
4.2.3 LONP1 and TFAM 81
4.2.4 Conclusion of LONP1 in mt gene expression 82
4.3 LONP1 in protein quality control 83
4.4 Summary 84
5 References 86
6 Supplementary data 105
Acknowledgements 118
Erklärung zur Dissertation 120

List of Figures

Figure 1.1 | The mitochondrion 1
Figure 1.2 | Oxidative phosphorylation 3
Figure 1.3 | Mitochondrial DNA 5
Figure 1.4 | TFAM regulates mtDNA metabolism by packaging mtDNA 6
Figure 1.5 | Mitochondrial replication 7
Figure 1.6 | Mitochondrial transcription 8
Figure 1.7 | The summary of RNA processing 10
Figure 1.8 | The mitoribosomal assembly 12
Figure 1.9 | Mitochondrial translation 13
Figure 1.10 | The enzymatic activity of Lon proteases 15
Figure 1.11 | PIM1 substrates 19
Figure 1.12 | A summary of LONP1 functions 21
Figure 3.1 | LONP1 deficiency causes embryonic lethality. 44
Figure 3.2 | LONP1 is not expressed in the KO heart 45
Figure 3.3 | General phenotypical description of the mouse model at 8 weeks of age 46
Figure 3.4 | The KO mice significantly deteriorate after 22 weeks of age. 47
Figure 3.5 | General phenotypical description of the mouse model at 20 weeks of age 48
Figure 3.6 | The LONP1 KO mitochondria accumulate electron dense particles 49
Figure 3.7 | LONP1 absence leads to a widescale loss of OXPHOS subunits 50
Figure 3.8 | LONP1 is not essential for supercomplexes (SC) 51
Figure 3.9 | The impairment of OXPHOS resulted in defective respiration 52
Figure 3.10 | General changes in the LONP1 KO heart proteome at 8 weeks of age 53
Figure 3.11 | General changes in the LONP1 KO heart proteome at 8 weeks of age 54
Figure 3.12 | An overview of the OXPHOS proteome 55
Figure 3.13 | Proteins involved in cytosolic and mitochondrial translation are upregulated in the LONP1 KO 56
Figure 3.14 | Loss of LONP1 resulted in a surge of mitoribosomal proteins 57
Figure 3.15 | LONP1 is necessary for mitoribosomal assembly 58
Figure 3.16 | Mitochondrial de novo translation is mildly decreased in the LONP1 KO 59
Figure 3.17 | LONP1 absence did not affect the mtDNA levels, but it led to a significant increase in mitochondrial transcription at 8 weeks of age. 60
Figure 3.18 | Loss of LONP1 lead to a general surge of proteins involved in mitochondrial gene expression at 8 weeks of age. 61
Figure 3.19 | Loss of LONP1 lead to a general surge of proteins involved in mitochondrial gene expression at 8 weeks of age. 62

Figure 3.20 | Detected changes in proteins involved in mitochondrial gene expression at 20 weeks of age 63
Figure 3.21 | Lonp1 KD in cells does not phenocopy the mouse model 65
Figure 3.22 | A general overview of the LONP1 KO heart transcriptome at 8 weeks of age 66
Figure 3.23 | Transcriptomics reveal a decline of OXPHOS subunits already on the transcript level. 67
Figure 3.24 | OXPHOS subunits are more affected on the protein level 68
Figure 3.25 | Comparison of the proteomic and transcriptomic datasets from the 8-week-old hearts. 69
Figure 3.26 | Comparison of changes of mitochondrially encoded genes on transcript and protein level 70
Figure 3.27 | Comparison of changes of genes in mitochondrial gene expression machinery on transcript and protein level 71
Figure 3.28 | A proteomic analysis of insoluble proteins in the LONP1 KO cardiac mitochondria 72
Figure 3.29 | Pooling the most interesting insoluble targets 73
Figure 3.30 | All 108 targets identified in the proteomic analysis of the insoluble mitochondrial proteins 74
Figure 3.31 | An OMICS approach to identify the most interesting candidates for LONP1 substrates 75

List of tables

Table 2.1 | Primer sequences used for mtDNA levels determination 33
Table 2.2 | Primer sequences used for mtDNA levels determination 34
Table 2.3 | Primary antibodies used for the western blot 37
Table 2.4 | Secondary antibodies used for the western blot 38
Table 3.1 | Heart KO and cell *Lonp1* siRNA comparison 64
Table 4.1 | Mouse models of mitochondrial gene expression. 76
Table 6.1 | Supplementary table for the Figure 3.27 105
Table 6.2 | Supplementary table for the Figure 3.24 109
Table 6.3 | Supplementary table for the Figure 3.30 113
Table 6.4 | Supplementary table for the Figure 3.31 116

Abbreviations

°C	degree Celsius
^{35}S-Met	radioactive methionine isotope
AAA+	ATPases Associated with diverse cellular Activities
Actb	β-actin
ADP	adenosine diphosphate
APS	ammonium persulfate
ARS2s	aminoacyl-tRNA synthetases 2, mitochondrial
ARSs	aminoacyl-tRNA synthetases, cytosolic
ATP	adenosine triphosphate
BN	Blue Native
BSA	bovine serum albumin
CAA	chloroacetamide
cDNA	copy DNA
CI	complex I
CII	complex II
CIII	complex III
CIV	complex IV
CJ	cristae junction
CKMM	Creatine-kinase muscle mitochondrial
CNX	calnexin
CV	complex V
D-loop	displacement loop
(d)dH_2O	(double) distilled water
DMEM	Dulbecco's Modified Eagle Medium
dNTP	deoxynucleoside triphosphate
dpc	days post coitum
DTT	dithiothreitol
ECL	enhanced chemiluminescence
EDTA	ethylenediaminetetraacetic acid
EGTA	ethylene glycol tetraacetic acid
EMMA	European Mouse Mutant Archive
En	embryonic day (e.g., embryonic day 1 – E1)
ETC	electron transport chain
EUCOMM	European Conditional Mouse Mutagenesis Program
$FADH_2$	flavin adenine dinucleotide
FCCP	carbonyl cyanide-p-trifluoromethoxyphenylhydrazone
Fe-S (cluster)	iron-sulphur (cluster)
fl	floxed
FLP	flippase
FRT	Flippase Recognition Target
GO	gene ontology
GOBP	gene ontology
H-strand	heavy strand of mitochondrial DNA

HCl	hydrogen chloride
HEPES	4-(2-hydroxyethyl)-1-piperazineethanesulfonic acid
Hmgu	Helmholtz Zentrum München GmbH
HRP	horseradish peroxidase
HSP	heavy strand promotor
HW/BW	Heart weight to body weight ratio
HZ	heterozygous
IRES	internal ribosome entry site
IMM	inner mitochondrial membrane
IMS	intermembrane space
ISR	integrated stress response
KCl	potassium chloride
KH_2PO_4	potassium dihydrogen phosphate
KO	knockout
L-strand	light strand of mitochondrial DNA
LB	lysogeny broth
LFQ	label free quantification
LSP	light strand promotor
MEF	mouse embryonic fibroblast
$MgCl_2$	magnesium chloride
MiR05	mitochondrial respiration medium 05
MOPS	3-(N-morpholino)propanesulfonic acid
MRG	mitochondrial RNA granules
mRNA	messenger RNA
MRP	mitoribosomal protein
MRPL	mitoribosomal protein of the large subunit
MRPS	mitoribosomal protein of the small subunit
mt	mitochondrial
mtDNA	mitochondrial DNA
mtLSU	mitochondrial ribosome (mitoribosome), the large subunit
mtPQC	mitochondrial protein quality control
mtSSU	mitochondrial ribosome (mitoribosome), the small subunit
MUT	mutant
$Na_3VO_4 \cdot 2H_2O$	sodium orthovanadate
NaCl	sodium chloride
NADH	nicotinamide adenine dinucleotide
NaF	sodium fluoride
NaOH	sodium hydroxide
ncDNA	nuclear DNA
NCR	non-coding region
ns	non-significant
O^H	origin of the heavy strand replication
O^L	origin of the light strand replication
OMM	outer mitochondrial membrane

OXPHOS	oxidative phosphorylation
PAGE	polyacrylamide gel electrophoresis
PBS	phosphate-buffered saline
PBST	phosphate-buffered saline + Tween 20
PCR	polymerase chain reaction
PMSF	phenylmethylsulphonyl fluoride
PTFE	polytetrafluoroethylene
RIPA	radioimmunoprecipitation assay
ROS	reactive oxygen species
rpm	rotation per minute
rRNA	ribosomal RNA
RT	room temperature
S.O.C.	super optimal broth with added glucose
SC	supercomplex
SD	standard deviation
SDS	sodium dodecyl sulphate
SSC	saline-sodium citrate
TBE	Tris/Borate/EDTA
TCA	tricarboxylic acid cycle
TEAB	tetraethylammonium bromide
TEM	transmission electron microscopy
TEMED	tetramethylethylenediamine
TES	N-[Tris(hydroxymethyl)-methyl]-2-aminoethanesulphonic acid
tm1a	targeted trap allele 1a
TMPD	tetramethylphenylendiamin
tRNA	transfer RNA
v/v	volume/volume percentage
w/v	mass/volume percentage
WT	wild type

Abstract

Mitochondria are a melting pot of several metabolic pathways and other cellular processes. Therefore, tight regulatory mechanisms must be in place and the maintenance of mitochondrial homeostasis is essential for the organism. Lon proteases are serine peptidases that are conserved throughout the kingdoms of living organisms. LON is encoded by the nuclear genome and belongs to the AAA+ protein family (ATPases associated with diverse cellular activities).

In the mammalian mitochondrial matrix, the key role of LONP1 is to preserve mitochondrial proteostasis. LONP1 recognizes and degrades unfolded or damaged proteins to prevent their aggregation. LONP1 is also involved in the regulation of several mitochondrial processes, as it was shown to target specific folded proteins. A few examples of these processes are the heme biosynthesis (ALAS1), the lipid metabolism (StAR), adaptation to hypoxic conditions (COX4-1), etc. LONP1 was also reported to regulate the mitochondrial gene expression, e.g., by targeting TFAM, the most abundant mtDNA-binding protein. Furthermore, LONP1 has been reported to be involved in the mitoribosomal assembly and processing of some newly imported proteins. In yeasts, a catalytically inactive Pim1/LON was proposed to promote assembly of complex IV which indicates a possible chaperone-like function of the protease. In mammals, the general loss of LONP1 in mice resulted in embryonic lethality around E7.5, demonstrating its essential function in the early embryonic development.

The goal of this project was to further understand LONP1 and its role in the mitochondrial gene expression, in the regulation of OXPHOS, and in the mitochondrial proteostasis. We established a conditional heart-specific model in C57BL/6N mice. Our results show that LONP1 absence in heart resulted in the accumulation of insoluble in mitochondria and downregulation of protein levels of OXPHOS complexes I, III, IV and V, but not complex II. Furthermore, the depletion led to an increase in the mitoribosomal proteins and a general upregulation of protein levels in factors involved in the mitochondrial gene expression. Interestingly, the *de novo* mtRNA synthesis is also increased, but it does not lead to a general accumulation of the steady-state levels of mtRNAs. The mitochondrial *de novo* protein synthesis in mildly decreased despite the accumulation of mitoribosomal steady-state protein levels. Collectively, these results suggest an important multitasking role of LONP1 in the mitochondrial biology.

1 Introduction

1.1 Mitochondria

Mitochondria are an energetic hub of most living cells. These key organelles harbour the oxidative pathways which are responsible for supplying approx. 90% of the cell's ATP. They were first observed by Richard Altmann in 1890 who considered these structures to be some simple bacteria-resembling organisms that live inside the cells. He called them "bioblasts" (Ernster and Schatz, 1981). Mitochondria are indeed of a prokaryotic origin. According to the endosymbiotic theory, a heterotrophic archaeal host engulfed a free-living proteobacterium which gave the origin to the eukaryotes (Martin et al., 2015). This theory is supported by mitochondria having their own genome. During evolution, mitochondria lost or transferred most of their genes to the nucleus. In mammals, out of 1130+ proteins, the mitochondrial genome contains only 37 genes which secure the expression of 13 core proteins of oxidative phosphorylation. The rest is encoded by the nucleus and the protein precursors must be imported into mitochondria through a complex system including translocases (Zimorski et al., 2014, Rath et al., 2021).

Mitochondria have two phospholipidic membranes, the outer (OMM) and the inner membrane (IMM). The membranes compartmentalize the organelle into two distinct environments – the intermembrane space (IMS) and the matrix (Iovine et al., 2021). The two membranes vary in their permeability and composition. The lipid-rich OMM is porous, and it allows solutes smaller than ~5 000 Da to pass freely through voltage-dependent anion channels (VDACs) (Colombini, 1989, Alberts et al., 2017). On the other hand, the IMM is very rich in protein content. It will let only specific molecules cross the membrane through selective transporters. Only water, oxygen, and carbon dioxide can permeate freely (Protasoni and Zeviani, 2021, Yang et al., 2021). The restricted permeability enables the IMM to maintain an electrochemical membrane potential of ~120–180 mV together with the enzymes of oxidative phosphorylation (OXPHOS) (Yang et al., 2021).

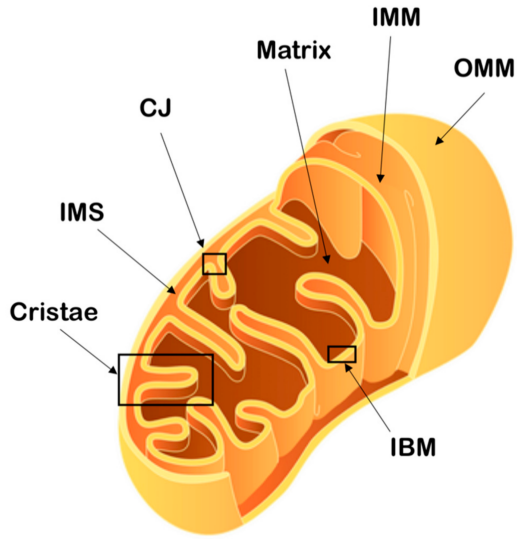


Figure 1.1 | The mitochondrion

OMM and IMM – outer and inner mitochondrial membrane, CJ – cristae junctions, IMS – intermembrane space, IBM – inner boundary membrane. Adapted from (Protasoni and Zeviani, 2021).

The IMM increases its surface by creating various tubular or lamellar protrusions called cristae. Cristae can

further create functionally distinct subcompartments called cristae junctions (CJ) (Iovine et al., 2021).

Mitochondria provide the cell with ATP mainly via oxidative phosphorylation (OXPHOS). Electrons in the electron transport chain (ETC) are donated by the electron carriers NADH and $FADH_2$. These electron carriers are recycled by the tricarboxylic acid cycle (TCA) and by the catabolic β-oxidation of fatty acids. Moreover, mitochondria also harbour many biosynthetic pathways to generate amino acid, lipids, or heme. They also regulate the synthesis of iron-sulphur clusters and nucleotides. Mitochondria also maintain the Ca^{2+} homeostasis and participate in signalling pathways with Ca^{2+}, acetyl-CoA, and reactive oxygen species (ROS). Mitochondria are also key players in the cell fate-determining processes, such as apoptosis (Nunnari and Suomalainen, 2012).

The size and the number of mitochondria present in one cell can vary across different organisms, tissues, and even different cell types. While none can be found in erythrocytes, a single oocyte may harbour as many as 100 000 mitochondria (Ikon and Ryan, 2017, Zhang et al., 2017). That is due to the different energy and metabolic demands of the specific cell type or tissue.

1.2 OXPHOS

Oxidative phosphorylation (OXPHOS) in mitochondria is the main mechanism for energy production in most living systems. Eukaryotes depend on OXPHOS for most of the energy production to meet the needs of most cell types and cell states. OXPHOS as a mechanism is based on electron transfer between a chain of four enzymatic complexes: Complex I (CI, or NADH: ubiquinone oxidoreductase); Complex II (CII, SDH or succinate dehydrogenase), Complex III (CIII, or cytochrome bc1 oxidoreductase), Complex IV (CIV or cytochrome c oxidase), and two mobile electron carriers: ubiquinol and cytochrome c, that are regarded as the electron transport chain (ETC). ETC is responsible for creating an electrochemical proton gradient across the IMM by coupling electron transfer with proton pumping from the mitochondrial matrix to the IMM. Complex I, III and IV have proton pumping activity, although they utilize different mechanisms (Jones et al., 2017, Mitchell, 1976, Snyder et al., 1999). The electrochemical proton gradient is then utilized by F_1F_o-ATP synthase (also referred to as Complex V or CV) to phosphorylate ADP to ATP. Complexes other than individual enzyme complexes also form supramolecular structures with each other, which are then dubbed as supercomplexes (Schagger and Pfeiffer, 2000). Supercomplex structures contain CI, CIII and CIV in different stoichiometries, and the best-established structure is called the respirasome, consisting of $CICIII_2CIV$. Although the function for supercomplexes is still heavily debated, its crystal structure has been solved recently, showing that respirasome is a stable and functional unit of OXPHOS (Letts et al., 2016, Gu et al., 2016). Other than the respirasome, $CICIII_2$ (Letts et al., 2019), $CIII_2CIV$ (Vercellino and Sazanov, 2021) and $CI_2CIII_2CIV_2$ (Guo et al., 2017) have been described.

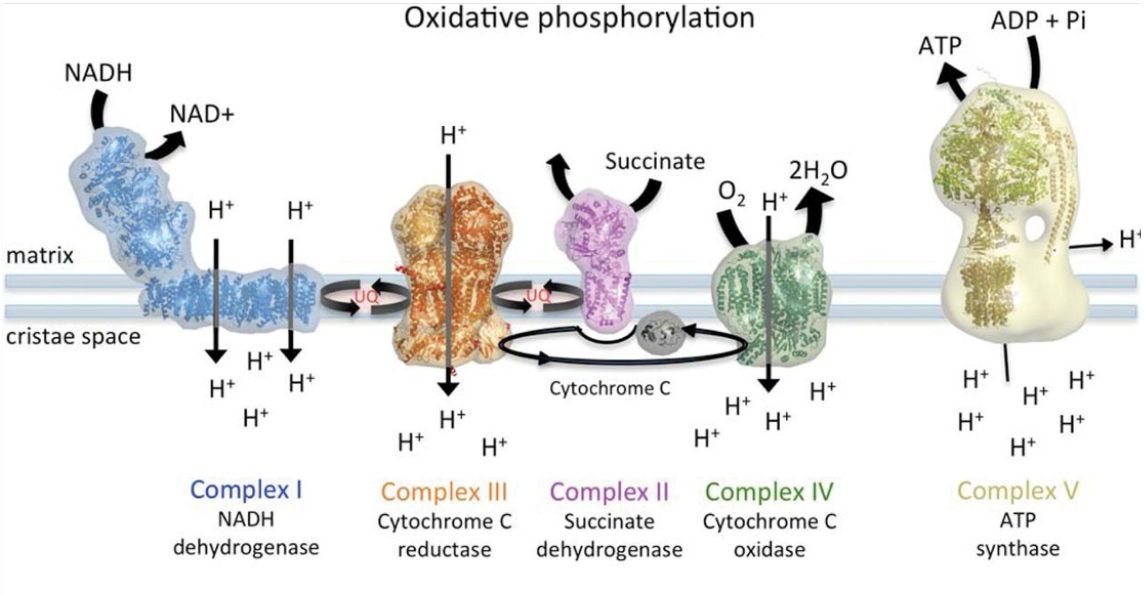


Figure 1.2 | Oxidative phosphorylation

Adapted from (Davies and Daum, 2013)

Electrons derived from metabolism of nutrients such as fatty acids, proteins, and sugars, enter ETC via electron donors such as NADH (for CI) and FADH (CII). These reducing equivalents, coming from the Krebs cycle and fatty acid oxidation, get oxidized by CI and CII, reducing ubiquinone, the membrane embedded electron carrier. This electron carrier is at the core of energetic flexibility of a cell; it accepts electrons from more than the two OXPHOS complexes. Other dehydrogenases that also donate electrons to ubiquinone are dihydroorotate dehydrogenase, glycerol 3-phosphate dehydrogenase, choline dehydrogenase, proline dehydrogenase, sulphide: quinone oxidoreductase (Alcazar-Fabra et al., 2021, Wang and Hekimi, 2016). Next step in ETC is CIII, which then accepts electrons from ubiquinol and further reduces cytochrome c. Finally, CIV accepts electrons from cytochrome c to reduce oxygen, the final electron acceptor.

OXPHOS components are multiprotein enzymatic complexes that are comprised of nuclear and mitochondrial encoded proteins. CII is the only complex that is entirely encoded by nuclear genes, while the rest of OXPHOS demands a high level of coordination between nuclear and mitochondrial gene expression machinery. Here are the compositions of OXPHOS complexes as known in mammals (as summarized in (Vercellino and Sazanov, 2022)):

The biggest complex is Complex I, with molecular size of 1 MDa and 45 subunits (14 core, 31 supernumerary), and several different cofactors (flavin mononucleotide and the Fe–S clusters) (Fiedorczuk et al., 2016, Zhu et al., 2016). Out of 44 subunits, 7 are encoded by mitochondrial DNA, the rest are nuclear encoded (Chomyn et al., 1985, Chomyn et al., 1986), and their assembly is regulated by 20 assembly factors hitherto identified (Guerrero-Castillo et al., 2017, Formosa et al., 2020). The seven

mitochondrially encoded subunits that are part of the enzymatic core form the matrix arm (hydrophilic arm) of CI, that is responsible for NADH oxidation. The rest of the core subunits are within the membrane, and the enzymatic core is encompassed by a network of supernumerary subunits, important for either assembly or stability of the complex (Stroud et al., 2016).

Complex II is composed of four subunits encoded by the nuclear genome (Rasheed and Tarjan, 2018), and subsequently transported to the mitochondria. Two matrix subunits SDHA and SDHB are linked to the IMM by membrane embedded SDHC and SDHD subunits, and their assembly is facilitated by four assembly factors: SDHAF1-F4 (Moosavi et al., 2019).

Complex III exists as a functional homodimer with three catalytic subunits: MT-CYB, encoded by mitochondrial DNA; UQCRFS1, which is an iron-sulphur protein, and CYC. The rest are eight supernumerary subunits, encoded by nuclear DNA (Xia et al., 2013). Consistent with CIII involvement in SC structures, its correct assembly is implicated in assembly and biogenesis of CI, with a role to help maturation and further stabilize CI and to an extent, CIV (Protasoni et al., 2020).

Complex IV is a 14-subunit enzyme complex, containing three mitochondrially encoded catalytic (core) subunits MT-CO1, MT-CO2 and MT-CO3, and 11 supernumerary subunits encoded by nuclear DNA. The assembly of CIV is dependent on 50 assembly factors (Timon-Gomez et al., 2018). CIV is the only enzyme of OXPHOS that contains isoforms for 6 of its supernumerary subunits. CIV assembly is proposed to be modular, where CIV assembles into three subcomplexes (modules), each containing one core subunit, which then join into a complete CIV. MT-CO1 forms the initial seed for CIV assembly, together with subunits COX4 and COX5A, with the regulation from HIGD1A (Vidoni et al., 2017). MT-CO1 expression is regulated post-transcriptionally through TACO1, LRPPRC and MITRAC7. It also shows translational plasticity as a regulatory mechanism, as absence of COX4 subunit leads to stalling of COX1 translation in mitochondria (Richter-Dennerlein et al., 2016). The rest of the assembly factors implicated in MT-CO1 assembly are involved in copper cofactor insertion, heme biosynthesis, processing of catalytic core subunits and membrane insertion.

Complex V is the last enzyme of OXPHOS. It is composed of 17 different proteins, where two are mitochondrially encoded – MT-ATP6, a core subunit forming the subunit a, and MT-ATP8, a supernumerary A6L subunit. Functionally, CV is formed by two main domains – the soluble F1 stalk and the F_o domain embedded in the IMM (Spikes et al., 2020). The F_o domain is formed by the c-ring, a membrane-embedded subunit, which is responsible for the rotation of itself and the central stalk. The rotation is fuelled by the passive translocation of protons, pumped to the IMS side by CI, CIII, and CIV, through the proton channel. The proton channel is formed at the interface between the c-ring and the subunit a. The F_1 domain consists of three α-subunits and three β-subunits, which form a globular catalytic head where the phosphorylation of ADP occurs. Furthermore, the F_1 domain contains two stalks. The peripheral stalk is composed of the soluble subdomain formed by the subunits b, OSCP, F6, d, and

a membrane subdomain consisting of the subunits f, e, g, a, ATP8, DAPIT and 6.8PL. The peripheral stalk immobilizes the catalytic head. The second stalk is the central stalk formed by the γ, δ, and ε subunits, which is directly attached to the c-ring of the F_o domain. The central translates the rotary movement of the c-ring directly to the catalytic head, changing the conformation of the head and allowing the phosphorylation of ADP (Pinke et al., 2020, Spikes et al., 2020). The assembly of CV is currently described as a modular process, where five modules are independently assembled with the help of five different assembly factors: ATPAF1, ATPAF2, TMEM70, C7orf55, and TMEM242 (Signes and Fernandez-Vizarra, 2018, Carroll et al., 2021). Apart from phosphorylation of ADP, CV was shown to form mitochondrial cristae by bending the IMM in its dimeric form (Blum et al., 2019). CV dimers were also reported to contribute to cell death by opening the permeability transition pore, although this is still discussed by the scientific community, and it requires more research (Mnatsakanyan et al., 2019, Pinke et al., 2020).

1.3 Mitochondrial gene expression in mammals

The mammalian mitochondrial DNA (mtDNA) is localized within the mitochondrial matrix. It is a circular molecule of a 16 kb length (Anderson et al., 1981). mtDNA encodes 13 core proteins of OXPHOS, and to maintain its independent protein synthesis machinery, it also expresses its own 22 tRNAs, and 2 rRNAs (Mercer et al., 2011). mtDNA consists of a heavy (H) strand and a light (L) strand. It also contains a non-coding control region, where promoters for each strand can be found (HSP or LSP, respectively) strand (Montoya et al., 1982, Gustafsson et al., 2016). An additional LSP

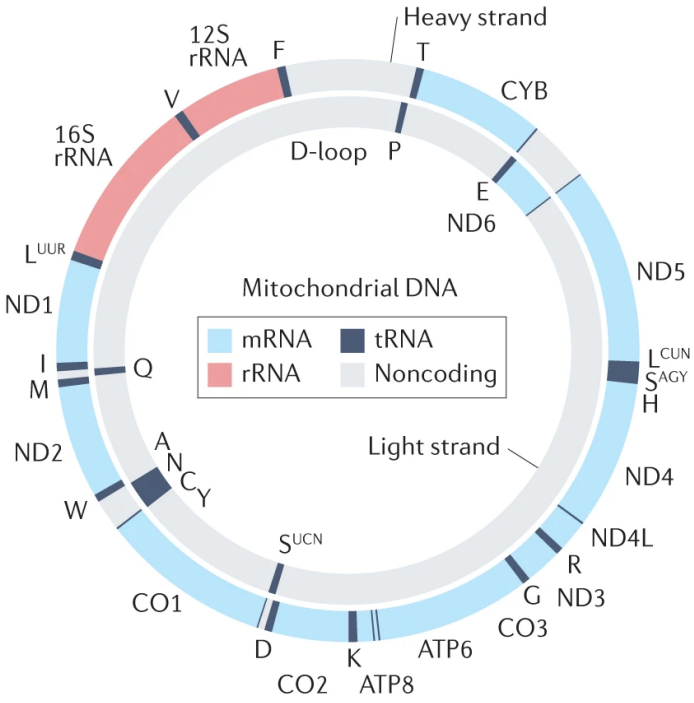


Figure 1.3 | Mitochondrial DNA

Adapted from (Rackham and Filipovska, 2022)

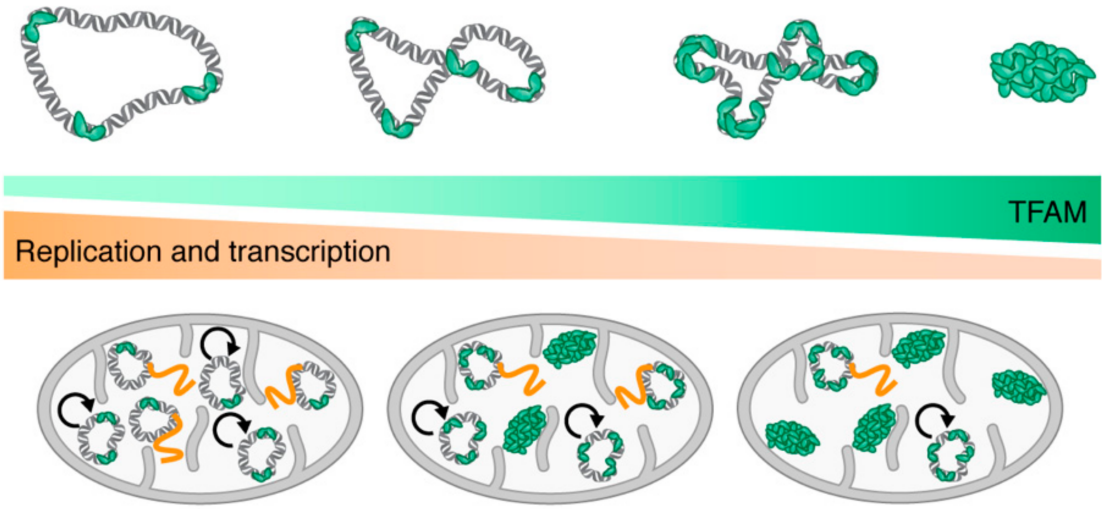


Figure 1.4 | TFAM regulates mtDNA metabolism by packaging mtDNA

Adapted from (Farge and Falkenberg, 2019)

(LSP2) has been recently discovered (Tan et al., 2022). Most of the mitochondrial genes encoding 12 messenger RNAs (mRNA), 14 transfer RNAs (tRNA), and 2 ribosomal RNAs (rRNA) are localized on the H-strand. The genes on the L-strand then encode the remaining 1 mRNA and 8 tRNAs (Mercer et al., 2011).

1.3.1 Replication of mtDNA

mtDNA is organized into nucleoids by mitochondrial transcription factor A (TFAM) (Kukat et al., 2011). TFAM is one of the most abundant proteins present in the mammalian nucleoid – one TFAM protein molecule coats 16–17 bp of mtDNA. (Bogenhagen, 2012). TFAM was shown to package mtDNA via cross-strand binding and loop formations. Increasing concentrations of TFAM also increased the compaction of mtDNA (Kukat et al., 2015). TFAM was also reported to introduce negative DNA supercoils (Shi et al., 2012). These characteristics allow TFAM to maintain mtDNA and regulate its replication and transcription (Gustafsson et al., 2016).

Given its ancestry, the mitochondrial replication machinery is simpler than in the nuclear one and it very much resembles the prokaryotic system. There are four main enzymes of the machinery – the replicase DNA polymerase gamma (POLG) (Gray and Wong, 1992), the helicase Twinkle (TWNK) (Spelbrink et al., 2001), the mitochondrial single-strand binding protein (SSBP1) (Tiranti et al., 1991), and the mitochondrial RNA polymerase (POLRMT) (Kelly et al., 1986, Greenleaf et al., 1986).

According to the widely accepted strand-displacement mode, mtDNA replication is continuous on both strands (Robberson et al., 1972). Replication of the H strand is initiated at the origin of replication of the H-strand (O_H) which is located within the so-called displacement loop (D-loop) in the NCR. POLRMT generates an RNA primer to provide the 3'-end for POLG to initiate DNA synthesis (Chang and Clayton, 1985). TWNK travels in front of POLG to unwind the two strands of DNA in the existing fork. SSBP1 coats and protects the displaced strand against nucleases, secondary structure formations, and random RNA synthesis by POLRMT (Jiang et al., 2021). SSBP1 was also shown to stimulate TWNK and POLG (Farr et al., 1999, Korhonen et al., 2003). After synthesizing approx. two thirds of the genome, the replication fork reaches the second origin of replication of the L-strand (O_L). The parental H-strand then forms a loop, which prevents SSBP1 from binding. That allows POLRMT to bind and prime the H-strand, which initiates the replication of the L-strand (Gustafsson et al., 2016). The replication then continues on both strands until its completion as the strand-displacement mode suggests (Gustafsson et al., 2016).

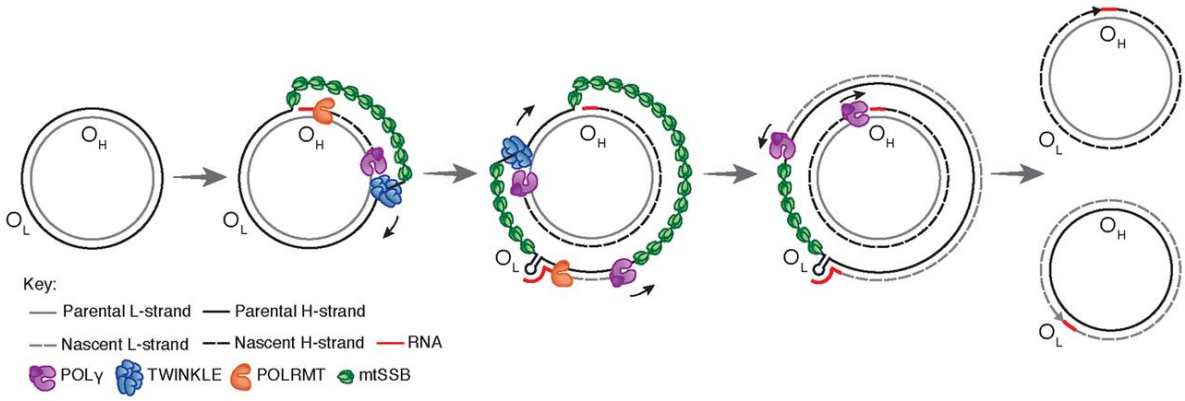


Figure 1.5 | Mitochondrial replication

Adapted from (Falkenberg, 2018)

1.3.2 Transcription of mtDNA

Transcription is under the control of HSP and LSP which are located proximally within the D-loop. The initiation complex constitutes of TFAM, POLRMT, and the mitochondrial transcription factor B2 (TFB2M) (Posse and Gustafsson, 2017). TFAM binds the upstream start site of HSP and bends the DNA (Ngo et al., 2014), which allows the recruitment of POLRMT to the promoter. This recruitment further changes the conformation and TFB2M is mobilized to stabilize the DNA opening in the D-loop (Hillen et al., 2017). This initiation complex is also essential for generating the RNA primer for mtDNA synthesis (Inatomi et al., 2022). A non-coding 7S RNA present within the D-loop then inhibits POLRMT by interacting with the enzyme which prevents POLRMT to initiate transcription (Zhu et al., 2022). The RNA synthesized under the control of LSP can additionally form stable G-quadruplexes between the newly formed RNA and a non-template DNA strand, which can also prematurely inhibit transcription (Hillen et al., 2017). To overcome these obstacles, POLRMT needs the mitochondrial

transcription elongation factor (TEFM) to stimulate the processivity of POLRMT (Minczuk et al., 2011, Agaronyan et al., 2015, Kuhl et al., 2016). TEFM then enhances POLRMT activity to synthesize full-length polycistronic transcripts (Posse et al., 2015). The termination of mitochondrial transcription is still poorly understood. The mitochondrial transcription termination factor 1 (MTERF1) was proposed to terminate transcription that is driven by the LSP (Terzioglu et al., 2013). How the HSP-driven transcription is terminated, is not clear, it does not depend on MTERF1, and might require another enzyme (Bouda et al., 2019).

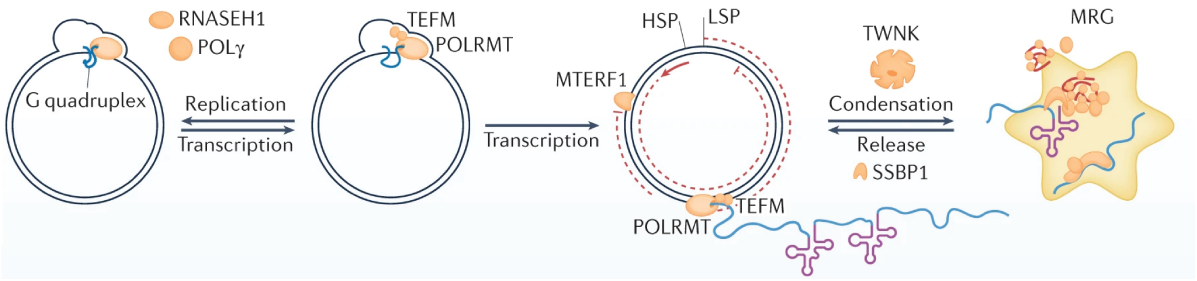


Figure 1.6 | Mitochondrial transcription

HSP – H-strand promoter, LSP – light strands promoter. MRG – mitochondrial RNA granule. Adapted from (Rackham and Filipovska, 2022)

1.3.3 Processing of the primary transcript

The tRNA punctuation model proposes that the processing of mitochondrial polycistronic transcripts starts with the endonucleolytic excision of mt-tRNAs. As mt-tRNAs are placed between most of the mt-rRNA and mt-mRNA coding sequences, excising mt-tRNAs also release these mt-RNAs (Ojala et al., 1981, Anderson et al., 1981). The cleavage of the 5' tRNA ends is carried out by the RNase P complex (Holzmann et al., 2008). The RNase P complex is constituted of three proteins – the tRNA methyltransferase TRMT10C (also MRPP1) and the 3-hydroxyacyl-CoA dehydrogenase type II HSD17B10 (also MRRP2), which are essential for the activity of the ribonuclease P catalytic subunit PRORP (also MRPP3) (Bhatta et al., 2021). The 3' tRNA ends are cleaved by RNase Z (zinc phosphodiesterase ELAC protein 2, also ELAC2). ELAC2 has two isoforms where the mitochondrial ELAC2 processes all 3' ends of all mitochondrial tRNAs and the nuclear ELAC2 processes the majority of nuclear pre-tRNAs (Siira et al., 2018). The 3' tRNA end cleavage occurs only after the excision of the 5' tRNA end (Rackham et al., 2016).

Nevertheless, not all the mRNAs are flanked by tRNAs – these are not cleaved by RNase P or ELAC2 (Sanchez et al., 2011). Instead, it is the proteins of the FASTK (Fas-activated Ser/Thr kinase) family that are involved in the processing of these mRNAs, however, the details of the mechanism are yet to be described (Popow et al., 2015, Boehm et al., 2017, Ohkubo et al., 2021).

1.3.4 tRNA maturation

There are in total 22 tRNAs encoded by mtDNA. A comprehensive analysis of the human mt-tRNAs revealed there are 18 different kinds of RNA modifications at 137 positions of mt-tRNAs. There are 34 different enzymes that were identified to date and that carry out these modifications (Suzuki et al., 2020). One of the modifications, the addition of a CCA trinucleotide at the 3' end, is catalysed by the RNA nucleotidyltransferase TRNT. This modification allows the attachment of an amino acid (Nagaike et al., 2001). Some modifications of the residues in the body of tRNAs are important for the tRNA stability (Bohnsack and Sloan, 2018) (e.g., methylation by MRPP1 which is independent on the RNase P complex activity (Vilardo et al., 2012)). Importantly, in contrast to the 497 cytoplasmic tRNA molecules, mitochondria had to deal with having only 22 mt-tRNAs to implement the genetic code. That is enabled by chemically modifying the anticodon region of the mt-tRNAs to facilitate non-Watson-Crick base pairing, which expands the recognition of codons during translation and increases the fidelity of translation (Suzuki et al., 2020). For example, enzymes NSUN3 and ABH1 catalyze 5-formylcytosine at the wobble position of $tRNA^{Met}$ (Haag et al., 2016). That allows the recognition of two start codons - canonical AUG and non-canonical AUA.

Mt-tRNAs are charged with amino acids by aminoacyl-tRNA synthetases (ARS2s), where 17 ARS2s are only mitochondrial, but GARS (glycyl-tRNA synthetase) and KARS (lysyl-tRNA synthetase) are involved in both cytoplasmic and mitochondrial translation (Konovalova and Tyynismaa, 2013).

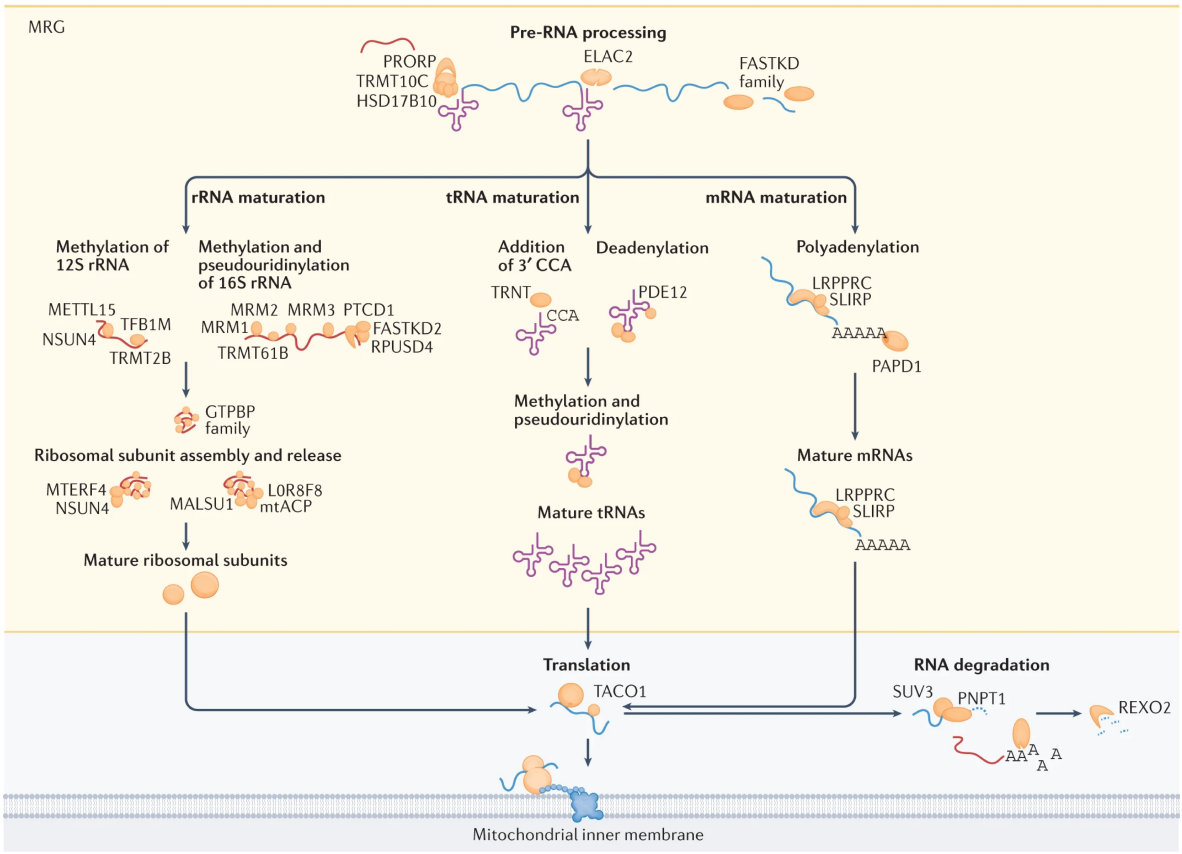


Figure 1.7 | The summary of RNA processing

Adapted from (Rackham and Filipovska, 2022)

1.3.5 rRNA maturation

12S rRNA and 16S rRNA are the integral components of the small mitoribosomal subunit (mtSSU) or the large mitoribosomal subunit (mtLSU), respectively. After being released, they undergo several chemical nucleotide modifications (e.g., base methylations, 2′-O-ribose methylations and pseudouridylation) (Bohnsack and Sloan, 2018). These modifications enable interactions with aminoacyl-tRNAs or mitoribosomal proteins (MRPs) and loss of the modifying enzymes can lead to defective mitochondrial ribosome assembly and impaired translation, e.g., TFB1M (Metodiev et al., 2009), NSUN4 (Metodiev et al., 2014) or MTERF4 (Camara et al., 2011).

1.3.6 mRNA maturation

After being released from the primary transcript, there are 12 mt-mRNAs from the H-strand and *MTND6* mRNA from the L-strand that need to be further processed. The HSP-derived mt-mRNAs are polyadenylated at their 3’ end by the mitochondrial poly(A) polymerase (mtPAP). As seven of these mRNAs lack a 3’ stop codon, the polyadenylation is also important for the completion of these open reading frames (Nagaike et al., 2005, Chang and Tong, 2012). The polyadenylation of the mt-mRNAs

is considered as generally stabilizing, however that does not have to be true for all mt-mRNAs. Deadenylating by the 2',5'-phosphodiesterase 12 (PDE12) elevated CI mt-mRNA levels, but reduced CIV mt-mRNA levels (Rorbach et al., 2011).

The leucine-rich PPR motif-containing protein (LRPPRC) is essential for the stability of all HSP-derived mt-mRNAs as its loss led to a significant decrease in the steady-state levels of mt-mRNAs and no other mt-RNAs (Ruzzenente et al., 2012). LRPPRC works in a complex with the SRA stem-loop-interacting RNA-binding protein (SLIRP), which protects LRPPRC from degradation (Sasarman et al., 2010, Lagouge et al., 2015). LRPPRC/SLIRP complex stabilizes the HSP-derived mt-mRNAs by acting like an RNA chaperone. The complex binds to mRNA, relaxes the secondary structure and exposes the appropriate sites for polyadenylation (Siira et al., 2017), while protecting the mRNA from degradation mediated by PNPT1 (polyribonucleotide nucleotidyltransferase 1) (Chujo et al., 2012).

Unlike the H-strand derived mt-mRNAs, the *MTND6* mRNA is not polyadenylated. *Nd6* mRNA requires FASTK for stability and maturation. FASTK binds to multiple sites of the *MTND6* precursor and together with the mitochondrial RNA degradosome processes the 3' end of *MTND6* (Jourdain et al., 2015).

1.3.7 DNA and RNA degradation

The RNA fragments used in the replication are degraded by the ribonuclease H1 (RNASEH1) and any mtDNA fragments are degraded by the mitochondrial genome maintenance exonuclease (MGME1) (Matic et al., 2018). Together with MTERF1, these enzymes control the switch between the replication and transcription (Gustafsson et al., 2016).

The main RNA degrading enzyme is the polyribonucleotide nucleotidyltransferase 1 (PNPT1), which, in tandem with the helicase SUV3, degrade antisense RNA in the matrix (Borowski et al., 2013). The G4-melting protein GRFS1 co-operates with PNPT1-SUV3 complex (the RNA degradosome) to mediate G-quadruplex RNA degradation (Pietras et al., 2018). A recently described 3'-5' oligoribonuclease REXO2 was reported to scavenge and degrade short RNA sequences generated by RNA processing or by the RNA degradosome (Szewczyk et al., 2020).

1.3.8 Mitoribosomal biogenesis

The mammalian mitochondrial ribosome (mitoribosome) assembly starts with generating mature 12S rRNA and 16S rRNA, which are the scaffolds of the 30 mitoribosomal proteins (MRPs) of the mtSSU (the small 28S mitoribosomal subunit), and 52 MRPs of the mtLSU (the large 39S mitoribosomal subunit). Together, mtLSU and mtSSU form the 55S monosome (Lopez Sanchez et al., 2021). The mitoribosome assembly factors that were discovered so far are various GTPases, helicases, methylases, and RNA-binding proteins. GTPases ERAL1 and NOA1 (also MTG3) are involved in maturation of the mtSSU (Szczepanowska et al., 2016, Paul et al., 2012, Kolanczyk et al., 2011). GTPases GTPBP5 (also MTG2) and GTPBP7 (also MTG1) promote methylation of 16S rRNA by MRM2 methyltransferase (Maiti et al., 2020, Kim

and Barrientos, 2018). Enzymes MALSU1, L0R8F8, and mtACP prevent the immature mtLSU to assemble with the mtSSU (Brown et al., 2017). The MTERF4-NSUN4 complex binds the mtLSU before the last protein bL36m joins mtLSU, also to prevent the premature joining of the two subunits (Cipullo et al., 2021). GTPBP6 facilitates the dissociation of the late mtLSU assembly factors (Lavdovskaia et al., 2020).

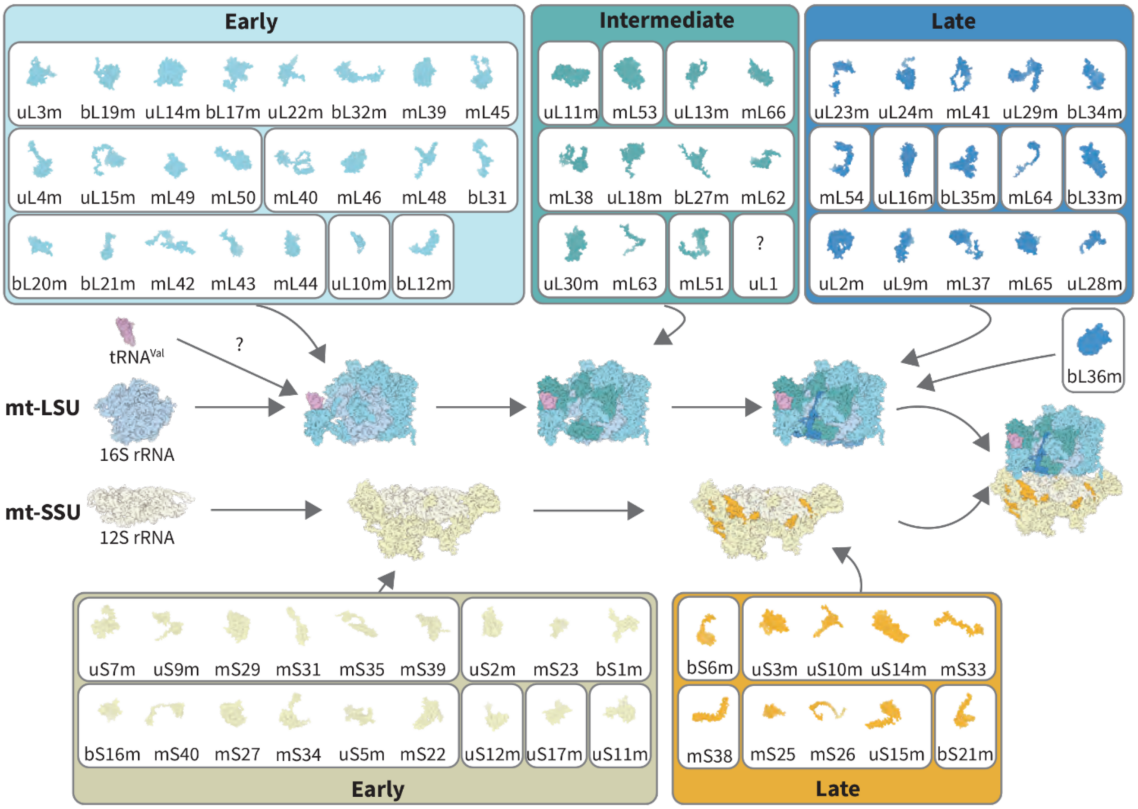


Figure 1.8 | The mitoribosomal assembly

Adapted from (Lopez Sanchez et al., 2021)

1.3.9 Mitochondrial translation

In mitochondria, the newly synthesized nascent protein is co-translationally inserted directly into the IMM, where it is aided by OXA1L, an insertase important for insertion of integral membrane proteins, and by mitochondrial cardiolipin (Kummer and Ban, 2021). Translation is initiated by the mitochondrial initiation factors MTIF3 and MTIF2. First, MTIF3 positions the start codons of the mRNA at the peptidyl site (P) in the mtSSU. LRPPRC in association with PTCD3 stabilizes and feeds the mRNA to the ribosome. Then MTIF2 is recruited to the mtSSU and orchestrates the assembly of the monosome and decoding of the start codon by formylmethionyl-tRNA (Rackham and Filipovska, 2022, D'Souza and Minczuk, 2018).

The elongation phase is carried out by mitochondrial elongation factors TUFM (EFTu), GFM1 (EFG1), and GUF1. TUFM delivers tRNA synthetases to the acceptor site (A), where the aminoacylated tRNAs continue to decode the codons. TUFM is then

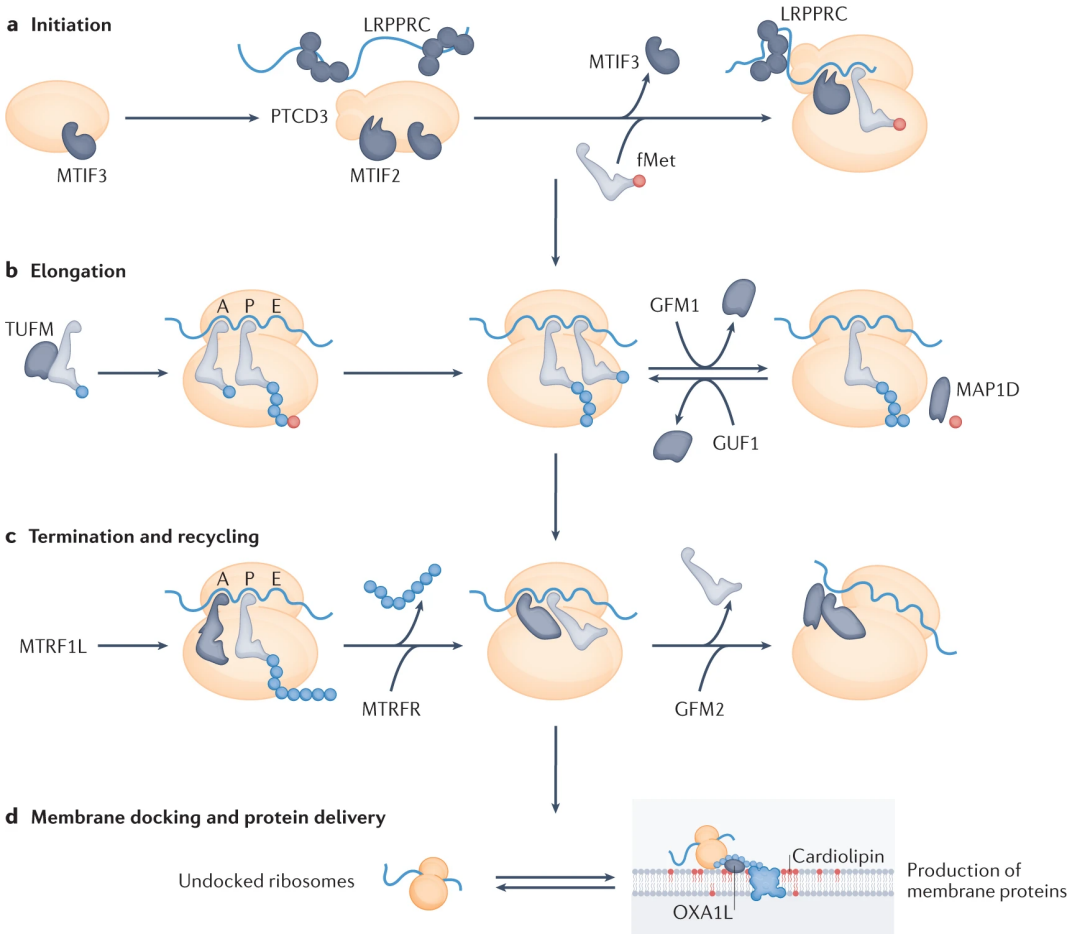


Figure 1.9 | Mitochondrial translation

Adapted from (Rackham and Filipovska, 2022)

released and GFM1 catalyses the translocation of the peptidyl-tRNA from the A and P site to the P and exit site (E), which moves the mRNA by one codon. On the other hand, GUF1 stimulates a one-codon back-translocation in the case of improper translation, ensuring the fidelity of the translation (Kummer and Ban, 2021). The methionyl aminopeptidase MAP1D (also METAP1D) removes the N-terminal methionine (Serero et al., 2003).

Translation is terminated when there is a stop codon at the A site. The termination is catalysed by ribosome release factors MTRFL1, MTRFR, and GFM2 (also EFG2). MTRFL1 recognizes a canonical stop codon and releases the peptide. MTRFR and GFM2 then facilitate the release of the mRNAs and tRNAs and promote the dissociation of the two ribosomal subunits (Rackham and Filipovska, 2022).

1.4 Protein quality control in mitochondria

The mitochondrial function is dependent on highly coordinated communication between nuclear and mitochondrial genome. Since the mitochondrial gene expression is largely dependent on nuclear encoded proteins and factors, their proper delivery to mitochondria is of key importance for mitochondrial function and organization. Nuclear encoded mitochondrial proteins depend on a highly specialized mitochondrial import

system, responsible for proper import, sorting and assembly of protein precursors (Wiedemann et al., 2004).

Owing it to their endosymbiotic origin, they have retained their own protein quality control (PQC) system which is very similar to the bacterial one (Voos et al., 2016). The PQC components are molecular chaperones and proteases from the AAA+ family (Voos, 2013).

Each mitochondrial compartment has its own group of proteases. There are a few membrane-embedded protein quality control (PQC) proteases. The *i*-AAA protease composed of six YME1L (yeast mtDNA escape 1-like) subunits active on the IMS side (Puchades et al., 2017).The *m*-AAA protease is active on the matrix side and can form a homooligomer of AFG3-like subunit 2 (AFG3L2), or heterooligomers of AFG3L2 and paraplegin (SPG7) (Koppen et al., 2007). Additionally, AFG3L1 is a third *m*-AAA subunit found in mice, which can also form homo- or heterooligomeric complexes of the *m*-AAA protease (Koppen et al., 2007). OMA1, a processing peptidase in the IMM, has an overlapping activity with the *m*-AAA protease (hence the acronym OMA1). OMA1 was recently shown to trigger the integrated stress response upon mitochondrial dysfunction by cleaving an IMS protein DELE1, which translocates to the cytosol and stimulates the activity of the canonical ISR kinase HRI (Guo et al., 2020, Fessler et al., 2020). Another IM protease is PARL (Presenilins-associated rhomboid-like protein), which was reported to interact with *i*-AAA and the stomatin-like protein 2 SLP2 (Wai et al., 2016). This proteolytic hub then prevents the activation of mitophagy by processing PINK1 (PTEN-induced kinase 1), after PINK1 translocates from the OMM to the IMM (Jin et al., 2010, Wai et al., 2016).

In the IMS, there are two serine proteases HTRA2 (high temperature requirement mitochondrial serine protease A2)/Omi (Vande Walle et al., 2010) and LACTB (β-lactamase-like protein) (Polianskyte et al., 2009).

Finally, in the mitochondrial matrix, there are two soluble proteases – LONP1 and CLPXP. CLPXP is composed of seven proteolytic CLPP (caseinolytic peptidase subunit P) subunits and of six chaperone-like CLPX (caseinolytic peptidase subunit X) subunits (Kang et al., 2005). LONP1 will be described more thoroughly in the next chapters as it is the focus of this study.

1.5 Lon proteases

Lon proteases are nuclear encoded serine peptidases that are highly conserved throughout all living species spanning from archaea and eubacteria to mammalian mitochondria and peroxisomes (Wlodawer et al., 2022). They belong to the AAA+ protein superfamily (ATPases Associated with diverse cellular Activities) whose members are characterized by harbouring an ATP-dependent domain (Lupas and Martin, 2002). In mammals, there are two isoforms of Lon – LONP1 (mitochondrial) and LONP2 (peroxisomal). Both isoforms are associated with degrading of oxidatively damaged proteins, although the role of LONP2 is still poorly understood and needs more investigation (Pomatto et al., 2017).

1.5.1 Structure

Lon proteases are divided into four subfamilies that differ in structure and origin (Wlodawer et al., 2022). The LonA subfamily is where the eukaryotic (organellar) and most of the eubacterial enzymes belong to. The LonB subfamily consists of archaeal enzymes, and LonC was discovered in thermophilic bacteria. The most recently described subfamily is LonBA, which was recently discovered in *Bacillus subtilis* (Gustchina et al., 2022). All the Lon protomers possess two functional domains: the ATPase domain (A-domain) with an ATP-dependent unfoldase activity, and the C-terminal proteolytic domain (P-domain) with the catalytic activity. The LonA subfamily additionally possesses a third functional N-terminal domain (N-domain) responsible for the substrate recognition and stability of the protease (Kereiche et al., 2016). The LonC enzymes are soluble cytoplasmic proteins, while the LonB enzymes are transmembrane proteins (Wlodawer et al., 2022). The LonBA proteases were reported to be anchored to the membrane like LonB, but they also carry the N-domain of the LonA subfamily (Gustchina et al., 2022).

The mammalian LONP1 is a nuclear encoded peptidase with a catalytic Ser/Lys dyad at its C-terminus. The functional N-, A-, and P- domains form one LONP1 monomer with a molecular mass of ~100 kDa. The monomers assemble into homohexamers. The A- and P- domains form a chambered structure, and the N domains are positioned as a trimer of dimers on top of the chamber (Kereiche et al., 2016). The homohexameric ring is common to all Lon proteases, including the yeast PIM1. PIM1 was thought to form a unique heptamer (Stahlberg et al., 1999), but a recent cryo-EM structure suggested a conserved hexameric conformation (Yang et al., 2022).

The mechanism of LONP1 is as follows: the N-domain recognizes a substrate, binds it, and translocates the peptide inside the chamber. The A-domain hydrolyzes

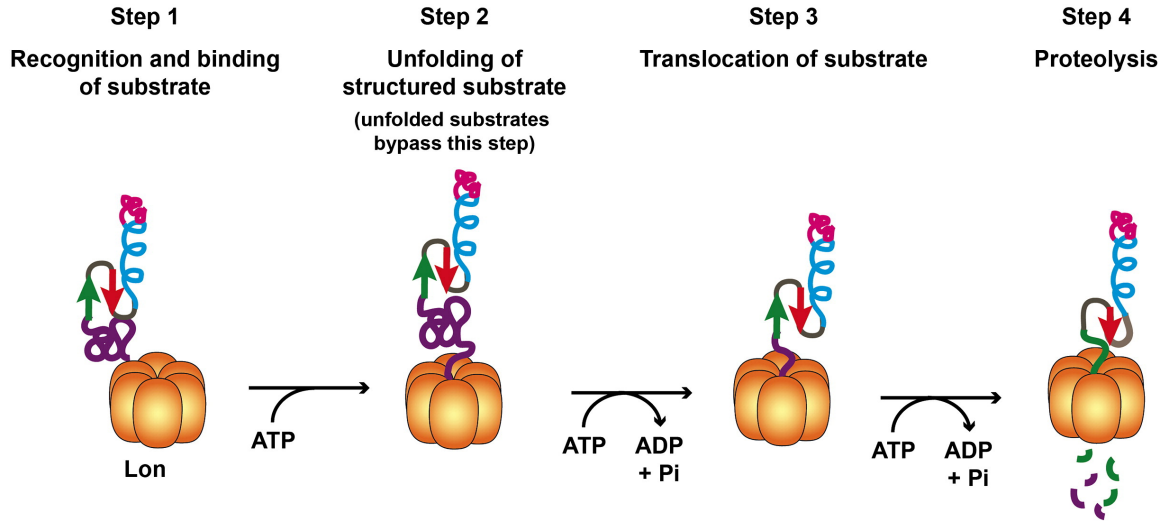


Figure 1.10 | The enzymatic activity of Lon proteases

Adapted from (Venkatesh et al., 2012)

ATP to unfold the peptide and translocates it further to the P-domain. Upon the interaction with the catalytic site, the substrate is cleaved, and the small peptides are released.

The study from *E. coli* proposes that the N-domain is capable of the regulation of the A-domain, because a partial deletion in the N-terminal region also impaired the ATPase activity (Cheng et al., 2012). A detailed human LONP1 structure offers another insight for LONP1 proteolysis mechanism (Shin et al., 2021b). The targeted peptide must not only enter the P domain, but also to interact with catalytic loops within the P-domain. This interaction activates the proteolytic activity of LONP1. The possibility of LONP1 to regulate the A- and the P-domain independently would support the ability of LONP1 functioning as an ATP-dependent chaperone. Intriguingly, LONP1 could potentially activate only a few catalytic subunits at a time, allowing it to possibly fine-tune the degradation of its substrates (Shin et al., 2021b).

A specific amino acid sequence by which Lon proteases recognize their substrates, has not been described yet. However, bacterial Lon was shown to recognize hydrophobic sequences, which are rich in aromatic residues and which are revealed only upon unfolding of the protein (Gur and Sauer, 2008).

1.5.2 Function

Lon proteases are the key guardians of the bacterial and mitochondrial protein homeostasis. They degrade unfolded or misfolded proteins as it was shown in bacteria (Rosen et al., 2002), yeast mitochondria (Wagner et al., 1994), and also mammalian mitochondria (Bezawork-Geleta et al., 2015) to prevent protein aggregation. Lon proteases also remove oxidatively damaged proteins (Bota and Davies, 2002). The proteases are aided by molecular chaperones (e.g., DnaK in bacteria, Hsp70 and Hsp60 in yeasts, mtHSP70 in mammals) to stabilize the proteins against aggregation, and then they either ensure the protein refolding, or the removal of the non-refoldable proteins (Kumaran and Munavar, 2019, Bender et al., 2011, Shin et al., 2021a).

The absence of Lon is not completely detrimental to all organisms. In bacteria, yeasts, and plants (*Arabidopsis thaliana*), the deletion of Lon leads to higher susceptibility to various stresses, and in case of mitochondrial Lon, also to the impairment of respiration (Chung and Goldberg, 1981, Van Dyck et al., 1994, Rigas et al., 2009). In mammals, however, when LONP1 is depleted in the whole body, it is embryonically lethal, proving LONP1 to be essential for embryonic development (Quiros et al., 2014).

1.5.3 Lon in bacteria

Lon proteases were first discovered in *Escherichia coli* – mutation in *lon* caused *E. coli* cells to grow in long forms after an exposure to UV light, as they were unable to divide. The long phenotype coined the name of the gene (Howard-Flanders et al., 1964). The enzyme was later isolated by Swamy and Goldberg and was named La. The discovery of this protease was confusing, as there was no other known protease

which would be stimulated by ATP (Swamy and Goldberg, 1981). The protease La was confirmed to be a *lon* gene product (Chung and Goldberg, 1981, Charette et al., 1981). Historically, the bacterial Lon protease had two names – La and CapR, however those labels were abandoned and the protease was named after its gene – Lon (Gur, 2013).

The long phenotype was caused by an accumulation of a cell division inhibitor SulA, later identified as Lon substrate (Mizusawa and Gottesman, 1983). The mutation in *lon* also led to a mucoid phenotype caused by an overproduction of capsule polysaccharides – that is due to the accumulation of another Lon substrate, a transcription activator RcsA (Torres-Cabassa and Gottesman, 1987).

Lon is a general stress response protease in bacteria – *lon* mutants accumulate abnormal and unfolded proteins and are more sensitive to heat shock, oxidative damage, puromycin and are less able to resist killing from these stresses (Robertson et al., 2000, Phillips et al., 1984).

There are also other specific Lon-dependent adaptations to stressful conditions in bacteria. A general mistranslation is a stress response to DNA damage in *E. coli* and is essential for the cell survival. Lon mitigates the consequences of the mistranslation as it combats the proteotoxic stress (Samhita et al., 2020). Stress-induced misfolded proteins competitively inhibit degradation of dCTP deaminase (CcrM) by Lon in *Caulobacter crescentus*. The elevated pool of dNTPs improves the cell's fitness as the cell can maintain replication capacity (Zeinert et al., 2020).

In *E. coli*, Lon degrades most ribosomal proteins like S2, L3 or L19 in the presence of inorganic polyphosphate (polyP). PolyP doesn't have a role as an energy source, but it stimulates the formation of the protease-substrate complex. As polyP concentration increases more than 100-fold during acute stresses, e.g., starvation, it probably does so to promote Lon degradation of free ribosomal proteins to provide the cell with amino acids (Kuroda et al., 2001). PolyP binds the proteins and Lon in a specific manner and induces conformational changes of Lon itself (Nishii et al., 2005).

The accumulation of active DnaA is key to triggering the bacterial DNA replication initiation. Under normal conditions, DnaK/J chaperone destabilizes the sigma factor σ^{32} in *E. coli* and in *Caulobacter*. Upon acute or severe stress, DnaK/J is saturated with misfolded proteins, which releases σ^{32}. σ^{32} then activates the stress response including the upregulated synthesis of Lon. Lon then degrades DnaA, which prevents the initiation of DNA replication and leads to cell cycle arrest in *Caulobacter* (Jonas et al., 2013). In *E. coli*, the polyP-dependent proteolysis was also found to target DnaA, but only when bound to ADP, not ATP (Gross and Konieczny, 2020). Excess DnaA-ATP binds to *dnaA* promoter, preventing its own transcription, while DnaA-ADP interacts with Lon. By regulating DnaA-ADP/DnaA-ATP balance, Lon-polyP is able to block replication initiation in stress conditions (Gross and Konieczny, 2020).

Lon was shown to bind a double-stranded DNA (dsDNA) (Zehnbauer et al., 1981) to a TG-rich DNA promoter element (Fu et al., 1997) through its A-domain, which was shown necessary for the degradation of DNA-binding substrates (Karlowicz et al., 2017).

The lack of Lon was reported to be compensated by upregulation of ClpYQ protease, which indicates a possible interplay between Lon and ClpYQ in bacteria (Kumaran et al., 2020).

1.5.4 Lon in yeasts

In *Saccharomyces cerevisiae*, Lon protease is encoded by *PIM1* gene (which stands for proteolysis in mitochondria) (Kutejova et al., 1993, Van Dyck et al., 1994), therefore the protease is known also as PIM1. Although *PIM1* is not an essential gene, Δ*pim1* strains are respiratory-deficient due to large mitochondrial DNA deletions. The mitochondrial dysfunction inhibits growth on non-fermentable carbon sources (Suzuki et al., 1994, Van Dyck et al., 1994, Wagner et al., 1997). The impaired proteolysis additionally resulted in the accumulation of electron-dense inclusions which are likely protein aggregates (Wagner et al., 1994, Suzuki et al., 1994, Van Dyck et al., 1994). It is PIM1 which is crucial for removing oxidatively damaged proteins in mitochondria, especially those containing iron-sulphur (Fe-S) clusters (Bender et al., 2010, Bayot et al., 2010). Degrading oxidized proteins also prevents their aggregation (Bender et al., 2011). In the Figure 1.11, the wide range of substrates targeted when oxidatively damaged are summarized (Bayot et al., 2010). This demonstrates the plethora of mitochondrial pathways that PIM1 regulates.

PIM1 is also required for longevity in yeasts - Δ*pim1* cells accumulated aggregates of oxidized proteins in the cytosol. There was also an increase in ubiquitinated proteins in the cytosol indicating an impaired 26S proteasome activity (Erjavec et al., 2013).

The chaperone-like properties of Lon proteases were first demonstrated in yeasts. The defective assembly of CIV and CV in Δ*pim1* was rescued by a catalytically inactive PIM1, but not by an A-domain mutant (Rep et al., 1996).

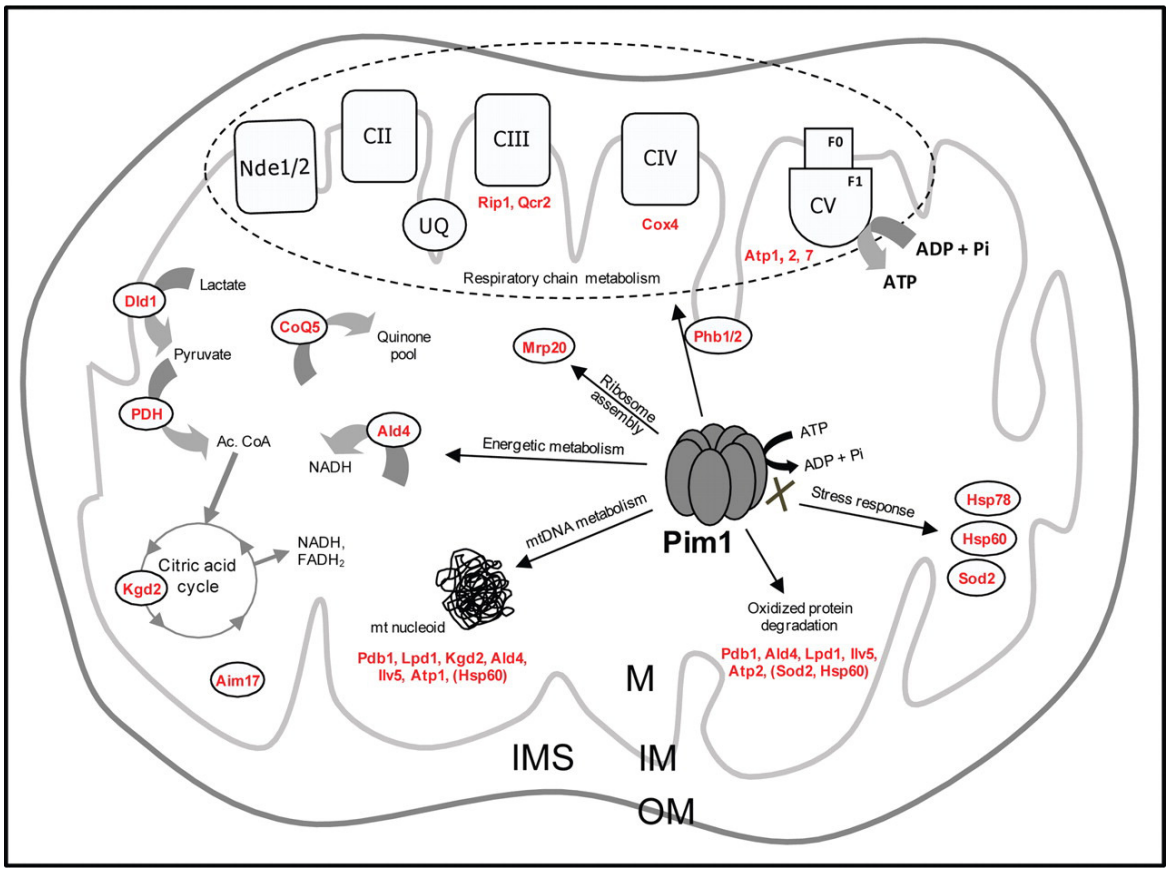


Figure 1.11 | PIM1 substrates

Adapted from (Bayot et al., 2010)

PIM1 is involved in the regulation of the mitochondrial nucleoid. Apart from targeting the above-mentioned substrates when oxidized, PIM1 also degrades two yeast proteins - ABF2 (a functional homologue of TFAM) and MGM101 (the mitochondrial genome maintenance protein) *in vitro* (Kunova et al., 2017). These proteins bind to mtDNA – this interaction protects them from PIM1 degradation. Whether PIM1 binds to DNA is not clear (Göke et al., 2020), but PIM1 colocalizes with the mitochondrial nucleoid (Kunova et al., 2017). A recently identified protein MRX6 forms a complex with PIM1 and localizes to mtDNA. There, MRX6 aids PIM1 to recognize and degrade proteins that stimulate replication (Göke et al., 2020).

PIM1 doesn't only promote CIV assembly, but the protease is also required for COX1 translation. The yeast mtDNA contains introns, therefore the pre-mRNA has to undergo splicing. PIM1 seems to be involved in COX1 pre-mRNA processing either by splicing introns, or by degrading RNA-binding proteins which prevent COX1 translation (van Dyck et al., 1998). PIM1 also targets mS38 – an mtLSU protein that is necessary for the translation of COX1, COX2, and COX3 (Wu et al., Mays et al., 2019).

1.5.5 LONP1 in mammals

The mammalian LONP1 was first isolated and characterized in 1993 in humans (Wang et al., 1993). It was shown that LONP1 is ubiquitously expressed in all human tissues. It is most present in brain, heart, skeletal muscle, and liver, whereas it is the least expressed in lung, kidney, pancreas, and immune cells (Wang et al., 1993).

LONP1 is a protein essential for life in mammals. A homozygous knockout of *Lonp1* resulted in embryonic death at 8.5 days post coitum (dpc) accompanied by a ~80% decrease in the mtDNA copy number at 7.5 dpc (Quiros et al., 2014).

1.5.5.1 LONP1 in protein quality control

LONP1 was shown to be the main protein quality control protease in the mitochondrial matrix. There are multiple studies reporting the accumulation of electron-dense inclusions in Lon-deficient models that are most probably aggregated proteins. These inclusions were observed in yeasts (Suzuki et al., 1994), human cells (Zurita Rendon and Shoubridge, 2018), and even human muscle biopsies (Nimmo et al., 2019). It was LONP1, and not CLPXP, which degraded misfolded proteins, protecting the mitochondria from accumulated aggregates (Bezawork-Geleta et al., 2015). The examples of misfolded LONP1 substrates are the mitochondrial glutaminase GLS after its native tetrameric conformation is destroyed (Kita et al., 2012), and a mildly oxidized mitochondrial aconitase ACO2 to prevent excessive oxidation and aggregation of the protein (Bota and Davies, 2002). LONP1 also possesses a chaperone-like function, where its ATPase activity is required. Together with mtHSP70 and TID1, they promote the folding of several matrix and IMM proteins (Shin et al., 2021a, Matsushima et al., 2021). LONP1, and not *m*-AAA or CLPP, has the ability to prevent protein aggregation (Matsushima et al., 2021).

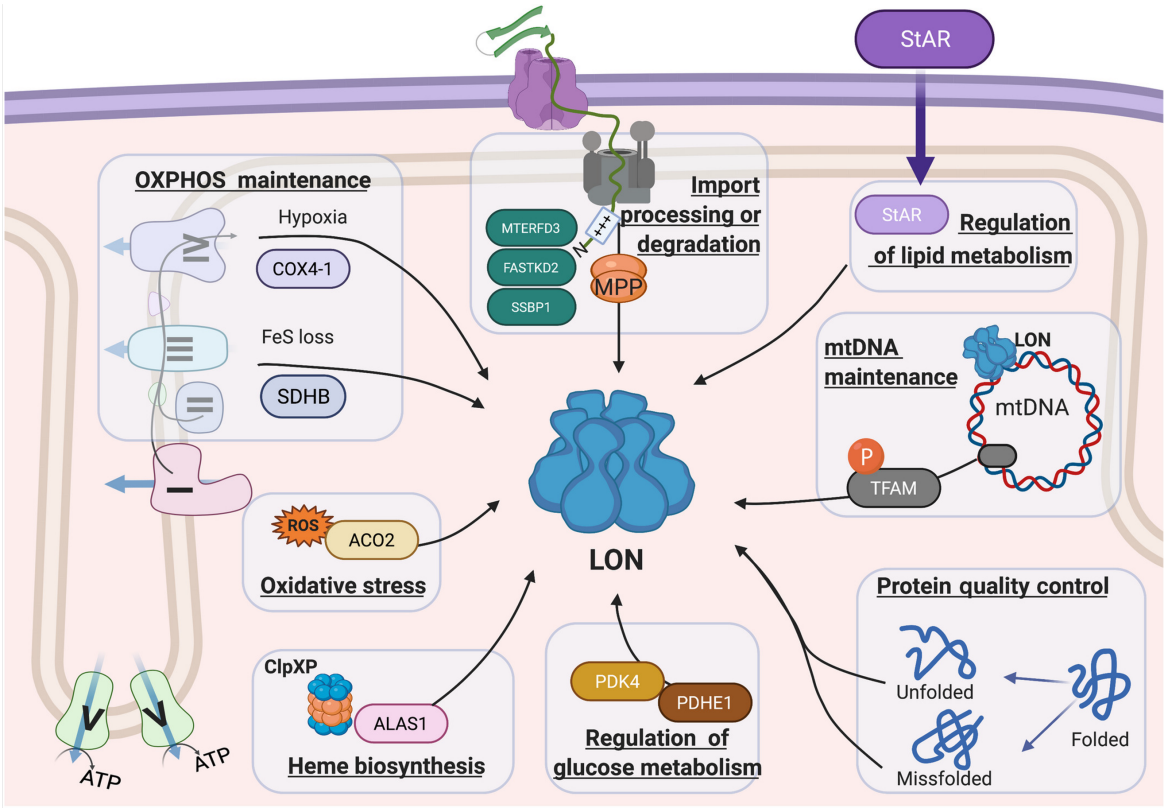


Figure 1.12 | A summary of LONP1 functions

Adapted from (Szczepanowska and Trifunovic, 2022)

There are also natively folded substrates that are targeted by LONP1. In steroidogenic cells, the availability of cholesterol on mitochondria is important for the synthesis of steroid. A steroidogenic acute regulatory protein StAR facilitates the transfer of cholesterol from the OMM to the IMM. StAR itself is readily degraded by LONP1, once it reaches the mitochondrial matrix (Granot et al., 2007).

LONP1 also regulates the activity of the pyruvate dehydrogenase (PDH) by degrading the phosphorylated E1α subunit (Nimmo et al., 2019). The phosphorylated E1α would otherwise inhibit PDH, which would rise the intracellular lactate concentration (Nimmo et al., 2019). PDH can be also inhibited by a pyruvate dehydrogenase kinase 4 PDK4, which is an integral component of PDH. When PDK4 dissociates from PDH, PDH is activated and PDK4 is degraded by LONP1 (Crewe et al., 2017).

Another example of a folded substrate of LONP1 is the 5-aminolevulinic acid synthase ALAS1 (Tian et al., 2011). ALAS1 controls the rate-limiting step of heme biosynthesis in the cell and catalyses the synthesis of the first heme precursor – 5-aminolevulinic acid. The synthesized heme then stimulates the degradation of ALAS1 in a negative feedback regulation (Yoshino et al., 2007), and LONP1 carries out the degradation itself (Tian et al., 2011).

1.5.5.2 LONP1 in OXPHOS

LONP1 targets COX5b and COX4i1 (CIV subunits) during hypoxia and myocardial ischemic injury (Fukuda et al., 2007). Under hypoxic conditions, the hypoxia-inducible factor 1 (HIF-1) is activated to regulate the oxygen homeostasis. HIF-1 stimulates the expression of *Lonp1* and *Cox4i2* genes. COX4i2 is another isoform of COX4, but it is also more adaptive to hypoxia. LONP1 selectively degrades COX4i1 to allow the switch to COX4i2 isoform (Fukuda et al., 2007). COX5b and COX4i1 must be phosphorylated to be recognized by LONP1 as mutations in the respective phosphorylation sites protected the substrates against LONP1. The phosphorylation is mediated by the protein kinase A (PKA) (Sepuri et al., 2017).

LONP1 could be involved in the regulation of Fe-S clusters in OXPHOS. It was reported to interact with CI subunit NDUFS8 (Kao et al., 2015) and overexpression of LONP1 also increased NDUFS8 levels, indicating LONP1's role in stabilizing NDUFS8 (Cheng et al., 2013). In frataxin-depleted heart mitochondria, LONP1, ClpP, and their overall proteolytical activity were upregulated. Simultaneously, the Fe-S containing OXPHOS subunits (NDUFS3, SDHB, and UQCRFS1) were downregulated on the protein level with no major change on the transcript level, making these proteins the putative substrates of LONP1 or ClpP (Guillon et al., 2009). Indeed, SDHB was reported to be degraded by LONP1 upon the loss of the CII assembly factor SDHAF1. SDHAF1 is needed for the incorporation of Fe-S cluster into SDHB (Maio et al., 2016).

Another CII assembly factor SDHAF2 (also known as SDH5) is required for flavination of SDHA (Hao et al., 2009). SDHAF2 is degraded by LONP1 when not bound to SDHA (Bezawork-Geleta et al., 2014).

1.5.5.3 LONP1 in mitochondrial gene expression

Human LONP1 was shown to bind to a single-stranded GT-rich element, which overlaps with LSP (Fu and Markovitz, 1998) and to GT-rich sequences found on the H-strand (Liu et al., 2004). MtDNA immunoprecipitation revealed LONP1 associates also with the region between the D-loop and COX1 (Lu et al., 2007). Interestingly, LONP1 binds GU-rich RNA as well (Liu et al., 2004), suggesting its potential role in regulation of both mtDNA and mtRNA. Furthermore, LONP1 was found to be a core nucleoid component (Rajala et al., 2015) and it interacts with some nucleoid-associated proteins – TWNK, POLG (Liu et al., 2004), and PDIP38 (Cheng et al., 2005).

There are also a few proposed LONP1 substrates. The most studied substrate is TFAM, which was shown to be degraded by LONP1 *in vitro* in *Drosophila melanogaster* and mammalian cell lines (Matsushima et al., 2010, Lu et al., 2013). However, in the mammalian cell line, only TFAM that was not bound to mtDNA and was phosphorylated by PKA on both Ser55 and Ser56 was targeted by LONP1 (Lu et al., 2013). By degrading TFAM, LONP1 is thought to participate in the regulation of the TFAM:mtDNA ratio (Matsushima et al., 2010, Lu et al., 2013). Further identified LONP1 substrates are the catalytic subunit of POLG – POLγA (Silva-Pinheiro et al., 2021), and TWNK (Kunova et al., 2017).

These discoveries propose a direct involvement of LONP1 in the regulation of the nucleoid composition itself, but also in the regulation of mtDNA replication and transcription.

LONP1 has been also implicated in maturation of imported mitochondrial matrix proteins. Together with the mitochondrial processing peptidase MPP, they cleave the matrix targeting sequence of the following proteins – SSBP1, MTERFD3, FASTKD2, and CLPX (Zurita Rendon and Shoubridge, 2018). These four proteins are also suggested by this study as bona fide LONP1 substrates. Zurita Rendon and Shoubridge also showed that depletion of LONP1 led to a decrease in mtDNA copy number. Furthermore, the depletion inhibited mitochondrial translation and decreased the protein levels of both mtLSU and mtSSU individual proteins and subunits (Zurita Rendon and Shoubridge, 2018). A co-immunoprecipitation experiment revealed an interaction of LONP1 with 11 mtLSU protein (Zurita Rendon and Shoubridge, 2018), and MRPL32 was targeted by LONP1 *in vitro* (Kunova et al., 2017), suggesting its role in mitoribosomal biogenesis.

1.5.6 LONP1 in disease

At first, mutations in LONP1 were linked to CODAS syndrome (cerebral, ocular, dental, auricular, and skeletal anomalies syndrome), an autosomal-recessive disorder characterized by developmental delay, short stature, hypotonia, ptosis, hearing loss, which are classical features of a mitochondrial disorder, but in addition, CODAS patients suffer from skeletal and dental anomalies (Strauss et al., 2015, Dikoglu et al., 2015). Lately, two other cases of LONP1-related disorders were described – one infant patient with congenital lactic acidosis, muscle weakness, brain MRI consistent with Leigh syndrome and profound deficiencies of mitochondrial oxidative phosphorylation associated with severe depletion of mtDNA (Peter et al., 2018). The other case are two siblings with hypotonia, muscle weakness, developmental delay, and severe neurological impairment with progressive cerebellar atrophy because of a newly classified pathogenesis of pyruvate dehydrogenase deficiency associated with LONP1 mutation (Nimmo et al., 2019).

1.6 Objectives

LONP1 was shown to be an essential mitochondrial protease. However, only a handful LONP1 substrates have been identified, although knowing the specific targets is the key to the understanding of a protease and its functions. That is due to the limited available methods and many challenges that studying mitochondrial proteases and their substrates entails, especially on a larger scale.

This study aimed to gain a deeper insight of LONP1 on the mouse heart biology with a special focus on the mitochondrial gene expression machinery. Even though mitochondria share many features with bacteria owing to their origin, we are just starting to understand the processes in the mitochondrial gene expression in detail. With the development of the experimental methods and advances in the structural cryo-EM studies, the publications in this field have been rapidly emerging in the last

couple of years. One of the pressing questions is what the regulating mechanisms in these processes are. To address this, we developed a mouse model with a heart and skeletal muscle specific depletion of LONP1. We also attempted to create a stable cell model of LONP1 depletion to perform experiments which are not compatible with the *in vivo* model and to be able to directly investigate the possible substrates of LONP1, however our efforts were unsuccessful. This mouse model allowed us to study the consequences of the LONP1 absence on the mRNA and protein levels not only in the regards to the mitochondrial gene expression, but also in OXPHOS. Through the investigation of insoluble proteins in the cardiac mitochondria, we also narrowed down a list of potential LONP1 substrates, which offers a future opportunity for an effective substrate screening (e.g., with a catalytically inactive protease combined with co-immunoprecipitation of trapped substrates and their proteomic analysis).

In summary, the goals of this study were:

1. Generating a viable mouse and cell model of the LONP1 deficiency.
2. Characterizing the general consequences of the condition in the heart.
3. Describing changes in the mitochondrial gene expression and in OXPHOS.
4. Characterizing new potential LONP1 substrates.

2 Materials and Methods

2.1 Materials

2-mercaptoethanol	Sigma-Aldrich	USA
3,3'-diaminobenzidine	Vector Laboratories	USA
Acetic Acid	AppliChem	USA
Acetone	AppliChem	USA
Adenosine 5'-triphosphate disodium salt	Sigma-Aldrich	USA
Adenosine 5'-diphosphate sodium salt	Sigma-Aldrich	USA
Agar bacteriology grade	AppliChem	USA
Agarose NEEO ultra quality	Roth	Germany
Agarose-LE	Ambion	USA
Alanine (L-)	Sigma-Aldrich	USA
Ammoniumpersulfat APS	Sigma-Aldrich	USA
Ampicillin sodium salt	AppliChem	USA
Antimycin A	Sigma-Aldrich	USA
Arginine mono-hydrochloride (L-)	Sigma-Aldrich	USA
Ascorbic Acid	Sigma-Aldrich	USA
Asparagine monohydrate (L-)	Sigma-Aldrich	USA
Aspartic Acid (L-)	Sigma-Aldrich	USA
Bis-Tris	Santa Cruz Biotechnology	USA
Bradford reagent	Sigma-Aldrich	USA
Bromophenol Blue	Merck	USA
BSA (Albumin from bovine serum) fatty acid free	Sigma-Aldrich	USA
Catalase, bovine liver	Sigma-Aldrich	USA
Chloro-D-Phenylalanine	Sigma-Aldrich	
Chloroacetamide	Sigma-Aldrich	USA
Chloroform	AppliChem	USA
Coomassie Brilliant Blue G250	AppliChem	USA
Creatine phosphate disodium salt tetrahydrate	Sigma-Aldrich	USA
Creatine Phosphokinase Type III, bovine	Sigma-Aldrich	USA
Cysteine hydrochloride monohydrate (L-)	Sigma-Aldrich	USA
Cytochrome c, bovine heart	Sigma-Aldrich	USA
DEPC	AppliChem	USA
Digitonin (HP)	Merck	USA
DMSO Dimethylsulfoxide	Sigma-Aldrich	USA
DTT Dithiothreitol	Sigma-Aldrich	USA
EDTA Ethylenediaminetetraacetic acid	Sigma-Aldrich	USA
EGTA Ethylene glycol-bis(2-aminoethylether)-N,N,N′,N′-tetraacetic acid	Sigma-Aldrich	USA
Ethidium Bromide (EtBr)	Sigma-Aldrich	USA
Ethanol abs.	AppliChem	USA
FCCP (Carbonyl cyanide-p-trifluoromethoxyphenylhydrazone)	Sigma-Aldrich	USA
Formaldehyde 38%	Roth	Germany
Glucose	AppliChem	USA

Glutamic Acid (L-)	Sigma-Aldrich	USA
Glutamine (L-)	Sigma-Aldrich	USA
Glutaraldehyde solution Grade I 50%	Sigma-Aldrich	USA
Glycerol	Sigma-Aldrich	USA
Glycine Molecular Biology grade	AppliChem	USA
GTP Guanosine 5'triphosphate sodium salt	Sigma-Aldrich	USA
HCl 37%	VWR	Germany
HEPES-Molecular biology grade	AppliChem	USA
Histidine mono hydrochloride monohydrate (L-)	Sigma-Aldrich	USA
Isoleucine (L-)	Sigma-Aldrich	USA
Isopropanol	AppliChem	USA
LB Medium - powder according to Miller	AppliChem	USA
LB Medium - powder according to Lennox	AppliChem	USA
Leucine (L-)	Sigma-Aldrich	USA
Lysine mono-hydrochloride (L-)	Sigma-Aldrich	USA
Lysyl Endopeptidase	Serva	Germany
Magnesium chloride hexahydrate	Sigma-Aldrich	USA
Malic acid	Sigma-Aldrich	USA
Mannitol Biochemica	AppliChem	USA
Methanol	AppliChem	USA
Methionine (L-)	Sigma-Aldrich	USA
Milk powder	AppliChem	USA
MOPS Mol Bio grade	AppliChem	USA
Nicotinamide adenine dinucleotide	Sigma-Aldrich	USA
Nitrotetrazolium Blue	Sigma-Aldrich	USA
PBS Buffer (10X Dulbecco's) Powder	AppliChem	USA
PBS Tablets	Calbiochem	USA
Phenol	AppliChem	USA
Phenol/Chloroform/Isoamylalcohol	Roth	Germany
Phenylalanine (L-)	Sigma-Aldrich	USA
Phenylmethanesulfonylfluorid PMSF	AppliChem	USA
Potassium acetate	Sigma-Aldrich	USA
Potassium chloride	AppliChem	USA
Potassium hydrogen phosphate	Merck	USA
Potassium dihydrogen phosphate	AppliChem	USA
Proline (L-)	Sigma-Aldrich	USA
Protein Standard	Sigma-Aldrich	USA
Proteinase K	AppliChem	USA
Protease Inhibitor Cocktail	Sigma-Aldrich	USA
Retinoic Acid	Sigma-Aldrich	USA
RNase A	AppliChem	USA
RNAse ZAP	Sigma-Aldrich	USA
Rotenone	Calbiochem	USA
Rotiphorese Gel 40 (29:1)	Roth	Germany
SDS granules	AppliChem	USA
Serine (L-)	Sigma-Aldrich	USA
Sodium acetate solution (3M, pH 5,2)	AppliChem	USA

Sodium azide	AppliChem	USA
Sodium chloride for molecular biology	Sigma-Aldrich	USA
Sodium deoxycholate	AppliChem	USA
Sodium fluoride	AppliChem	USA
Sodium hydroxide	Sigma-Aldrich	USA
Sodium Orthovanadate	AppliChem	USA
Sodium Phosphate dibasic	Sigma-Aldrich	USA
Sodium Phosphate monobasic	Sigma-Aldrich	USA
Sodium pyruvate	Sigma-Aldrich	USA
Sodium succinate dibasic hexahydrate	Sigma-Aldrich	USA
Sorbitol	AppliChem	USA
Subtilisin A	Sigma-Aldrich	USA
Succinic Acid	Sigma-Aldrich	USA
Sucrose	Sigma-Aldrich	USA
TEMED	Sigma-Aldrich	USA
TES Buffer grade	AppliChem	USA
Threonine (L-)	Sigma-Aldrich	USA
TMPD Tetramethyl-p-phenylenediamin	Sigma-Aldrich	USA
Triethylammonium bicarbonate TEAB	Sigma-Aldrich	USA
Tri-sodium citrate dihydrate	AppliChem	USA
Tricine	Roth	USA
Triton X-100, molecular biology grade	AppliChem	USA
Trizma Base	Sigma-Aldrich	USA
TRIzol reagent	Invitrogen	USA
TrypanBlue	Sigma-Aldrich	USA
Trypsin from bovine pancreas	VWR	Germany
Tryptophan (L-)	Sigma-Aldrich	USA
Tween 20	AppliChem	USA
Tyrosine (L-)	Sigma-Aldrich	USA
UltraPure distilled water	Gibco	USA
Urea	Fluka Analytical	USA
Valine (L-)	Sigma-Aldrich	USA
Yeast extract granulate for Microbiology	Merck	USA

2.2 Cell culture

The immortalised mouse embryonic fibroblasts were maintained in a humidified atmosphere at 37 °C containing 5% CO_2. The complete cell culture medium consisted of DMEM (4.5g/L glucose, glutamin, pyruvate; Gibco, USA), 10% fetal bovine serum South America (Biowest, France), and penicilin-streptomycin (Gibco, USA). The cells were split whenever the confluency was between 70 to 90% via trypsinisation (0.05% trypsin/EDTA; Gibco, USA). The splitting ratio ranged from 1:2 to 1:20 depending on the intended use.

2.2.1.1 RNA interference

MEFs were transfected with siRNA oligonucleotide duplex (*Lonp1* siRNA 1, *Lonp1* siRNA 2, or control siRNA (SR-CL-000-005); Eurogentec, Belgium) using the Lipofectamine RNAi MAX reagent (Invitrogen, USA) following the manufacturer's instructions for the reverse transfection. The transfected cells were harvested after 48h of the treatment and further analysed via SDS-PAGE and western blot analysis.

The siRNA-mediated knockdown of MEFs was performed by Dr. Karolina Szczepanowska.

2.3 Mouse experiments

2.3.1 Animal care

The mice with the C57BL/6 background were bred and cared for in the CECAD *in vivo* Research facility. They were kept in the groups of 2-5 mice in individually ventilated cages at an ambient temperature (22–24 °C) in 12h light/dark cycles starting at 6 am. The mice had *an ad libitum* access to drinking water and a normal chow diet (R/M-H-V1554, sniff Spezialdiäten GmbH, Germany). The animals were sacrificed at 8 weeks, 20 weeks or at a terminal age by cervical dislocation. All animal experiments were approved by the local governmental authorities (Landesamt für Natur, Umwelt und Verbraucherschutz Nordrhein-Westfalen, LANUV). All animal handling was performed according to the guidelines and recommendations of the Federation of European Laboratory Animal Science Associations (FELASA).

2.3.2 Experimental mouse models

2.3.2.1 Lonp1tm1a(EUCOMM)Hmgu

The *Lonp1*$^{tm1a(EUCOMM)Hmgu}$ (or *Lonp1*^{tm1a}) mouse line was purchased from the European Mouse Mutant Archive (EMMA). A knockout-first cassette consisting of an IRES:lacZ trapping cassette and a neo cassette (Skarnes et al., 2011) was inserted between exon 1 and 2 of the *Lonp1* gene, and it was flanked by FRT sites. Two loxp sites were positioned around the exon 2 of the *Lonp1* gene.

2.3.2.2 *Lonp1$^{fl/fl}$*

To generate the *Lonp1$^{fl/fl}$* line, the *Lonp1$^{tm1a/tm1a}$* mouse line was intercrossed with a FLP deleter mouse (Actb:Flp, (Dymecki, 1996)). The FLP recombinase recognizes and targets the FRT sites and therefore deletes the FRT-flanked sequence. The mice were further mated to generate the *Lonp1$^{fl/fl}$* homozygous line without the Actb:Flp allele.

2.3.2.3 *LONP1 KO*

The conditional heart and skeletal muscle-specific knockout LONP1 KO mouse line was obtained by intercrossing *Lonp1$^{fl/fl}$* mice with heterozygous *Ckmm-Cre* transgenic mice (Wang et al., 1999). The mice with the genotypes *Lonp1$^{fl/fl}$; Ckmm-Cre$^{wt/wt}$* and *Lonp1$^{fl/wt}$; Ckmm-Cre$^{wt/wt}$* were used as the control mice and labelled LONP1 WT or only WT. The genotype *Lonp1$^{fl/fl}$; Ckmm-Cre$^{tg/wt}$* is the knockout genotype and the mice were labelled LONP1 KO or KO.

2.3.3 Isolation of crude DNA

A piece of tissue was incubated with 500 µL DNA lysis buffer (100 mM Tris-HCl, pH 8.5; 5 mM EDTA, pH 8.0; 0.2% w/v SDS; 200 mM NaCl; 0.1 mg/mL Proteinase K) at 55 °C while shaking (1400 rpm) for 1 hour or until dissolved. One volume of isopropanol was added, samples were vortexed and centrifuged at full speed/4 °C/20 min. Afterwards, the supernatant was discarded. The pellets were washed with 500 µL 70% ethanol and centrifuged at full speed 4 °C/15 min. Supernatants were discarded, pellets were air-dried at room temperature and resuspended in 50–200 µL H_2O.

2.3.4 Genotyping

The polymerase chain reaction (PCR) was used to determine the genotypes of the animals. The reactions were performed using the GoTaq G2 Flexi DNA polymerase (Promega, USA). The PCR reaction mix was as follows:

DNA	0.5 µL
5x GoTaq Reaction Buffer	4 µL
$MgCl_2$ (25 mM)	1.2 µL
dNTP mix (1.25 mM each)	1 µL
Primers (10 mM)	0.8 µL each
GoTaq polymerase	0.05 µL
ddH_2O	Up to 20 µL

PCR program for all genes:

Duration	**Temperature**
5 minutes	95 °C

35 cycles:	
30 seconds	95 °C
30 seconds	annealing [°C]
90 seconds	72 °C
Final extension:	
10 minutes	72 °C
Hold	4 °C

The primers (in the 5'–3' direction) and their annealing temperatures:

Lonp1

Annealing temperature	57 °C
Forward primer	AGGTGACTGTGGAGAGATTCC
Reverse primer	CTTCACTAGTGTCACAGACCT
MUT primer	CAACGGGTTCTTCTGTTAGTCC

Actb:Flp

Annealing temperature	54 °C
Forward primer	TTAGTTCAGCAGCACATGATG
Reverse primer	GGAGGATTTGATATTCACCTG

Ckmm-Cre

Annealing temperature	63 °C
Forward primer (Cre)	GTGAAACAGCATTGCTGTCACTT
Reverse primer (Cre)	TAAGTCTGAACCCGGTCTGC
Forward primer (control)	CAAATGTTGCTTGTCTGGTG
Reverse primer (control)	GTCAGTCGAGTGCACAGTTT

2.3.5 Agarose gel electrophoresis

The PCR products were analysed by agarose gel electrophoresis. The agarose (Carl Roth, Germany) was boiled in 0.5x TBE buffer (AppliChem, Germany) to form a 1.5% gel. After boiling, ethidium bromide (Sigma-Aldrich, USA) was added (4 µL per 100 mL of agarose suspension). Then, the gel was poured into a gel cast with slot combs and left to cool down and polymerise.

The electrophoresis was performed in chambers filled with 0.5x TBE at 135 V until the PCR products were sufficiently separated. The GeneRuler Ladder Mix (Thermo

Fisher Scientific, USA) was used as a size marker for the separated DNA fragments. The gels were analysed using the GelDoc system (BioRad, USA).

2.4 Transmission electron microscopy

Small 1 mm^3 cubes of freshly dissected mouse heart were cut with sterile razors. The cubes were placed in the fixative solution (2% glutaraldehyde, 2% formaldehyde in 0.1 M cacodylate buffer (pH 7.3)) and incubated for 48 hours at 4 °C in the dark. Afterwards, the samples were submitted to the CECAD Imaging core facility to be further processed for the electron microscopy analysis according to the standard protocols of the facility. The samples were washed in 0.1 M cacodylate buffer (AppliChem, USA) and post-fixed in a solution of 2% osmium tetroxide (Science Services, Germany) in 0.1 M cacodylate buffer at 4 °C for 2 h. The samples were desiccated with the ascending ethanol series (AppliChem, USA), which was followed by a transfer to propylene oxide (Merck, USA) and embedding in epoxy resin (Sigma-Aldrich, USA).

Ultrathin 70 nm sections were sliced with a diamond knife on the EM-UC6 ultramicrotome (Leica Microsystems, Germany) and contrasted with 1.5% uranyl acetate and lead citrate. Images were obtained with the transmission electron miscroscope JEM 2100 Plus (JEOL, Japan), and the OneView 4K camera (Gatan, USA) with DigitalMicrograph software at 80 kV at RT.

2.5 Molecular biology

2.5.1 Transformation of chemically competent *Escherichia coli*

The DH5α strain (Thermo Fisher Scientific, USA) was used for the transformations. 50 µL of the competent cells was thawed on ice for 15 min which was followed by the addition of 1 µL of DNA (1-10 ng). After 30 min of incubation on ice, the cells were exposed to 42 °C for 30 s and then put back on ice for 2 min. Then, 950 µL of S.O.C. medium (Thermo Fisher Scientific, USA) was added, and the cells were incubated at 37 °C for 1 h at 250 rpm. Afterwards, the cells were pelleted at 1300 rpm/1 min and resuspended in 50 µL of LB medium. 10-20 µL was plated on selective LB agar plates and grown overnight at 37 °C. The plates were stored at 4 °C.

2.5.2 Isolation of plasmid DNA

A single colony of bacteria transformed with the desired plasmid DNA was inoculated in 200 mL of a selective LB medium overnight at 37 °C/160 rpm. Afterwards, the plasmid was isolated using the ZymoPURE II Plasmid Maxiprep kit (Zymo Research, USA) according to the manufacturer's instructions.

2.5.3 Isolation of RNA

For total RNA isolation, approximately 25 mg of the frozen heart was homogenized in 1 mL of TRIzol reagent (Invitrogen, USA) using 1.4 mm ceramic beads (Omni International, USA) and Precellys tissue homogenizer (Bertin Technologies, France)

(5000 rpm, 30 s). Afterwards, the samples were incubated at room temperature (RT) for 5 min. Next, 200 µL of chloroform was added and the samples were vigorously mixed. The samples were then centrifuged at 12 000 g/15 min/4 °C, which separated protein, DNA, and RNA. RNA, which was present in the top aqueous layer, was carefully collected and precipitated with 500 µL of isopropanol followed by a 10 min incubation at RT and subsequent centrifugation at 12 000 g/15 min/4 °C. The RNA pellet was washed with 1 mL of ice-cold 75% ethanol by centrifugation at 7 500 g/5 min/4 °C. After a short period of air-drying, the pellet was resuspended in 50 µL of UltraPure water (Gibco, USA) and the RNA was stored in –80 °C.

2.5.4 Quantification of the nucleic acid concentration

To measure the concentration of nucleic acids, NanoDrop 8000 Spectrophotometer was utilised (Thermo Fisher Scientific, USA). It was used to determine the absorbance and to calculate the concentration of the samples. The purity of nucleic acids was estimated by absorbances ratios. 260 nm is the absorbance maximum of nucleic acids, 280 nm is the absorbance maximum of proteins, and 230 nm absorbance signifies a presence of other contaminants (e.g., residual phenol, guanidine, salts…). Pure DNA has the 260/280 ratio ~1.8, whereas pure RNA has the 260/280 ratio ~2. And the 260/230 ratio in the range of 1.8 – 2.2 is accepted as pure for both RNA and DNA.

2.5.5 mRNA quantification with Quantitative PCR (qPCR)

RNA isolated according to the protocol 2.5.3 was further treated with DNase I (New England Biolabs, USA) to digest the residual DNA following this reaction mix:

RNA	10 µg
10x DNase I Reaction Buffer	3 µL
DNase I	1 µL
UltraPure water	Up to 30 µL

This reaction mix was incubated for 10 min at 37 °C and then another 10 min at 75 °C for heat-inactivation of DNase I. Afterwards, the concentration of the samples was adjusted to 200 ng/µL.

Next, copy DNA (cDNA) was synthesized from the digested samples using the High-Capacity Reverse Transcription kit (Applied Biosystems, USA). The reaction mix (total volume 20 µL) was prepared as follows:

RNA (200 ng/µL)	10 µL
10x RT buffer	2 µL
10x Random Primers	2 µL
25x dNTP mix	0.8 µL
MultiScribe Reverse Transcriptase	1 µL

UltraPure water	4.2 µL

The reaction mix was subjected to the following PCR program:

Annealing	25 °C	10 min
Elongation	37 °C	120 min
Denaturation	85 °C	5 s
Hold	4 °C	

The cDNA samples were stored at –20 °C.

2.5.6 Quantitative PCR (qPCR)

The qPCR experiments were performed on 96-well plates. 50 ng of DNA was mixed with the Brilliant III Ultra-Fast SYBR Green qPCR Master Mix kit (Agilent Technologies, USA). The reactions were performed in the QuantStudio 7 Flex Real-Time PCR System (Thermo Fisher Scientific, USA) with the following PCR program:

Denaturation	95 °C	3 min
For 40 cycles:		
Denaturation	95 °C	5 s
Annealing and elongation	60 °C	15 s
Dissociation curve		
Denaturation	95 °C	15 s
Annealing	60 °C	1 min
	95 °C	15 s

The relative gene expression was normalised to the endogenous housekeeping gene *Hprt* and was quantified using the $2^{-\Delta\Delta Ct}$ method.

Table 2.1 | Primer sequences used for mtDNA levels determination

Gene	Forward primer [5'– 3']	Reverse primer [5'– 3']
Hprt	GCCCCAAAATGGTTAAGGTT	TTGCGCTCATCTTAGGCTTT
Lonp1	ATGACCGTCCCGGATGTGT	CCTCCACGATCTTGATAAAGCG
Nppa	ATGGGCTCCTTCTCCATCA	CCTGCTTCCTCAGTCTGCTC
Nppb	GGATCTCCTGAAGGTGCTGT	TTCTTTTGTGAGGCCTTGGT
Pgc1a	TATGGAGTGACATAGAGTGTGCT	CCACTTCAATCCACCCAGAAAG

2.5.7 mtDNA quantification via qPCR

mtDNA levels were determined according to a previously described method (Quiros et al., 2017). The DNA obtained from mouse hearts was quantified by qPCR as

described in section 2.5.6. *16S* and *Nd1* were used as markers of mtDNA levels and were normalized to the nuclear *Hk2* DNA levels. Used primers are listed below.

Table 2.2 | Primer sequences used for mtDNA levels determination

Gene	Forward primer [5'– 3']	Reverse primer [5'– 3']
16S	CCGCAAGGGAAAGATGAAAGAC	TCGTTTGGTTTCGGGGTTTC
Nd1	CTAGCAGAAACAAACCGGGC	CCGGCTGCGTATTCTACGTT
Hk2	GCCAGCCTCTCCTGATTTTAGTGT	GGGAACACAAAAGACCTCTTCTGG

2.5.8 mtDNA quantification via Southern blot

A quarter of a frozen heart was cut and lysed in 400 µL of tissue lysis buffer (0.5 % v/v SDS; 0,1 M NaCl; 50 mM Tris-HCl, pH 8; 2.5 mM EDTA; 0.4 mg/mL Proteinase K) at 900 rpm and 55 °C for 2–12 hours. After lysis, 75 µL of 8 M potassium acetate and 500 µL of chloroform was added. Samples were centrifuged at full speed/4 °C/15 min. Upper aqueous phase was collected, supplemented with 2 volumes of ice-cold 100% ethanol, mixed and centrifuged at full speed/4 °C/15 min. Supernatant was discarded. Pellet was washed with ice-cold 70% ethanol and centrifuged at full speed/4 °C/5 min. Ethanol was completely removed, and DNA was dissolved in 100–200 µL of dH_2O.

10 µg of DNA was digested by a restriction enzyme SacI (NEB, USA) at 37 °C overnight in a following reaction:

DNA	10 µg
SacI	6 µL
CutSmart 10X	20 µL
10% BSA (10 mg/mL)	2 µL
dH_2O	up to 200 µL

To precipitate the DNA, 10 µL of 5 M NaCl was added together with 3 volumes of ice-cold 95% ethanol and the samples were placed in –80 °C for 30 min. Afterwards, the precipitated DNA was pelleted at 14 000 rpm/15 min/4 °C and washed with 70% ethanol with another centrifugation. The pellet was dissolved in 20 µL dH_2O.

The DNA samples were mixed with a 6x Gel Loading Dye (NEB, USA) and were separated in an 0.8% agarose gel supplied with 4% ethidium bromide using the Sub-Cell GT Horizontal Electrophoresis System (BioRad, USA). The electrophoresis was performed overnight at constant 35 V until the DNA reached ¾ of the gel. The progress of the electrophoresis and the final picture used as a loading control were visualised using the GelDoc system (BioRad, USA).

The gel was later soaked in 0.2 M HCl for 10 min. Following a rinse in dH_2O, the gel was soaked in a denaturing solution (1.5M NaCl; 0.5M NaOH) 2x for 20 min. After a rinse in dH_2O, the gel was soaked in a neutralizing solution (1.5M NaCl; 1M Tris-HCl, pH 7.5) 2x for 20 min. After another rinse in dH_2O, the gel and the Amersham Hybond-

N+ nylon membrane (Cytiva, USA) were soaked in 20x SSC (3 mM NaCl; 0.3 mM sodium citrate) for 20 min. The gel was then soaked in 1x SSC for 20 min. Afterwards, an overnight capillary Southern blot with 20x SSC was assembled to transfer the DNA to the membrane. After the transfer, the membrane was soaked in 2x SSC for 2 min with a subsequent air-drying of the membrane. Then it was baked for 1.5 hours at 80 °C.

The membrane was prehybridised for 30 min at 65 °C in 10 mL of Rapid-hyb buffer (Cytiva, USA) in a glass bottle and incubated overnight with a ^{32}P-dCTP labelled pAM1 probe which was prepared with the Random Primers DNA Labelling system (Thermo Fisher Scientific, USA) according to the manufacturer's instructions. After the overnight hybridisation, the membrane was washed in 2x SSC/0.1% w/v SDS for 20 min at RT, which was followed by a wash in 1x SSC/0.1% w/v SDS for 20 min at 65 °C. The membrane was exposed to the Amersham Hyperfilms MP (Cytiva, USA) and the film was developed in an automatic X-ray film processor (Kodak, USA).

2.6 Biochemistry

2.6.1 Protein isolation from cells

Cells were trypsinized, collected and washed with PBS. The cell pellet was lysed with radioimmunoprecipitation assay (RIPA) buffer (50 mM Tris-HCl, pH 7.4; 1% v/v Triton-X; 0,5% w/v sodium deoxycholate; 0,1% w/v SDS; 150 mM NaCl; 2 mM EDTA; 50 mM NaF; 1x protease inhibitor cocktail) and incubated on ice for 30 min with occasional vortexing. Afterwards, the lysate was subjected to 10 cycles of sonication at 30 s intervals at 4 °C with Bioruptor Pico (Diagenode, Belgium). Cell debris was pelleted at 14 000 g/4 °C/15 min. Supernatant was collected and stored at –80 °C.

2.6.2 Protein isolation from tissues

A piece of frozen tissue was cut and placed in organ lysis buffer (50 mM HEPES, 1% v/v Triton X-100, 50 mM NaCl, 0.1 M NaF, 10 mM $Na_3VO_4 \cdot 2H_2O$, 10 mM EDTA, 0.1% v/v SDS, 1x protease inhibitor cocktail, 2 mM PMSF, pH 7.4) and homogenized using 1.4 mm ceramic beads (Omni International, USA) and Precellys tissue homogenizer (Bertin Technologies, France) (5500 rpm, 2x20", pause 30"). Homogenates were centrifuged at full speed/4 °C/45 min, the supernatant was collected and stored at −80 °C.

2.6.3 Isolation of mitochondria

A freshly dissected heart was weighed and placed in ice-cold mitochondria isolation buffer with BSA (MIB+BSA; 100 mM sucrose, 50 mM KCl, 1 mM EDTA, 20 mM TES, 0,2% w/v BSA free from fatty acids) in 50 mL Falcon tube. Prior to homogenization, subtilisin A was added (1 mg protease per 1 g tissue) to the tissue and everything was subsequently transferred to a glass homogenizer tube. The tissue was homogenized with PTFE pestle using Potter S homogenizer (Sartorius AG, Germany) with 20 strokes at 1000 rpm. The homogenate was transferred to a 50 mL

Falcon tube and centrifuged at 8 500 g/4 °C/5 min. Afterwards, supernatant was discarded, the pellet was resuspended in 25 mL MIB+BSA and centrifuged at 800 g/4 °C/10 min. The supernatant was collected to a new 50mL tube and kept on ice. The pellet was resuspended in another 25 mL MIB+BSA and re-centrifuged at 800 g/4 °C/10 min. The supernatants were combined and centrifuged at 8 500 g/4 °C/5 min. The mitochondrial pellet was resuspended in 600–800 µL MIB without BSA, transferred to a 1,5 mL tube and centrifuged at 8 500 g/4 °C/5 min. The supernatant was discarded, and the pellet was resuspended in 50–200 µL MIB without BSA, snap-frozen in liquid nitrogen and stored at −80 °C.

2.6.4 SDS polyacrylamide gel electrophoresis (SDS-PAGE) and western blot

Concentration of the protein samples was quantified using the Bradford reagent (Sigma-Aldrich, USA) according to the manufacturer's instructions. The samples were subsequently mixed with the Laemmli buffer (50 mM Tris-HCl, pH 6.8; 2% w/v SDS; 10% v/v glycerol; 1% β-mercaptoethanol; 12.5 mM EDTA; 0.02% Bromophenol Blue) and denatured at 95 °C for 5 min.

SDS-PAGE was performed using the Mini-PROTEAN Tetra Cell system (BioRad, USA). Samples were loaded on a 8–12% polyacrylamide gel (stacking gel: 5% acrylamide/bis-acrylamide (29:1), 12.5 mM Tris-HCl, 0.1% w/v SDS, 0.25% APS, 0.25% TEMED, pH 6.8; separating gel: 8–12% acrylamide/bis-acrylamide (29:1), 37.5 mM Tris-HCl, 0.1% w/v SDS, 0.1% APS, 0.1% TEMED, pH 8.8; the percentage was dependent on the desired protein size separation) in a chamber containing a running buffer (25 mM Tris-HCl, 250 mM glycine, 0.1% w/v SDS, pH 8.3). PageRuler Prestained Protein Ladder (Thermo Fisher Scientific, USA) was used as a marker for protein size.

First, the electrophoresis was performed at a constant 75 V for 15 min to allow the protein to enter the stacking gel. Afterwards, the constant voltage was raised to 150 V and the electrophoresis continued until the loading dye reached the end of the gel.

For western blotting, the Criterion Blotter (BioRad, USA) was utilised according to the manufacturer's instructions. The Amersham Protran 0.45 nitrocellulose membrane (Cytiva, USA) was used for the transfer of proteins. The transfer of proteins was performed at constant 400 mA/4 °C/2 h in a transfer buffer (30 mM Tris-HCl, 240 mM glycine, 0.037% SDS, 20% methanol). Afterwards, the membrane was washed shortly in dH_2O and stained by Ponceau S solution to assess the quality of the loading and the transfer of proteins. The Ponceau S staining was later removed by a wash in PBST (1x PBS, 0.1% w/v Tween-20) and the membrane was blocked in 5% milk-PBST. Primary and secondary antibodies were prepared according to the manufacturers. The membranes were incubated in the primary antibodies overnight at 4 °C, which was followed by 3 rounds of a wash in PBST for 5 min. Afterwards, an incubation in the HRP-conjugated secondary antibodies was performed at RT for 1 hour, which was followed again by 3x washing in PBST for 5 min. To activate the chemiluminescence of the secondary antibodies, Pierce ECL Western Blotting substrate (Thermo Fisher

Scientific, USA) was applied to the membrane according to the manufacturer's instructions. Afterwards, the membranes were exposed to Super RX-N films (Fujifilm, Japan) and the films were developed in an automatic X-ray film processor (Kodak, USA).

Table 2.3 | Primary antibodies used for the western blot

Protein	Manufacturer	Catalogue number
ATP5A1	abcam	ab14748
CNX	Calbiochem	208880
COX1	Molecular Probes	459600
COX4	Molecular Probes	A21348
COX7C	Sigma-Aldrich	SAB4301750
EFG1	abcam	ab6107496
EIF2A	Cell Signaling Tech. (CST)	5324
ERAL1	Proteintech	29465-1-AP
HSC70	Santa Cruz	sc-7298
LONP1	Proteintech	15440-1-AP
LRPPRC	NG Larsson group	(Harmel et al., 2013)
MRPL12	abcam	ab58334
MRPL37	Sigma-Aldrich	HPA025826
MRPS30	Proteintech	18441-1-AP
MRPS35	Proteintech	16457-1-AP
MTHFD2	abcam	ab56772
NDUFA9	Molecular Probes	459100
NDUFB11	abcam	ab183716
NDUFS1	Proteintech	12444-1-AP
NDUFS3	MitoSciences	MS112
OXPHOS cocktail	abcam	ab110413
p-EIF2A	abcam	ab32157
PNPT1	Proteintech	14487-1-AP
POLG	abcam	ab128899
POLRMT	NG Larsson group	(Harmel et al., 2013)
SDHA	MitoSciences	MS204
SHMT2	abcam	ab224428
SSBP1	Atlas Antibody	HPA002866
TEFM	NG Larsson group	(Jiang et al., 2019)
TFAM	abcam	ab131607
TFB2M	abnova	64216-A01
TWNK	NG Larsson group	(Milenkovic et al., 2013)
UQCRC1	Molecular Probes	459140
VDAC	CST	4661

Table 2.4 | Secondary antibodies used for the western blot

Antibody	Manufacturer	Catalogue number
ECL anti-mouse IgG-peroxidase	Sigma-Aldrich	A4416
ECL anti-rabbit IgG-peroxidase	Sigma-Aldrich	A6154

2.6.5 Blue native PAGE (BN-PAGE) and *in gel* activity

To prepare samples for BN-PAGE, the NativePAGE Sample Prep Kit (Invitrogen, USA) was used according to the manufacturer. 10 – 15 µg freshly isolated or frozen mitochondria were lysed in 4% digitonin on ice for 15 min. Afterwards, the samples were centrifuged at 13 000 rpm/30 min/4 °C to pellet the non-lysed debris. The supernatant was loaded on a 4 to 16% Bis-Tris gradient gel. The electrophoresis was conducted in XCell SureLock Mini-Cell Electrophoresis system (Life Technologies, USA) according to the manufacturer. The proteins were transferred to the Amersham Hybond P 0.45 PVDF membrane (Cytiva, USA) following the western blot protocol in the section 2.6.4.

For the *in gel* activity assay for CI, the BN-PAGE gel was incubated in the CI activity buffer (0.1 mg/mL NADH; 2.5 mg/mL nitrotetrazolium blue; 5 mM Tris-HCl, pH 7.4) for 1 hour at 37 °C.

For the CIV *in gel* activity, the gel was incubated in the CIV activity buffer (1 mg/mL cytochrome c; 1 mg/mL 3,3'-diaminobenzidine; 0.4 mg/mL catalase; 50 mM Tris-HCl, pH 7.4) overnight at 37 °C.

The gels were destained in a destaining solution (50% v/v methanol; 10% v/v acetic acid) for 2 h at RT and then rehydrated in dH_2O.

The BN-PAGE and *in gel* activities were performed together with Lea Isermann and Milica Popovic.

2.6.6 Sucrose density gradient

Sucrose gradients were prepared in 13.2mL Open-Top Thinwall Ultra-Clear Tubes (Beckman Coulter, USA) by mixing equal volumes of 10% and 30% sucrose gradient buffer (10% or 30% w/v sucrose; 100 mM KCl; 20 mM $MgCl_2 \cdot 6$ H2O; 10 mM Tris-HCl, pH 7.5; 1x protease inhibitor cocktail) using the Gradient Master (BioComp Instruments, Canada) and were kept at 4 °C. Two adult mouse hearts per condition were collected in mitochondria isolation buffer (320 mM sucrose; 10 mM Tris-HCl, pH 7.5) and homogenized with 20 strokes at 1200 rpm. Homogenate was centrifuged at 800 g/4 °C/10 min. Supernatant with mitochondria was collected, pellet was resuspended in mitochondria isolation buffer and re-centrifuged at 800 g/4 °C/10 min. Both supernatants were combined and centrifuged at 10 000 g/4 °C/10 min to pellet mitochondria. Supernatants were discarded and pellets resuspended in 400 µL

mitochondria isolation buffer. The protein concentration was determined with the Bradford reagent (Sigma-Aldrich) according to the manufacturer.

Two milligrams of mitochondria were pelleted at 10 000 g/4 °C/5 min and lysed in 200 µL lysis buffer (260 mM sucrose; 100 mM KCl; 20 mM $MgCl_2 \cdot 6\ H_2O$; 10 mM Tris-HCl, pH 7.5; 1% v/v Triton-X) on ice for 20 min with occasional vortexing. The lysates were centrifuged at 9 200 g/4 °C/45 min. The supernatants were transferred to a new tube and 165 µL of the supernatant was loaded on top of the gradient. The rest of the supernatant was kept as input and stored in –80 °C. The gradients with loaded lysate were subjected to an overnight ultracentrifugation at 71 000 g/4 °C/15 h. The following day, the gradients were fractionated by collecting 750 µL for each fraction. The fractions were subjected to SDS-PAGE analysis or stored in –80 °C.

The sucrose density gradient was performed together with Dr. Karolina Szczepanowska.

2.6.7 *In organello* transcription

Fresh mitochondria were isolated from heart tissue according to the protocol in the section 2.6.3, and protein concentration was measured with the Bradford reagent (Sigma-Aldrich, USA) according to the manufacturer. One milligram of mitochondria was pelleted by centrifugation at 9000 g/4 °C/5 min. The pellet was resuspended with 500 µL incubation buffer (25 mM sucrose; 75 mM sorbitol; 100 mM KCl; 10 mM K_2HPO_4; 50 µM EDTA; 5 mM $MgCl_2 \cdot 6\ H_2O$; 10 mM Tris-HCl, pH 7.4; 1 mM ADP; 10 mM glutamate; 2.5 mM malate; 1 mg/mL fatty acid free BSA) and centrifuged at 9000 g/4 °C/5 min. The pellet was resuspended again with 500 µL incubation buffer, 40 µCi ^{32}P-UTP was added, and mitochondria were incubated at 37 °C on a rotary shaker (20 rpm) for 1 h. Mitochondria were subsequently centrifuged at 13 000 g/4 °C/2 min, and the supernatant was discarded. The pellet was washed 2x in 500 µL washing buffer (10% glycerol; 10 mM Tris-HCl, pH 6.8; 0.15 mM $MgCl_2 \cdot 6\ H_2O$). The pellet was resuspended in 1 mL Trizol and RNA was isolated according to the protocol in the section 2.5.3.

The RNA Sample Loading buffer (Sigma-Aldrich, USA) was added to the isolated RNA (1/2 to 1/5 of the sample volume). The RNA was separated using an RNase-free agarose gel (1.2% agarose LE; 1x MOPS; 18% formaldehyde). The electrophoresis was carried out at constant 90 V in the Sub-Cell GT Horizontal Electrophoresis System (BioRad, USA), the tank was filled with 1x MOPS buffer. The electrophoresis was stopped when the loading dye reached ¾ of the gel. The gel was subsequently washed 3x for 15 min in a nuclease-free water. The RNA was transferred to the Amersham Hybond-N+ nylon membrane (Cytiva, USA) with a capillary northern blot system soaked in 20x SSC (3 mM NaCl; 0.3 mM sodium citrate). After the overnight transfer, the membrane was baked at 80 °C for 1.5 hours. The membrane was then exposed to the Amersham Hyperfilms MP (Cytiva, USA) to detect the radioactive signal and the films were developed in an automatic X-ray film processor (Kodak, USA).

2.6.8 *In organello* translation

Fresh mitochondria were isolated according to the protocol in the section 2.6.3 and the protein concentration was determined with the Bradford reagent (Sigma-Aldrich, USA) according to the manufacturer. 1 mg of mitochondria per condition was pelleted at 8500 g/4 °C/2 min. The pellet was resuspended in 1 mL translation buffer + ^{35}S-methionine [1x translation mix, pH 7.4 (100 mM mannitol; 10 mM sodium succinate; 80 mM KCl; 5 mM $MgCl_2$; 1 mM KH_2PO_4, pH 7.4; 25 mM HEPES, pH 7.4); 60 µg/mL amino acids (Ala, Arg, Asp, Asn, Cys, Glu, Gln, Gly, His, Ile, Leu, Lys, Phe, Pro, Ser, Thr, Trp, Tyr, Val); 5 mM ATP; 20 µM GTP; 6 mM creatine phosphate; 60 µg/mL creatine kinase; 7 µL ^{35}S-methionine] and incubated at 37 °C for 1 hour on a rotating wheel. Mitochondria were pelleted at 8500 g/2 min and resuspended with 1 mL translation buffer without ^{35}S-methionine. Half of the sample was re-pelleted, resuspended in 50 µL SDS-PAGE loading buffer (50 mM Tris-HCl, pH 6.8; 2% w/v SDS; 10% v/v glycerol; 1% v/v β-mercaptoethanol; 12.5 mM EDTA; 0.02% bromophenol blue), lysed for 30 min at room temperature and kept as “pulse” fraction. The rest was re-pelleted, resuspended in 500 µL translation buffer with non-radioactive methionine and incubated for 3 hours at 37 °C on a rotating wheel. Subsequently, the sample was pelleted, resuspended in 50 µL SDS-PAGE loading buffer, lysed for 30 min at room temperature and kept as “chase” fraction.

The proteins from pulse and chase fractions were separated using SDS-PAGE – 10 µL of the sample was loaded in a 15% polyacrylamide gel placed in SE600X Chroma Deluxe Dual Cooled Vertical Protein Electrophoresis Unit (Hoefer Inc, USA) filled with a running buffer (25mM Tris-HCl, 250mM Glycine, 0.1% w/v SDS, pH 8.3) and the electrophoresis was performed at constant 75 V overnight. The gel was stained with InstantBlue Coomassie Protein Stain (Thermo Fisher Scientific) for 30 min and placed in the Model 583 Gel Dryer (Bio-Rad Laboratories, Hercules, USA) for 2 hours at 80 °C.

The dried gel was exposed to the Amersham Hyperfilms MP (Cytiva, USA) to detect the radioactivity and the films were developed in an automatic X-ray film processor (Kodak, USA).

The *in organello* translation assay was performed in collaboration with Dr. Alexandra Kukat.

2.6.9 High resolution respirometry

Fresh mouse hearts were dissected and transferred to the ice-cold isolation buffer (225 mM mannitol; 75 mM sucrose; 1 mM EGTA, pH 7.4; 2.5 mg/mL BSA fatty acid free). The tissue was then cut into small pieces and transferred to a 5 mL glass potter. 3 mL of the isolation buffer was added, and the tissue was homogenized at 1000 rpm while being passed 8 to 10 times. The homogenate was transferred to a 50 mL Falcon tube and ~20 mL of the isolation buffer was added. The homogenate was centrifuged at 800 g/10 min/4 °C and the supernatant was transferred to a new Falcon tube. The pellet was resuspended in 25 mL of the isolation buffer and the centrifugation step was

repeated. The supernatants were collected, combined, and centrifuged at 10 000 g/10 min/4 °C to pellet mitochondria. The mitochondria were resuspended in 600 µL of the isolation buffer without BSA and centrifuged again at 10 000 g/10 min/4 °C. The supernatant was discarded, and the mitochondria resuspended in 100 – 200 µL of the isolation buffer without BSA and kept on ice. The protein concentration of the mitochondrial pellet was determined using the Bradford reagent (Sigma-Aldrich, USA) according to the manufacturer and 50 µg was used for the respiration measurements.

The respiration measurement was performed using the high resolution respirometry OROBOROS Oxygraph-2k (Oroboros Instruments, Austria). The chambers were filled with the MiR05 kit respiration medium (Oroboros Instruments, Austria). The measurement was commenced by the addition of mitochondria into the chambers followed by the addition of pyruvate (5 mM) and malate (2 mM) to observe the respiration fuelled by the NADH-linked substrates (CI-dependent respiration) without adenylates. Afterwards, ADP (1 mM) was added to observe the CI-dependent respiration with the activated OXPHOS. Glutamate (10 mM) and succinate (10 mM) were added to saturate the citric acid cycle and to observe the capacity of a fully active OXPHOS. The system was further titrated with FCCP (0.25 µM with every 0.5 µL titrated) to uncouple OXPHOS and to stimulate the maximum ETC activity. Addition of rotenone (0.5 µM) inhibited the CI-dependent respiration and addition of antimycin A (2.5 µM) completely inhibited the respiration and allowed to read the residual respiration (respiration background). To stimulate and observe the function of CIV, TMPD (0.5 mM) was added to donate the electrons to CIV, and ascorbate (2 mM) was added in parallel to keep TMPD in the reduced state and prevent its uncontrollable autooxidation. CIV was inhibited by adding of sodium azide (100 mM). The CIV activity was determined by subtracting the respiration after inhibiting CIV from the respiration before inhibiting CIV, because of the autooxidation of TMPD, which is then read by the machine as respiration.

2.7 Omics analysis

2.7.1.1 Label free quantification of the heart proteome

A small piece of the frozen heart was ground to powder in liquid nitrogen and the powder was resuspended in 100 µL of the urea lysis buffer (8 M Urea; 50 mM triethylammonium bicarbonate (TEAB); 1x protease inhibitor). The sample was sonicated with the Bioruptor Pico sonication device (Diagenode, Belgium) – cycle 30/30 s for 10 min. Afterwards, the sample was centrifuged at 20 000 g/15 min/4° C to pellet and discard the debris. The protein concentration of the samples was determined using the Bradford reagent (Sigma-Aldrich, USA) according to the manufacturer and 50 µg of the sample was transferred to a new tube. The sample was treated with dithiothreitol (DTT, final conc. 5 mM) and incubated at 25 °C for 1 h. Then chloroacetamide was added (CAA, final conc. 40 mM) and incubated for 30 min in the dark. Afterwards, lysyl endopeptidase (Lys-C) was added at the protease:sample

protein ratio 1:75 and the incubation lasted 4 h at 25 °C. The sample was diluted with 50 mM TEAB buffer to reach the final concentration of 2 M Urea. Then trypsin was added in the 1:75 ratio and the trypsinisation occurred overnight at 25 °C.

The following day, the sample was acidified with formic acid (final conc. 1%) to stop the digestion. The lysates were loaded on SDB RP StageTips supplied by the CECAD proteomics core facility and submitted to the facility for the mass spectrometry analysis according to the standard procedures of the facility. The raw data were analysed with the MaxQuant proteomics software.

2.7.1.2 Label free quantification of the insoluble proteins in cardiac mitochondria

To analyse the insoluble proteins in mitochondria, 300 µg of freshly isolated cardiac mitochondria was pelleted at 8 500 g/10 min/4 °C and lysed in 100 µL of lysis buffer (0.5% Triton X-100; 30 mM Tris-HCl, pH 7.4; 200 mM KCl; 5 mM EDTA; 0.5 mM PMSF; 1x protease inhibitor cocktail; pH 7.4) by shaking at 750 rpm/15 min/4 °C. The lysates were centrifuged at 4000 g/10 min/4 °C to sediment the insoluble material and debris. The supernatant was collected and divided into two 50 µL aliquots. One of these aliquots was saved at the total or input fraction. The second aliquot was centrifuged at 125 000 g/60 min/4 °C to pellet the insoluble proteins – the insoluble fraction. The supernatant was saved as the soluble fraction.

All the samples were precipitated in ice-cold acetone which was added in 4x the sample volume. Then the samples were incubated for 15 min at –80 °C, which was followed by 90 min of incubation at –20 °C. The supernatants were discarded. Another 500 µL of ice-cold acetone was added to the protein pellet and the samples were centrifuged at 16 000 g/15 min/4 °C. The supernatant was discarded and the wash in 500 µL of acetone was repeated. The pellet was air-dried and resuspended in 100 µL of 8 M Urea buffer. The samples were sonicated with Bioruptor Pico sonication device (Diagenode, Belgium) – cycle 30/30 s for 10 min. Afterwards, the samples were subjected to an incubation at 37 °C for 40 min and the insoluble fraction was subjected to another sonication in Bioruptor to aid the dissolution of the sample. All the samples were centrifuged at 20 000 g/15 min/4 °C to pellet anything that did not dissolve and was therefore unsuitable for the mass spectrometry analysis.

Only the total and insoluble fraction were further processed for the proteomic analysis. The samples were further supplied with SP3 buffer (5% w/v SDS in 1x PBS) and reduced with DTT (final conc. 5 mM) at 55 °C for 30 min. Afterwards, CAA was added (final conc. 40 mM) and incubated at RT in the dark. Then the samples were centrifuged at 20 000 g/15 min/4 °C. 10 µg of protein was submitted to the CECAD proteomics core facility for the data-independent acquisition mass spectrometry analysis according to the standard procedures of the facility. The raw data were processed and analysed with the MaxQuant software.

2.7.1.3 RNA sequencing (RNAseq)

A maximum of 25 mg of frozen hearts from 8-week-old male mice were used for the RNA isolation for RNAseq. RNA was isolated using the miRNeasy Mini kit

(QIAGEN, Germany) and the RNase-Free DNase Set (QIAGEN, Germany) according to the manufacturer's instructions. The purified samples were submitted to the Cologne Center for Genomics and were validated by the 4150 TapeStation System (Agilent, USA). The facility used the TruSeq Total RNA Ribo-Zero prep kit (Illumina, USA) for the preparation of the libraries and the NovaSeq 6000 (Illumina, USA) for the sequencing. The data obtained by RNAseq were analysed in the collaboration with the research group of Prof. Aleksandra Filipovska from the Harry Perkins Institute for Medical Research, Perth, Australia.

2.8 Image processing and data analyses

Western blot films were digitalized with the V800 transparency scanner (Epson, Japan) at 800 dpi 16Bit colour depth. Fiji (Schindelin et al., 2012) was used for densitometric analyses. Graphpad Prism 9 was used for generating graphs and for statistical analyses (Student's t-tests). Adobe Illustrator was used for cropping scanned films and generating figures and figure arrangements. Instant Clue (Nolte et al., 2018) was used to generate hierarchical clusterings, heatmap illustrations, and volcano plots.

3 Results

3.1 Generation of the mouse model

The initial study of LONP1 deficiency in mice reported embryonic lethality at day 8.5 days post coitum (dpc) in homozygous deletion of *Lonp1*, while embryos heterozygous for *Lonp1* were viable and developed normally (Quiros et al., 2014). This implies that LONP1 is essential for mammalian embryonic development. To confirm this finding, a mouse strain *C57BL/6N-Lonp1*$^{tm1a(EUCOMM)Hmgu}$*/Ieg* with a knockout-first allele tm1a (**Error! Reference source not found.** A) was used to generate a mouse model with a whole-body depletion for *Lonp1* (*Lonp1*$^{tm1a/tm1a}$). The genotype was confirmed with PCR (**Error! Reference source not found.** B). As expected, this mating did not produce any *Lonp1*$^{tm1a/tm1a}$ mice at the time of weaning. As mentioned before, the whole-body depletion of LONP1 led to the embryonic death after embryonic day 8.5, or E8.5 (Quiros et al., 2014). Next, we isolated and analysed embryos at 7.5

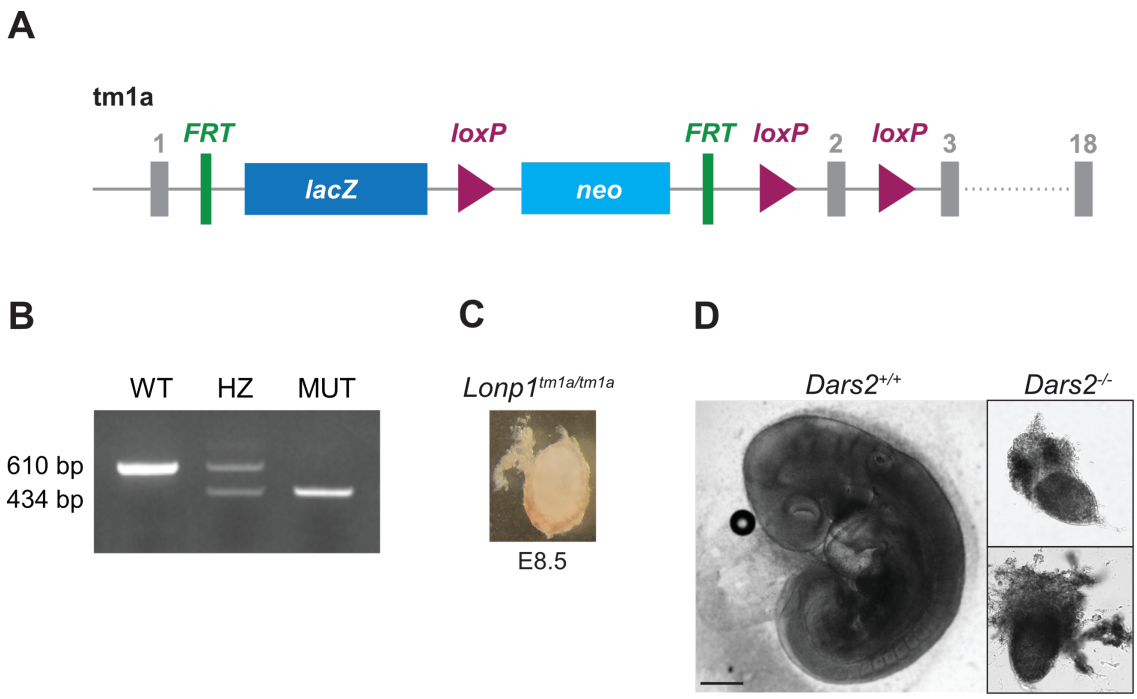


Figure 3.1 | LONP1 deficiency causes embryonic lethality.

(A) A scheme of the knockout-first allele. An IRES:lacZ trapping cassette and a floxed promoter-driven neo cassette were inserted upstream to a critical exon, disrupting the expression of the gene of interest. (B) Genotyping agarose gel electrophoresis of *Lonp1*$^{+/+}$ – WT, *Lonp1*$^{tm1a/+}$ – HZ and *Lonp1*$^{tm1a/tm1a}$ – MUT. (C) A null *Lonp1* embryo in arrested development. (D) A comparable phenotype in a mouse model for DARS2 depletion (Dogan et al., 2014). Depicted embryos are at E8.5, *Dars2*$^{-/-}$ embryos are arrested at the stage of an egg cylinder.

– 8.5 dpc.

Embryos at 7.5 dpc form half-turned embryos. Using a stereomicroscope, there were no visible differences in the different genetic backgrounds at this age. At E8–

E8.5, as the early organogenesis begins, the head and the heart start to form and the embryo grows. *Lonp1*$^{+/+}$ (n = 6) and *Lonp1*$^{tm1a/+}$ (n = 20) embryos showed normal development and displayed no visible phenotype while *Lonp1*$^{tm1a/tm1a}$ mice (n = 12) did not advance from the egg cylinder stage – their development was arrested (**Error! Reference source not found.** C). Thus, the essential role of LONP1 in early embryonic development was confirmed. This phenomenon was reported also for other mouse models with depletion of essential proteins involved in mtDNA gene expression and maintenance – e.g. DARS2 (**Error! Reference source not found.** D, (Dogan et

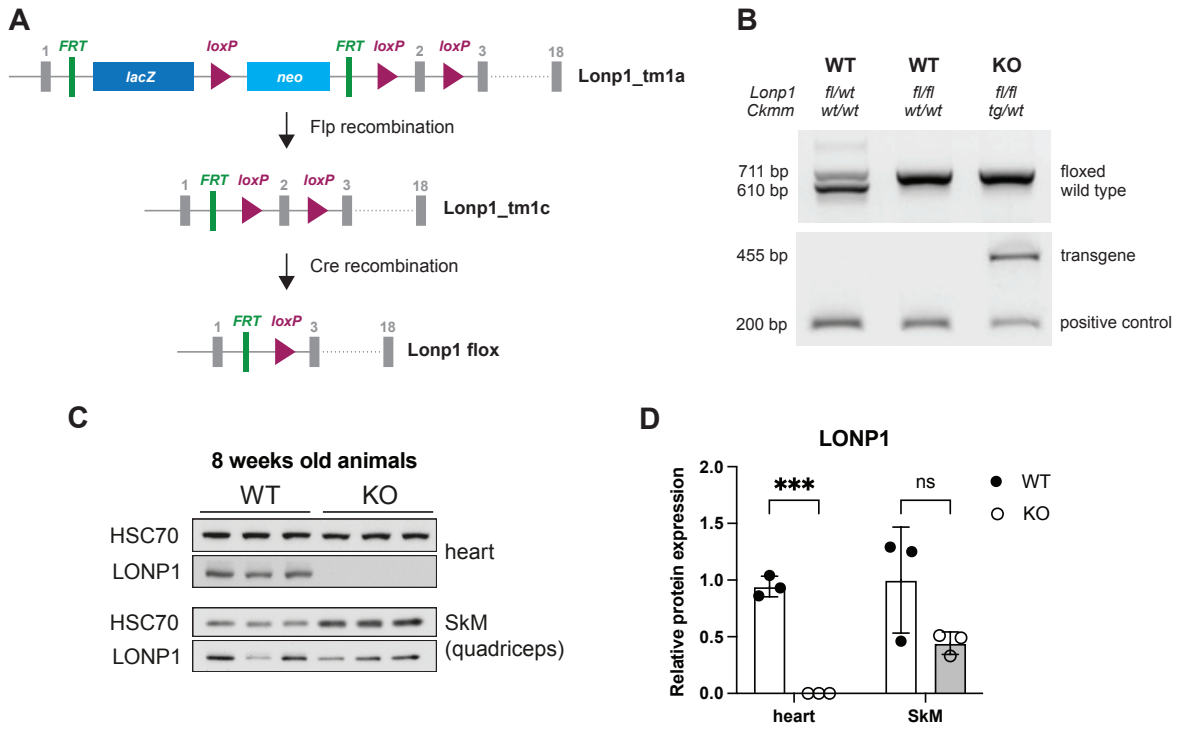


Figure 3.2 | LONP1 is not expressed in the KO heart

(A) A scheme of the generation of KO mice. (B) Genotyping agarose gel electrophoresis. (C) and (D) Immunoblot of LONP1 expression in the whole heart/quadriceps lysate (n = 3 per condition).
***$p < 0.001$, ns = no statistical difference between WT and KO. Values are means ± SD.

al., 2014), TWNK (Milenkovic et al., 2013), TFAM (Larsson et al., 1998), and POLRMT (Kühl et al., 2016).

The mouse strain *C57BL/6N-Lonp1*$^{tm1a(EUCOMM)Hmgu}$*/Ieg* was further used for generating a mouse model for a tissue specific LONP1 deficiency in the heart and the skeletal muscle using a Ckmm-cre promoter (summarized in Figure **3.2** A). The expression of the Cre recombinase is driven by the Ckmm-cre promoter. The promoter becomes fully active after E13 (Li et al., 2000).

The genotype was verified with PCR (Figure **3.2** B) shortly after weaning. *Lonp1*$^{fl/fl}$; *CkmmCre*$^{tg/wt}$ genotype was named LONP1 KO. The loss of LONP1 was tested with western blot at 8 weeks of age (Figure **3.2** C, D). The depletion of LONP1 was

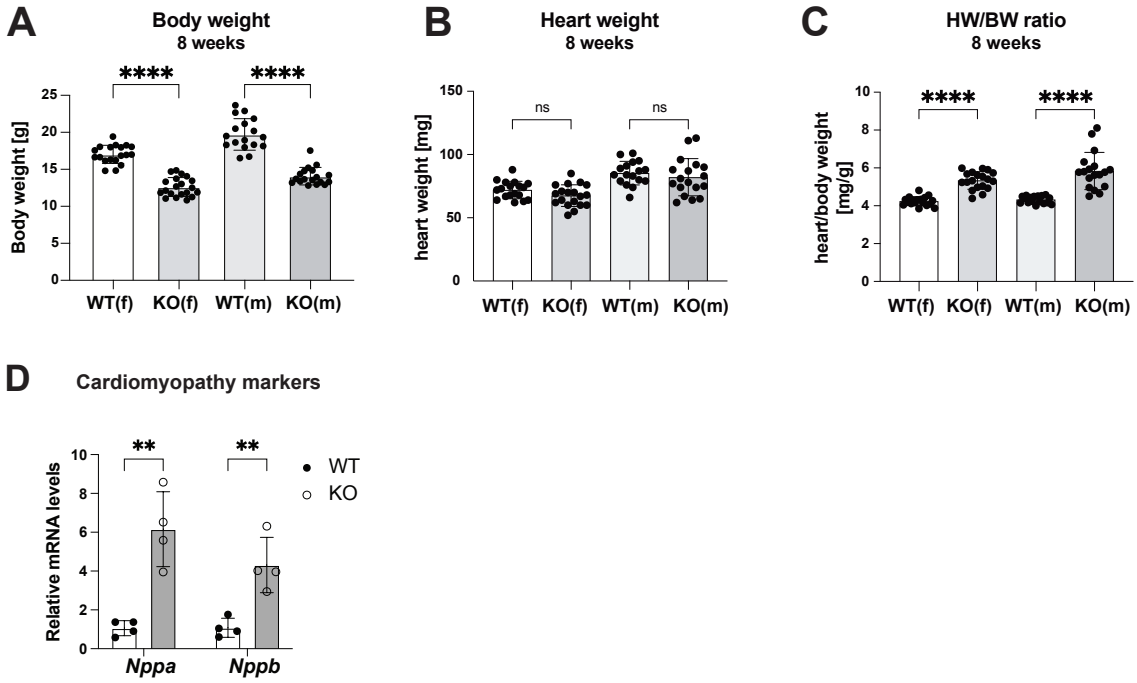


Figure 3.3 | General phenotypical description of the mouse model at 8 weeks of age

(A) The body weight in grams, f – female, m – male; n = 17–20. (B) The heart weight in milligrams; n = 17–19. (C) The heart weight to body weight ratio; n = 17–19. (D) A qPCR analysis of *Nppa* and *Nppb* – the markers for heart failure, normalized to *Hprt*; n = 4.
***p* < 0.01, *****p* < 0.0001, ns = no statistical difference between WT and KO. Values are means ± SD.

confirmed in the heart. However, in the skeletal muscle (quadriceps) LONP1 was still present although its expression was decreased. One of the possible explanations for this observation could be low mitochondrial protein turnover in the skeletal muscle, hence LONP1 could be retained for a longer period, as previously observed when TFAM was depleted (Wang et al., 1999).

Initially, we analysed the mice at 8 weeks of age. LONP1 KO mice were significantly smaller (Figure **3.3** A). Despite cardiomyopathy markers were highly upregulated (Figure **3.3** D), the heart weight in LONP1 KO remained comparable to LONP1 WT mice (Figure **3.3** B). The heart weight to body weight (HW/BW) ratio is typically higher in the mice lacking the components of mitochondrial gene expression due to the severely dilated and enlarged heart. Surprisingly, in the LONP1 KO mice, it is the smaller body weight which increases the ratio (Figure **3.3** C). Phenotypically, LONP1 KO mice did not show any signs of suffering at this age.

As the phenotype was milder than expected the survival rate of LONP1 KO was reassessed, and the mice were followed and observed until their condition significantly worsened. At the point when they had to be humanely terminated, the mice exhibited a sudden drop in their weight, and they developed a prominent kyphosis (Figure **3.4** A).

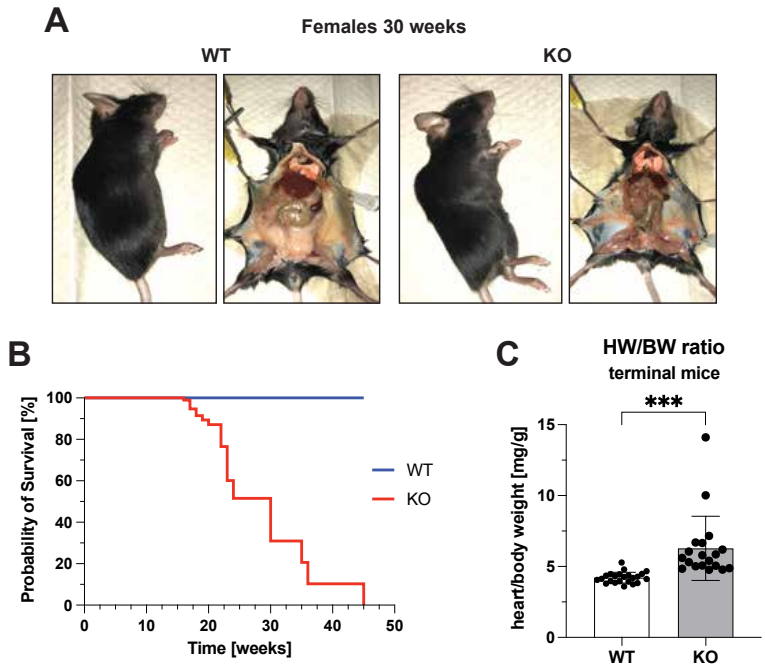


Figure 3.4 | The KO mice significantly deteriorate after 22 weeks of age.

(A) A comparison of a terminal KO mouse with a WT. (B) A Kaplan–Meier analysis of survival, median = 30 weeks (WT – n = 191; KO – n = 184). (C) The heart weight to body weight ratio of the WT and the terminal KO mice; n = 19–23.
***$p < 0.001$, ns = no statistical difference between WT and KO. Values are means ± SD.

Upon dissection, we observed a notable loss of the white adipose tissue in their abdomen (Figure **3.4** A). The humane endpoint differed between the mice – the range spanned from 16 weeks of age to 45 weeks of age with majority of the KOs being sacrificed at 22–23 weeks of age (n = 8) (Figure **3.4** B). The HW/BW ratio of the terminal animals remained increased although it was greatly skewed by two atypically enlarged hearts (Figure **3.4** C).

To describe how the dysfunction progresses with age, a second timepoint for the analysis was set at 20 weeks of age, before the animals deteriorate. Apart from the smaller body weight (Figure **3.5** A), the old KO mice displayed also a significantly smaller heart (Figure **3.5** B). The HW/BW ratio remained increased (Figure **3.5** C).

The heart mitochondrial ultrastructure was analysed with transmission electron microscopy (TEM) at both 8 and 20 weeks of age (Figure 3.6). LONP1 absence did not seem to have a profound effect on mitochondrial morphology as no excessively fused or fragmented mitochondria were observed.

The most notable difference between WT and KO mitochondria was a presence of round electron dense occlusions found inside of the KO mitochondria. They vary in size (~0.1 μm – 1 μm in diameter) and number. Although the occlusions were present only in a small portion of mitochondria, some of the organelles harboured even tens of these particles. Given that LONP1 is an essential matrix protease, these occlusions

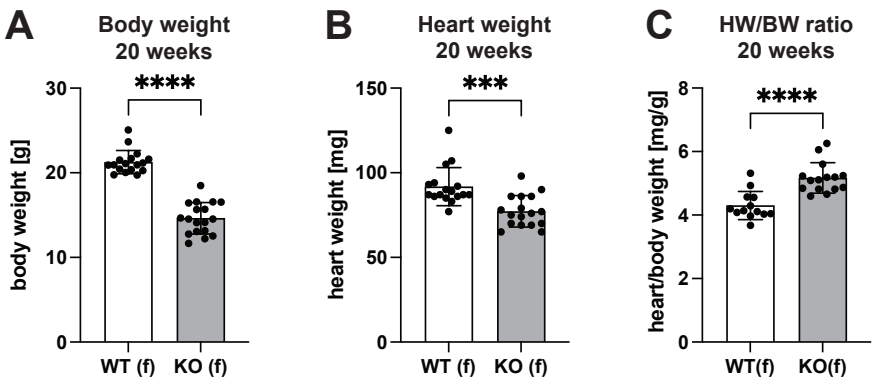


Figure 3.5 | General phenotypical description of the mouse model at 20 weeks of age

A) The body weight in grams, f – female; n = 17–18. (B) The heart weight in milligrams; n = 17. (C) The heart weight to body weight ratio; n = 17.
***p < 0.001, ****p < 0.0001, ns = no statistical difference between WT and KO. Values are means ± SD.

could be accumulated misfolded proteins and/or specific substrates of LONP1 which are not being degraded by another protease.

The consequences of the loss of LONP1 are not as detrimental as it was previously described for other models with mitochondrial dysfunction. Besides the aforementioned heart and skeletal muscle specific depletion of genes involved in mtDNA expression and/or maintenance, it is also the disruption of essential OXPHOS subunits and assembly factors that leads to a serious phenotype (e.g. COX10 (Ahola et al., 2022), NDUFAB1 (Hou et al., 2019), COX7C and SDHA (unpublished work from our group). These mice suffer from dilated cardiomyopathy, have increased heart to body weight ratio, and die latest at 7 weeks of age.

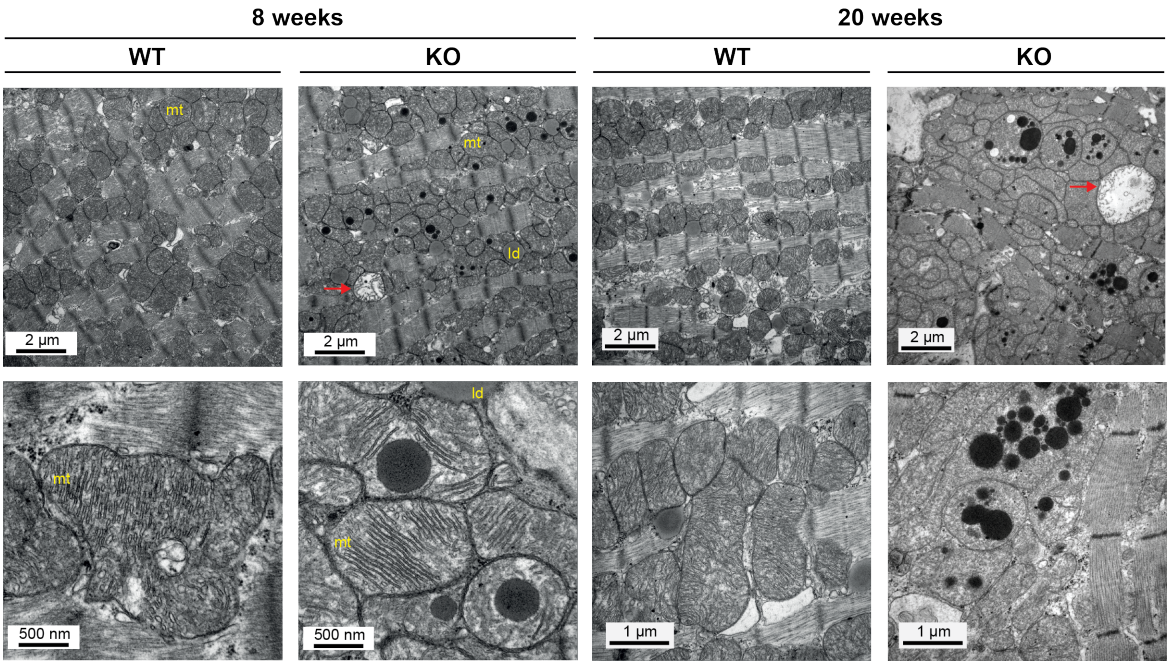


Figure 3.6 | The LONP1 KO mitochondria accumulate electron dense particles

Transmission electron microscopy images (TEM) of 8- and 20-weeks old mitochondria; mt (yellow) – mitochondrion, ld (yellow) – lipid droplet, red arrow – damaged mitochondrion.

3.2 LONP1 deficiency causes a profound OXPHOS dysfunction

Next, the state of OXPHOS in LONP1 KO was examined. By 8 weeks of age, the depletion of LONP1 already caused a prominent decrease of individual subunits in the complexes I (CI) and IV (CIV) (Figure **3.7**). The decline in the protein levels also explains the lower *in gel* activity of CI and CIV (Figure **3.7** G). Remarkably, a similar level of decrease in CI and CIV subunits was observed also at 20 weeks of age and in terminal mice (Figure **3.7** D–F).

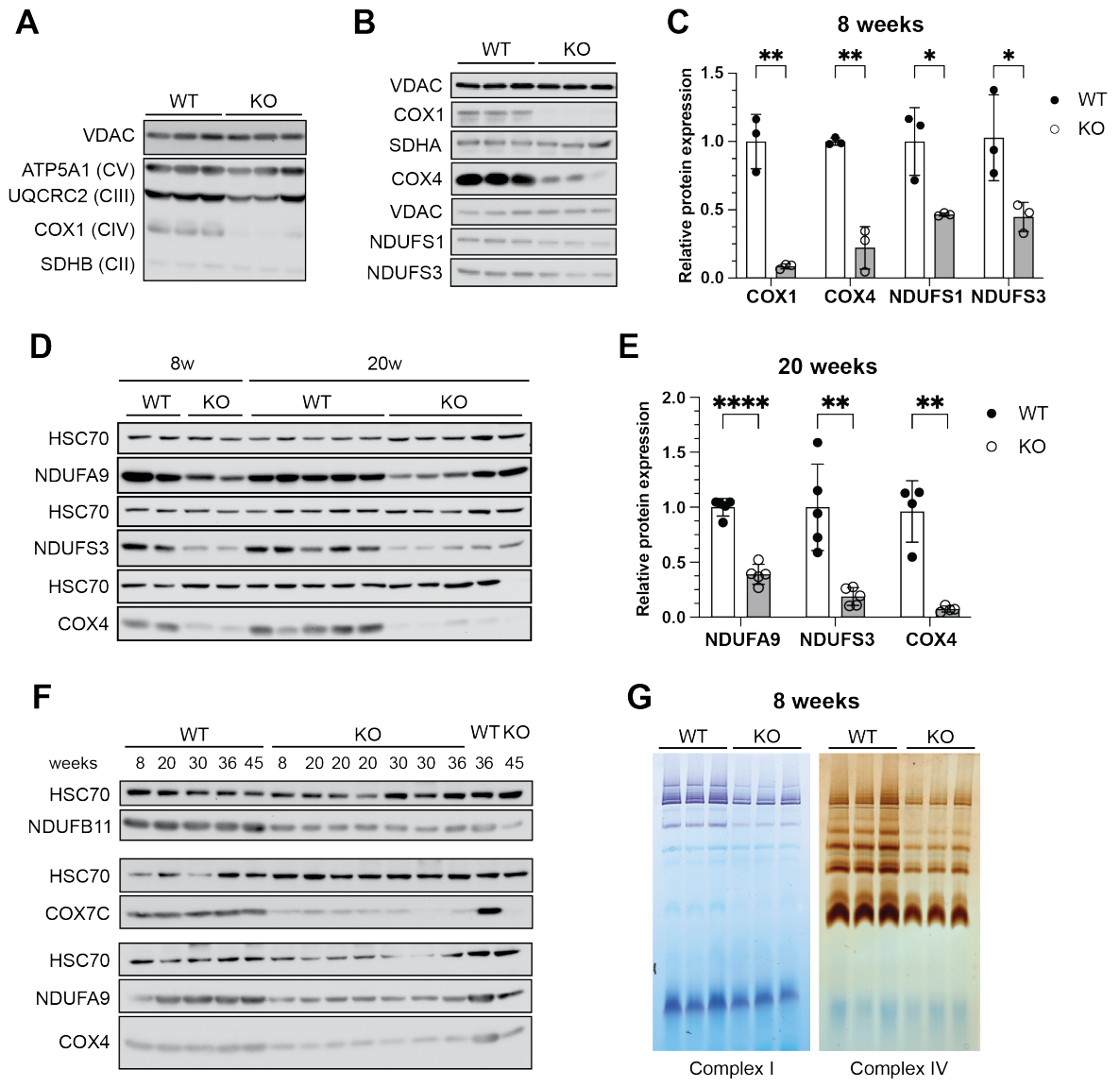


Figure 3.7 | LONP1 absence leads to a widescale loss of OXPHOS subunits

A) and B) Immunoblot of lysed cardiac mitochondria isolated from 8-weeks-old mice. (C) A quantification of B), normalized to VDAC and SDHA; n = 3. D) Immunoblot analysis of a whole heart protein lysate in 8- and 20-weeks-old mice, E) a quantification of 20-weeks-old samples, normalized to HSC70; n = 4–5. F) A comparison of the whole heart lysates from 8- and 20-weeks-old mice with the terminal mice; HSC70 used as a loading control. G) *In gel* activities of the complexes I and IV in isolated cardiac mitochondria.
*$p < 0.05$, **$p < 0.01$, ****$p < 0.0001$. Values are means ± SD.

The loss of CI and CIV proteins is further reflected in the loss of assembled complexes (Figure 3.8 A). The decline on the level of supercomplexes seems to be proportional to the loss of the individual complexes (Figure 3.8 A, B). It also appears that the overall protein levels of the individual complexes are additionally, but very mildly, reduced in the 20-week-old animals.

The impairment is less severe for CIII and CV. While the levels of UQCRC2 and ATP5A1 are probably decreased on the individual protein levels (Figure **3.8** A) it's only CIII-containing supercomplexes that are decreased (Figure **3.8** B). The loss in CIII supercomplexes is probably caused by the decline in CI and CIV complexes. The CIII monomer fraction seems to be in fact enriched (Figure **3.8** B), possibly due to

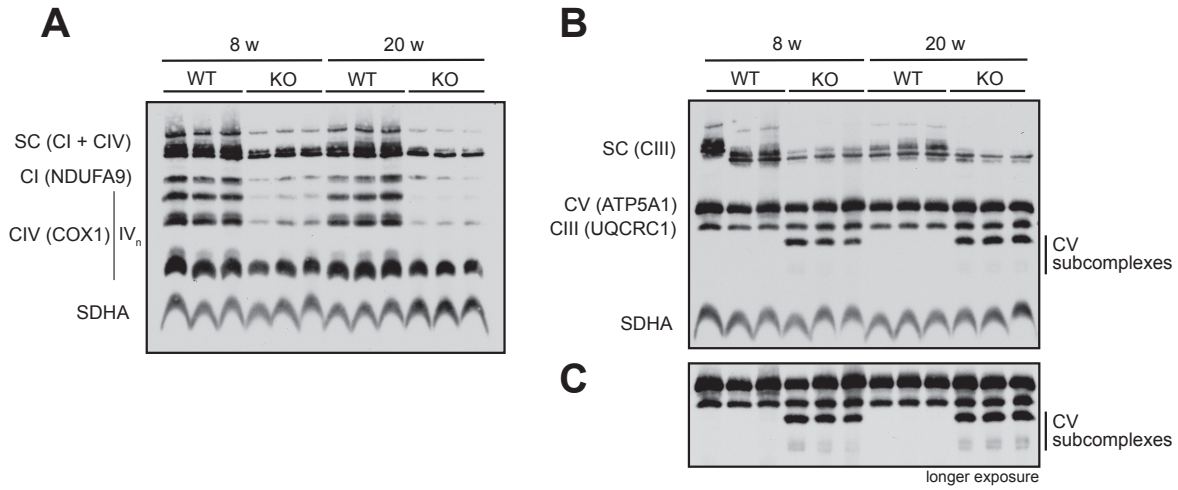


Figure 3.8 | LONP1 is not essential for supercomplexes (SC)

BN-PAGE analysis of isolated cardiac mitochondria solubilized with 4% digitonin. A) Immunoblot of CI and CIV; SDHA is used as a loading control; IV_n – possible CIV mono- and oligomers. B) Immunoblot of CIII and CV; SDHA is used as a loading control. C) A longer exposure of CV shown already in B).

redistribution of the oligomeric CIII. The CV monomer levels do not seem to be altered. However additional bands appeared in KO mitochondria, which could be the F1 subcomplex (Figure **3.8** B, C).

Respiration was measured in mitochondria isolated from 20 weeks old heart (Figure **3.9** A, B). The samples were first treated with pyruvate, malate, and ADP to assess CI-dependent respiration. Afterwards, the system was fuelled with glutamate and succinate to saturate OXPHOS and to measure the OXPHOS capacity. Titrating FCCP into the saturated system allows to evaluate the capacity of ETC, as FCCP dissipates the mitochondrial membrane potential which then stimulates the complexes I, III and IV. As they try to restore the uncoupled proton gradient, the maximal respiration is reached. After inhibiting respiration using rotenone (CI inhibitor) and antimycin A (CIII inhibitor), CIV activity can be assessed by adding artificial electron donors (TMPD + ascorbate) and a CIV inhibitor (e.g., sodium azide). Determining the maximal CIV activity only after adding the inhibitor is crucial as TMPD

undergoes autoxidation and the inhibition allows to subtract the background "respiration".

Although only two measurements were performed and therefore the statistical significance could not be judged, the values show a clearly decreased OXPHOS capacity and CIV activity in KO mitochondria (Figure **3.9** B). Additional measurements must be performed to test the statistical significance of these observations.

Overall, these results demonstrate an indispensable role of LONP1 in the regulation of OXPHOS as the changes on individual and complex levels resulted in decreased respiration.

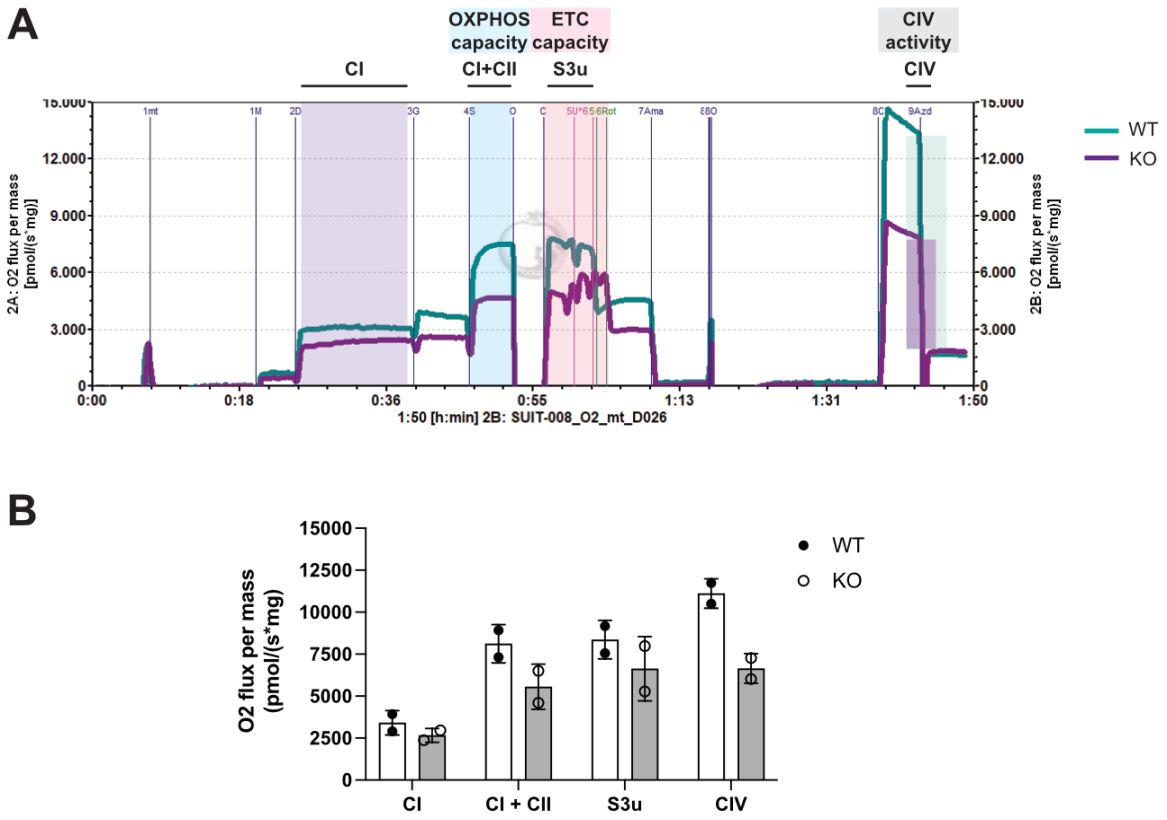


Figure 3.9 | The impairment of OXPHOS resulted in defective respiration

A) A representative respiration measurement. 1mt – mitochondria added, 1M – pyruvate and malate, 2D – ADP, 3G – glutamate, 4S – succinate, O + C – reoxygenation of the chamber, 5U – CCCP, 6Rot – rotenone, 7Ama – antimycin A, 8O + 8C – TMPD + ascorbate followed by reoxygenation, 9Azd – sodium azide. Axes: X – time [h], Y1 – O_2 concentration [µM], Y2 – O2 flux [pmol/(s*mg). B) A summary of the respiration measurements, normalized to protein mass (25 µg/mL); n = 2.

3.3 Whole heart proteomic analysis revealed a wide-scale change in the LONP1 KO heart proteome

To assess global changes in LONP1 KO, the label-free proteomic analysis of the heart proteome at 8 weeks of age was employed. In total, 3084 proteins were detected. Statistically significant changes were observed for 1580 proteins where the expression

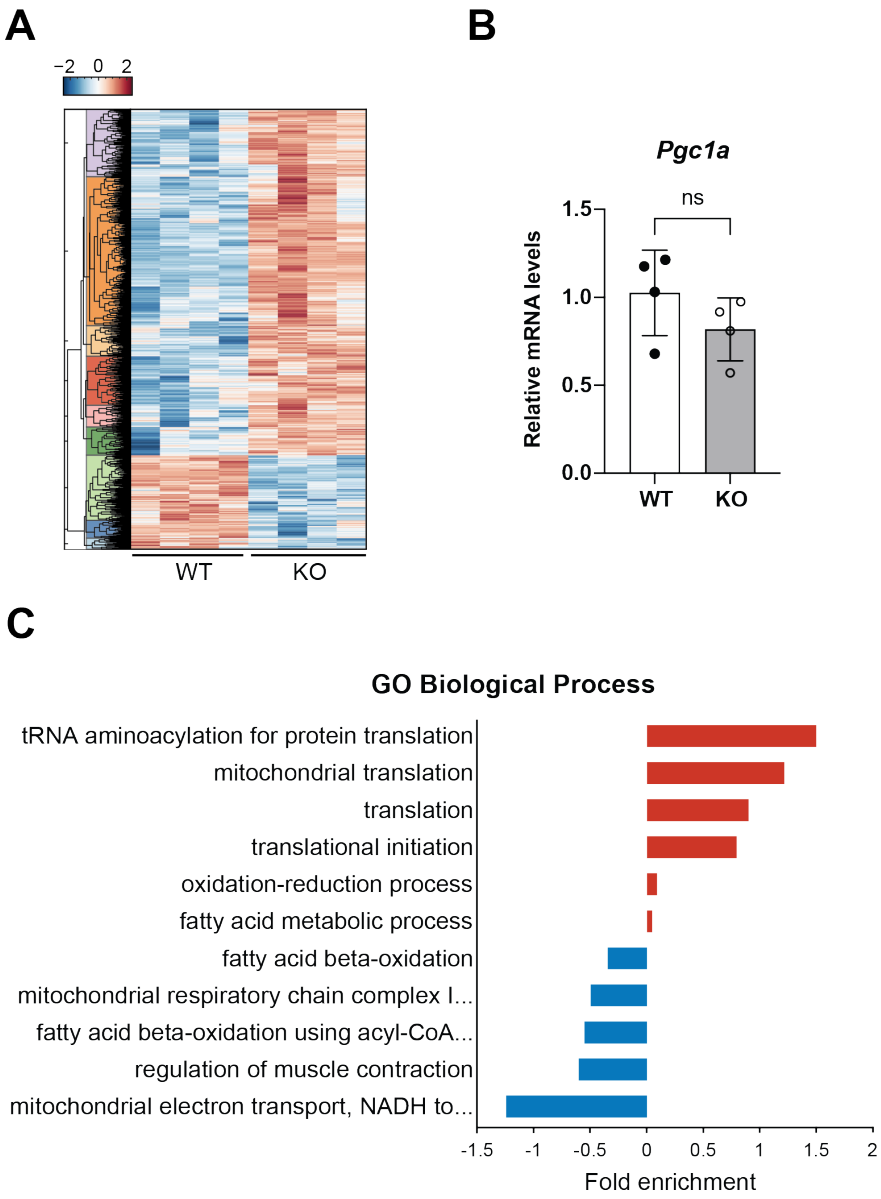


Figure 3.10 | General changes in the LONP1 KO heart proteome at 8 weeks of age

A) Hierarchical clustering of *Z*-scores of log_2-transformed label-free quantification (LFQ) intensities of significant changes (1580 proteins); n = 4. (B) *Pgc1a* mRNA levels analysed by qPCR, normalized to *Hprt*; n = 4. C) Gene ontology (GO) enrichment for biological processes of the significantly changed proteins.
ns = no statistical difference between WT and KO. Values are means ± SD.

of most of the proteins (1242) was upregulated (Figure **3.10** A). Out of 765 detected mitochondrial proteins, 312 was upregulated and 148 downregulated.

Mitochondrial biogenesis was not increased in KO heart as the mRNA level of *Pgc1a*, the major regulator of mitochondrial biogenesis, was not significantly changed (Figure **3.10** B). Gene ontology (GO) enrichment for biological processes (BP) of upregulated proteins revealed a significant enrichment in translation-related pathways (cytosolic and mitochondrial), while downregulated proteins were enriched in pathways involved in fatty acid beta-oxidation and OXPHOS (Figure **3.10** C). Among the most upregulated proteins were notably proteins involved in the integrated stress response

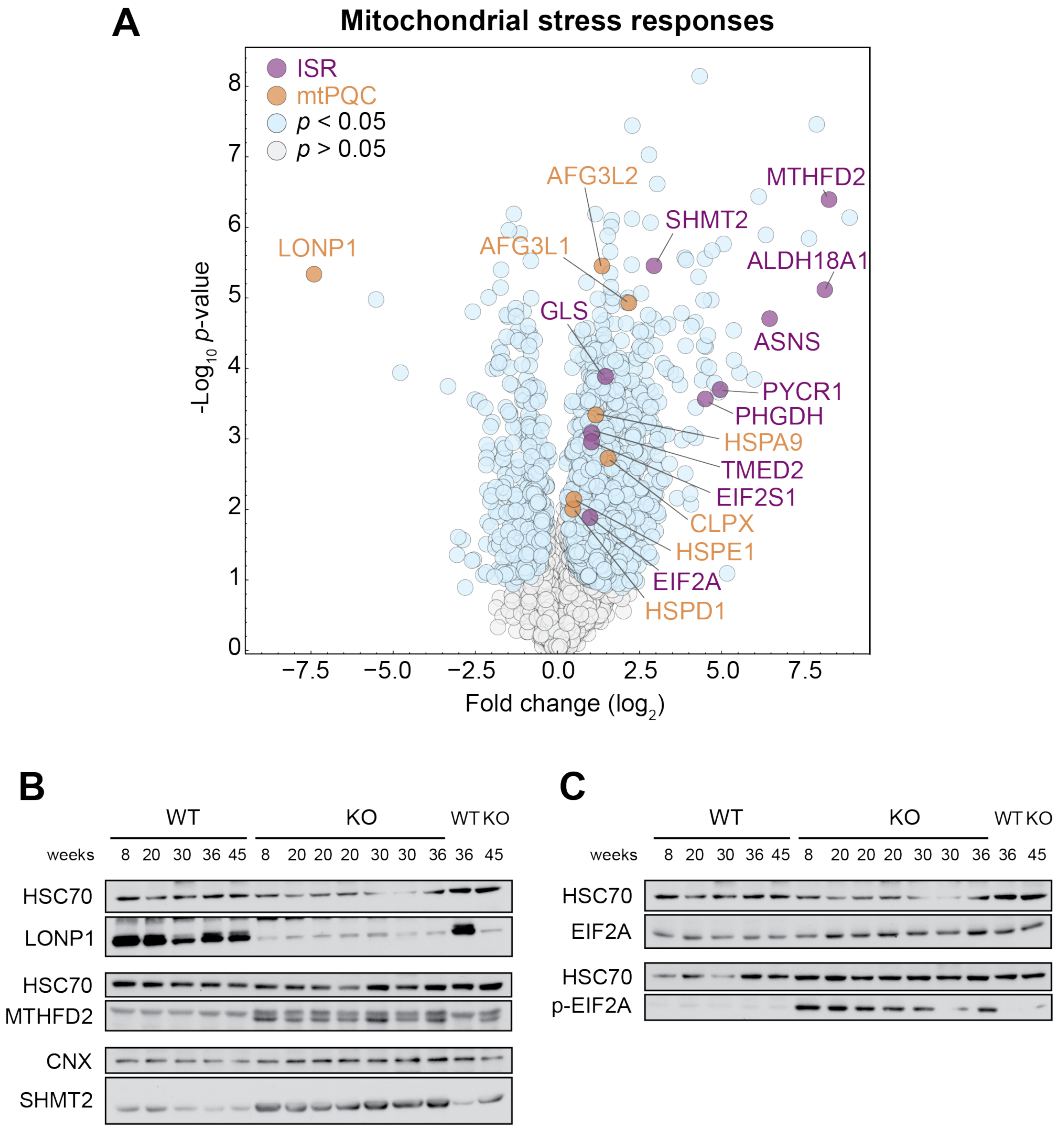


Figure 3.11 | General changes in the LONP1 KO heart proteome at 8 weeks of age

A) A volcano plot of the whole proteome (3084 proteins). Significantly changed mitochondrial stress markers are highlighted. B) A western blot analysis of the whole heart lysate. The stress markers are compared in mice at 8 and 20 weeks of age vs. the terminal mice. CNX and HSC70 are used as the loading controls.

(ISR) (Figure **3.11** A). Their increase in the heart KO was also shown with western blot analysis (Figure **3.11** B). Beside ISR, the protein quality control (mitoPQC) proteases and chaperones were to a lesser degree increased as well (Figure **3.11** C).

Proteomic analysis confirmed and revealed a large-scale decline in the levels of OXPHOS individual subunits with the strongest decrease in the CI and CIV subunits steady-state levels (Figure **3.12**). A significant increase of protein levels was observed in several assembly factors for all OXPHOS complexes, surprisingly also for CII, although its protein levels were not altered. Notably, three assembly factors – UQCC3 (CIII), COA7, and PET100 (both CIV) – were downregulated in KO hearts, which suggests a specific role of LONP1 for these assembly factors.

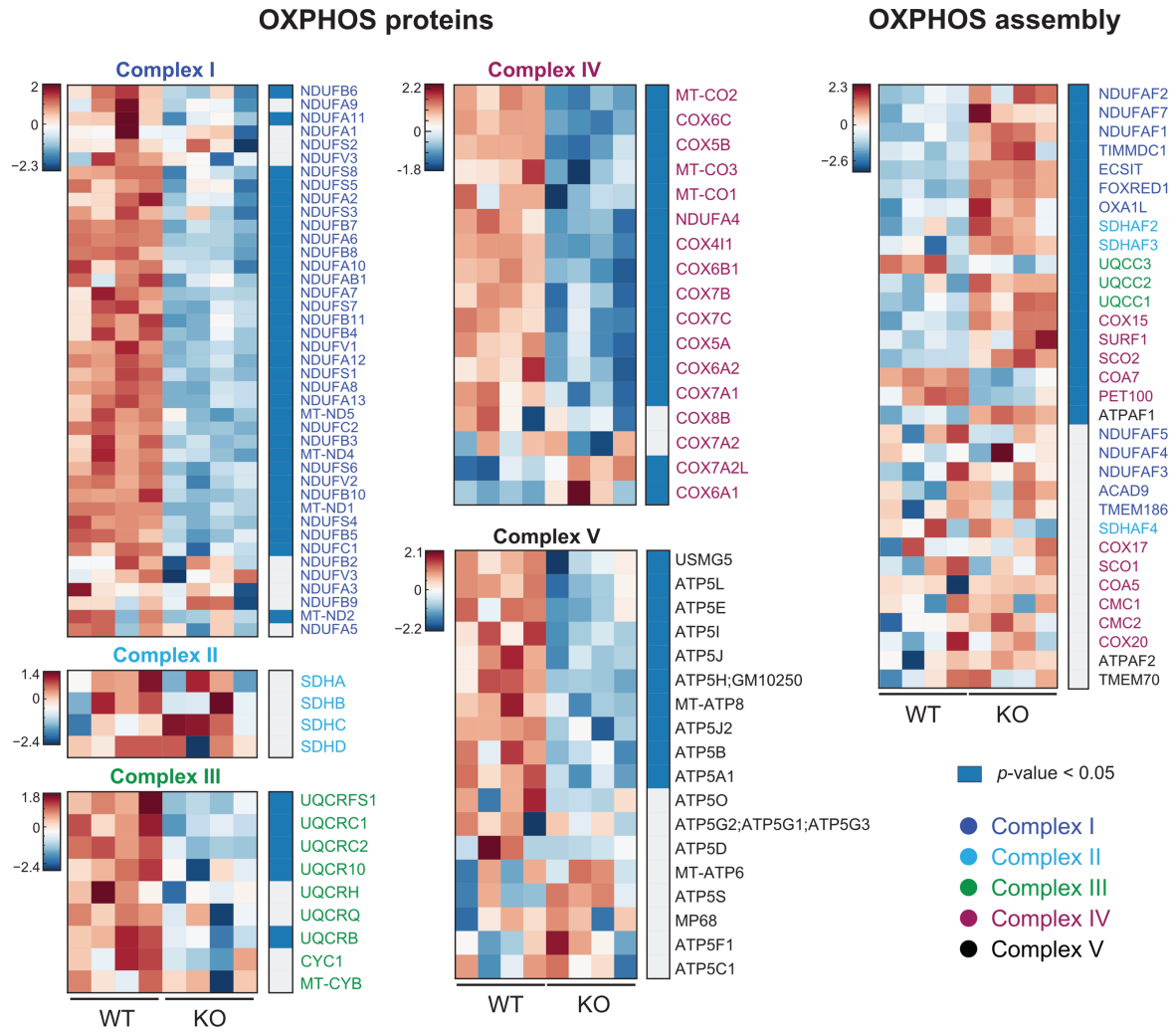


Figure 3.12 | An overview of the OXPHOS proteome

Heatmaps of *Z*-scores of log_2-transformed LFQ intensities in the 8-week-old heart lysates. Shown are all proteins that were detected in the dataset. In the columns placed on the right to the heatmaps, the statistical significance is depicted (blue – $p < 0.05$, white – ns); n = 4.

As the GO enrichment analysis suggested, there was an overall increase in proteins involved in translation (**Error! Reference source not found.**). A surge of eukaryotic translation initiation factors and ribosomal proteins was detected (**Error!**

Reference source not found. A). We observed an upregulation of aminoacyl-tRNA synthetases as well (**Error! Reference source not found.** B), both cytoplasmic and mitochondrial. An increase in the levels of the proteins is one of the hallmarks of ISR (Kilberg et al., 2012). More interestingly, other mitochondrial translation proteins were increased as well (**Error! Reference source not found.** C), particularly mitochondrial

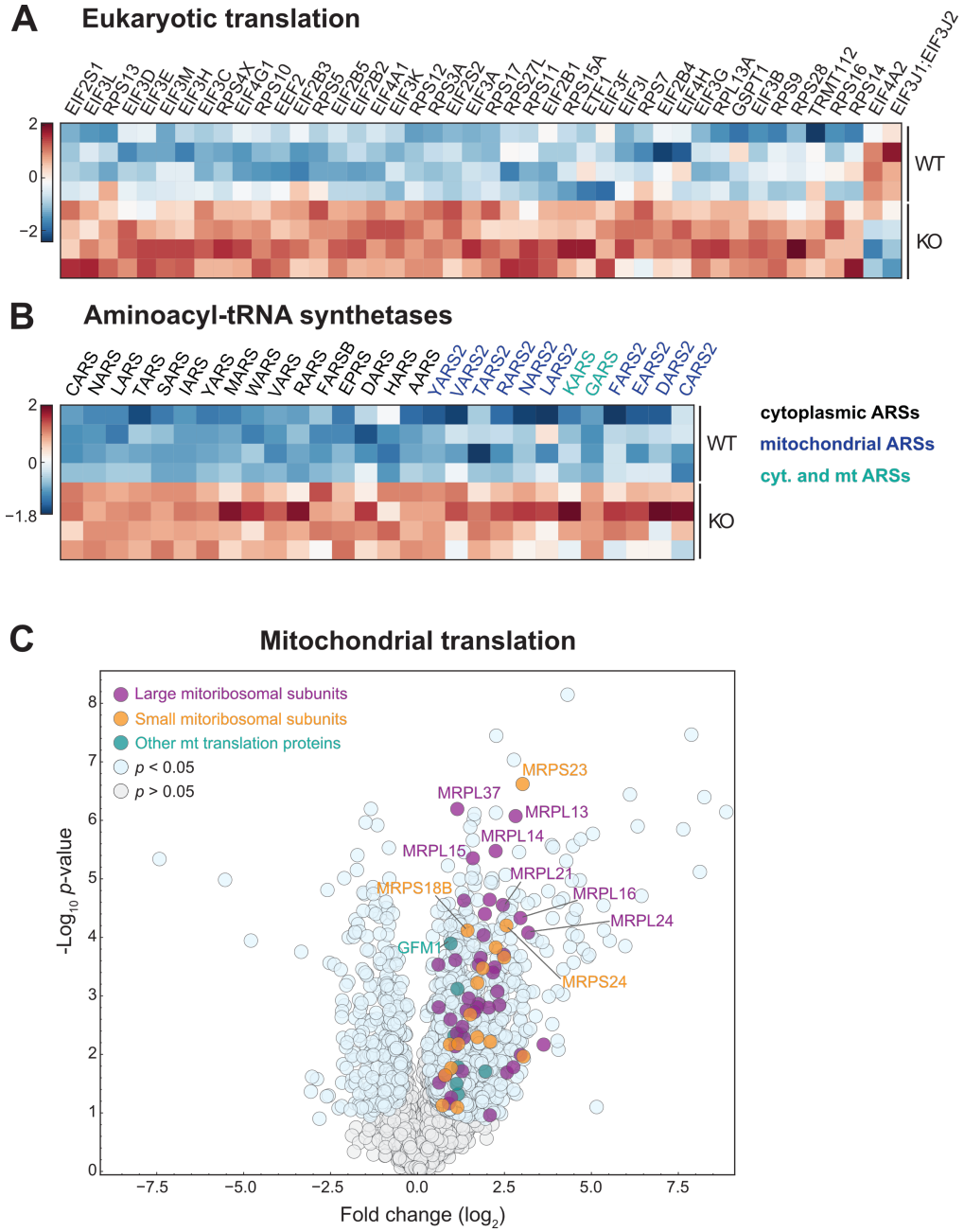


Figure 3.13 | Proteins involved in cytosolic and mitochondrial translation are upregulated in the LONP1 KO

Heatmaps of *Z*-scores of log_2-transformed LFQ intensities of significantly changed A) cytoplasmic translation factors and B) aminoacyl-tRNA synthetases. C) A volcano plot of the whole proteome. Highlighted are all significantly changed mitochondrial translation proteins.

ribosomal proteins (MRPs).

3.4 Loss of LONP1 led to an accumulation of mitoribosomal proteins

Closer inspection of MRPs unveiled a substantial increase in most of the proteins of the large mitoribosome (mtLSU) already at 8 weeks of age (Figure **3.14** A). There was also an increase in the small mitoribosomal proteins (mtSSU) but to a much lesser degree (Figure **3.14** A). This observation was confirmed by a western blot analysis of chosen MRPs (MRPL12, MRPL37) in all studied ages (Figure **3.14** B–E). However, the same cannot be said about MRPS35 which is unchanged in the proteomic analysis, but it is even decreased by 50% in the western blot analysis.

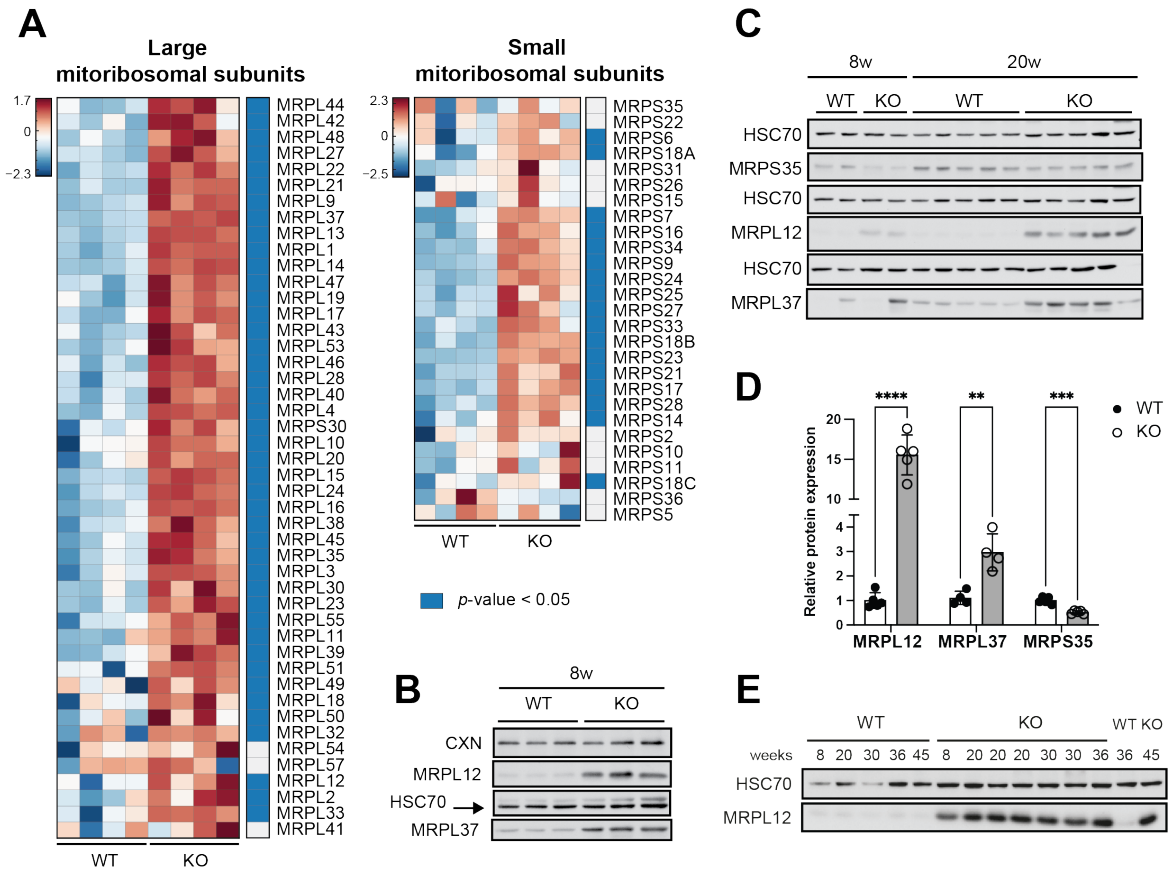


Figure 3.14 | Loss of LONP1 resulted in a surge of mitoribosomal proteins

A) Heatmaps of *Z*-scores of $\log_2$-transformed LFQ intensities of all detected MRPs in the 8-week-old heart lysates; n = 4. B), C), E) Immunoblots of chosen MRPs in the whole heart lysate; CXN and HSC70 are used as a loading control. D) Protein quantification of MRPs of the 20-week-old samples in C); n = 4–5
$^{**}p < 0.01$, $^{***}p < 0.001$, $^{****}p < 0.0001$. Values are means ± SD.

To determine the stability of the mitoribosomes, a ribosome profile of mitochondrial proteins was established using a sucrose density gradient. The gradient confirmed an increase in the steady-state levels of the individual mtLSU proteins in the KO. However, the increase was reflected mostly in the single assembled mtLSU, where the strongest signal was detected (Figure 3.15 A, fractions 9 and 10). In the WT mitochondria, the strongest signal was localized in the fractions 12 and 13 where the

fully assembled mitoribosome is expected. This indicates an accumulation of the single mtLSU, although a full mitoribosome is still being assembled in the KO. We faced a lot of technical difficulties when attempting to detect the mtSSU on the ribosomal profiles, as the available antibodies performed poorly and inconsistently even in the WT conditions. In Figure 3.15 B, the proteins from individual sucrose fractions were precipitated which increased their concentration and that also increased the mtSSU signal. We detected the strongest signal in the 55S monosome which suggests that the majority of mtSSU is present in the fully assembled mitoribosome.

The proteomic analysis also showed an increase in mitoribosomal maturation and assembly factors for 12S, 16S rRNA and mtLSU and mtSSU, respectively (Figure 3.15 C).

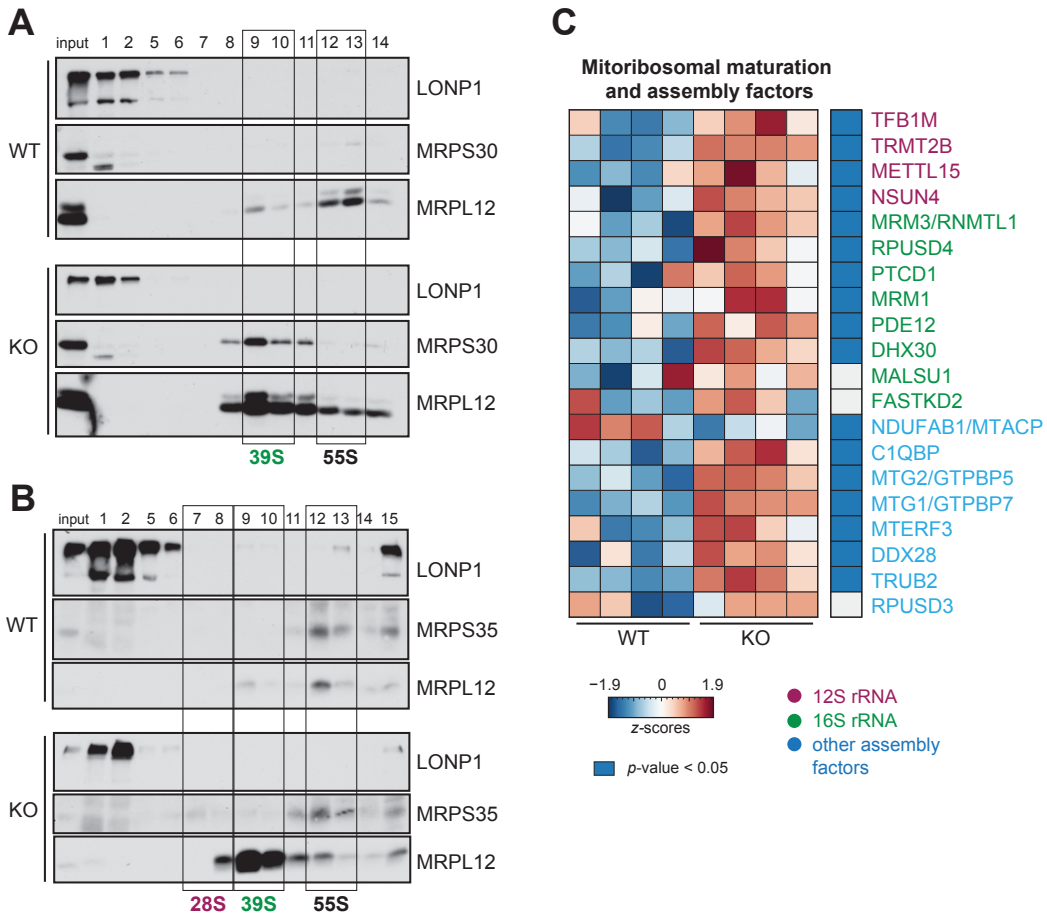


Figure 3.15 | LONP1 is necessary for mitoribosomal assembly

A) and B) Immunoblot of sucrose density gradient of mitoribosomes isolated from 8-week-old mitochondria; MRPL12 and MRPS30 are mtLSU proteins, MRPS35 is a mtSSU protein; n = 1. C) Heatmaps of *Z*-scores of log_2-transformed LFQ intensities of proteins involved in maturation and assembly of the mitoribosomes; n = 4.

3.5 LONP1 deficiency altered the *de novo* synthesis of mtRNA and mt proteins, but not mtDNA levels

The increased levels of mitoribosomal proteins and the dysfunctional mitoribosomal profile suggests a dysfunctional synthesis of mitochondrially encoded proteins. In order to assess the quality of *de novo* translation, we performed *in organello* translation using radioactive labelling ^{35}S-Met in freshly isolated cardiac mitochondria from 8 weeks old mice. This analysis demonstrated a significant decline in the overall *de novo* translation in KO by ~27% (Figure 3.16 A, B). A chase with a cold methionine that followed pulse-labelling did not reveal any differences in the

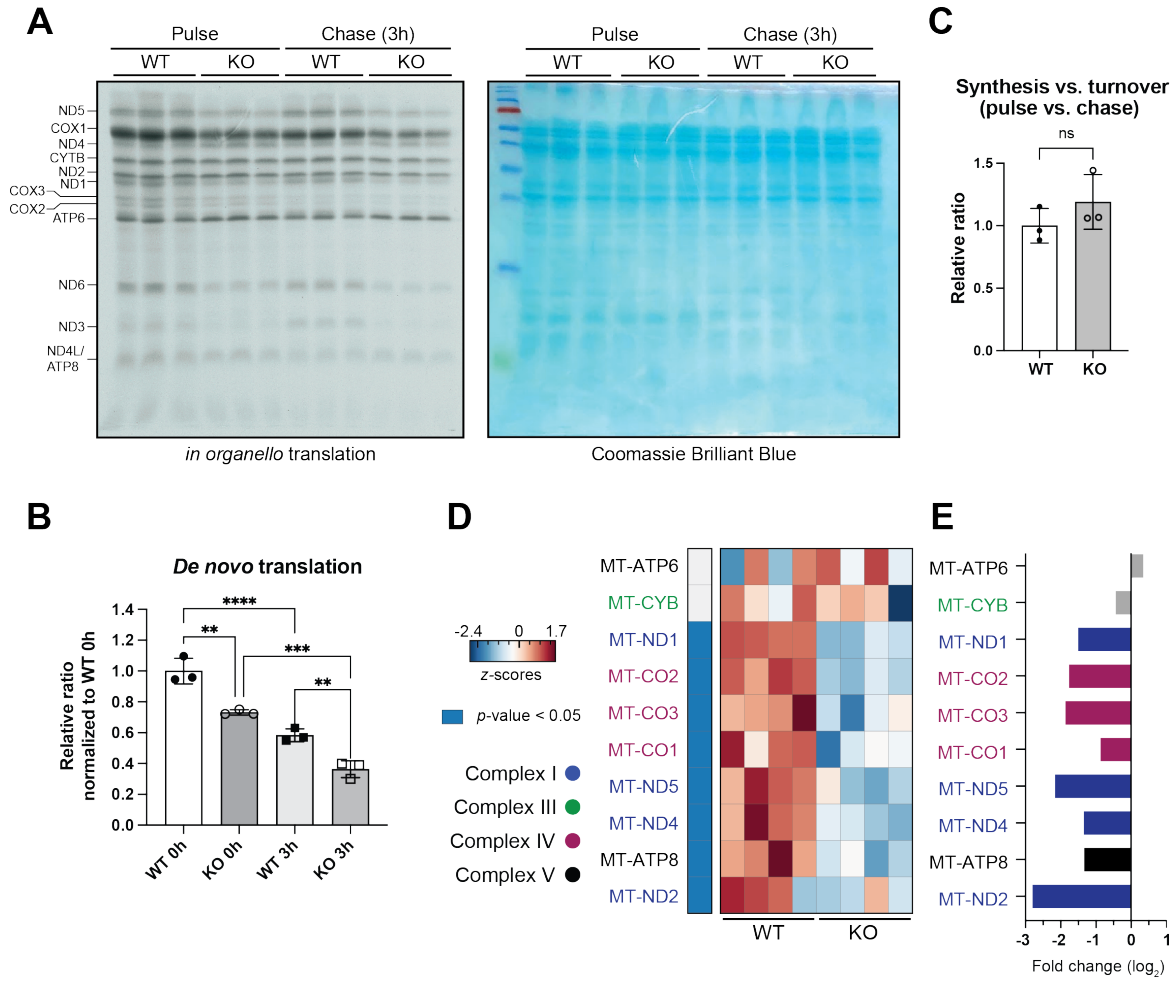


Figure 3.16 | Mitochondrial de novo translation is mildly decreased in the LONP1 KO

A) *De novo* synthesized proteins isolated from fresh cardiac mitochondria (8w). ^{35}S-Met was used for 1h pulse-labelling which was followed with a 3h cold chase. Coomassie Brilliant Blue was used to stain the gel for a loading control. B) Relative quantification of the respective lane intensities in A); n = 3. C) Relative quantification of the overall protein synthesis and turnover (pulse ÷ chase). D) Heatmaps of *Z*-scores of $\log_2$-transformed LFQ intensities of mitochondrially encoded proteins (8w); n = 4. E) $\log_2$ fold changes of proteins in D); statistically non-significant changes are labelled grey.

$^{**}p < 0.01$, $^{***}p < 0.001$, $^{****}p < 0.0001$, ns = no statistical difference. Values are means ± SD.

protein turnover as the further decline in KO translation was by ~22% and the synthesis vs. turnover ratio did not differ (Figure 3.16 C).

Although the translation defect was only mild, the steady-state levels of most of the mitochondrial-encoded proteins were additionally reduced with the changes ranging from 46% decrease of COX1 to 86% decrease of ND2 (Figure 3.16 D and E). Only CYTB and ATP6 were not affected and ND3, ND4L, and ND6 were not detected. Together with the large-scale loss of OXPHOS proteins (Figure 3.12), these data further suggest a post-translational role of LONP1 in maintaining OXPHOS.

Next, the way LONP1 depletion affected processes upstream of translation was investigated. We have not observed any deletions or duplications in the KO mtDNA (Figure 3.17 A) and the mtDNA levels were also not altered (Figure 3.17 B). *In*

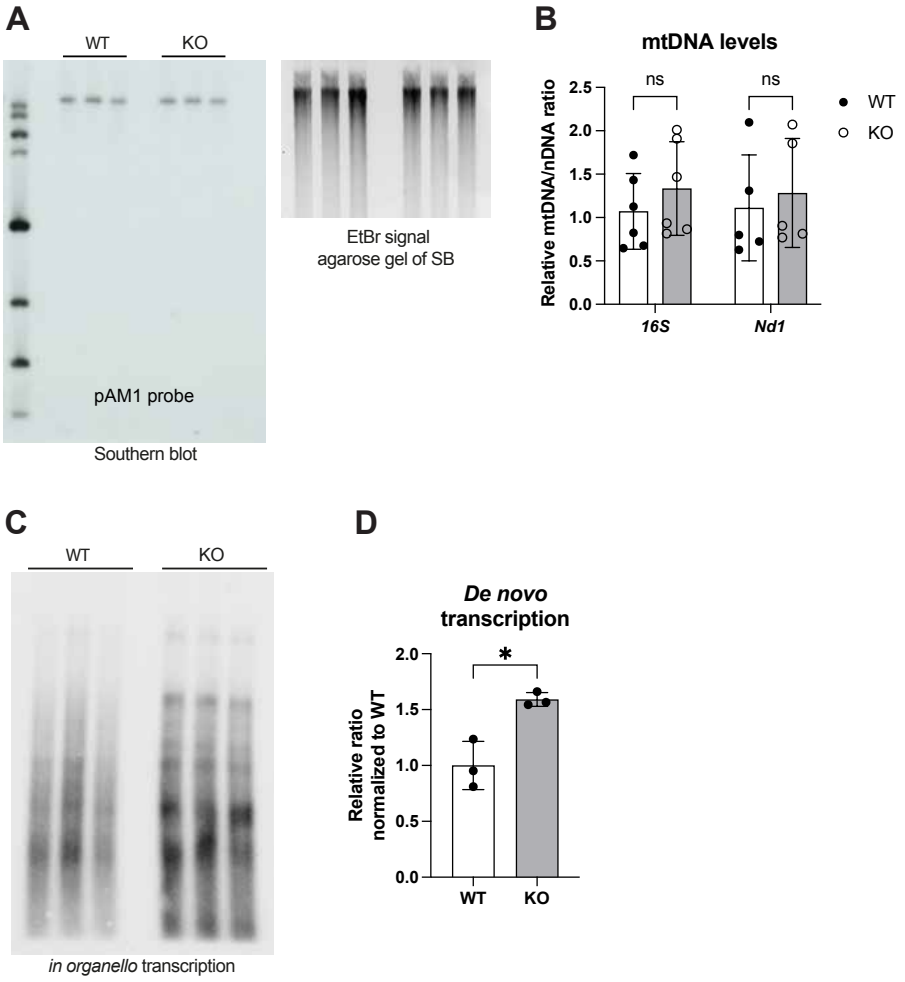


Figure 3.17 | LONP1 absence did not affect the mtDNA levels, but it led to a significant increase in mitochondrial transcription at 8 weeks of age.

A) Southern blot analysis of the steady-state mtDNA levels using ^{32}P-dCTP labelling; n = 3. EtBr signal is showed to estimate a correct loading. B) A qPCR quantification of mtDNA, normalized to *Hk2*; n = 6. C) *De novo* mtRNA synthesis in freshly isolated heart mitochondria. ^{32}P-dUTP labelling was used. D) Relative quantification of the respective lane intensities in C); n = 3.

*$p < 0.05$, ns = no statistical difference. Values are means ± SD.

organello transcription was subsequently employed to determine the transcription rate in KO mitochondria which was 1.5x higher than WT (Figure 3.17 C, D). That is in a direct contrast to the decrease in translation observed earlier in LONP1 KO mitochondria.

Western blot analysis was used to evaluate the state of proteins involved in mitochondrial gene expression (Figure 3.18). From the proteins involved in mtDNA maintenance and replication only POLRMT and SSBP1 were changed. Their protein

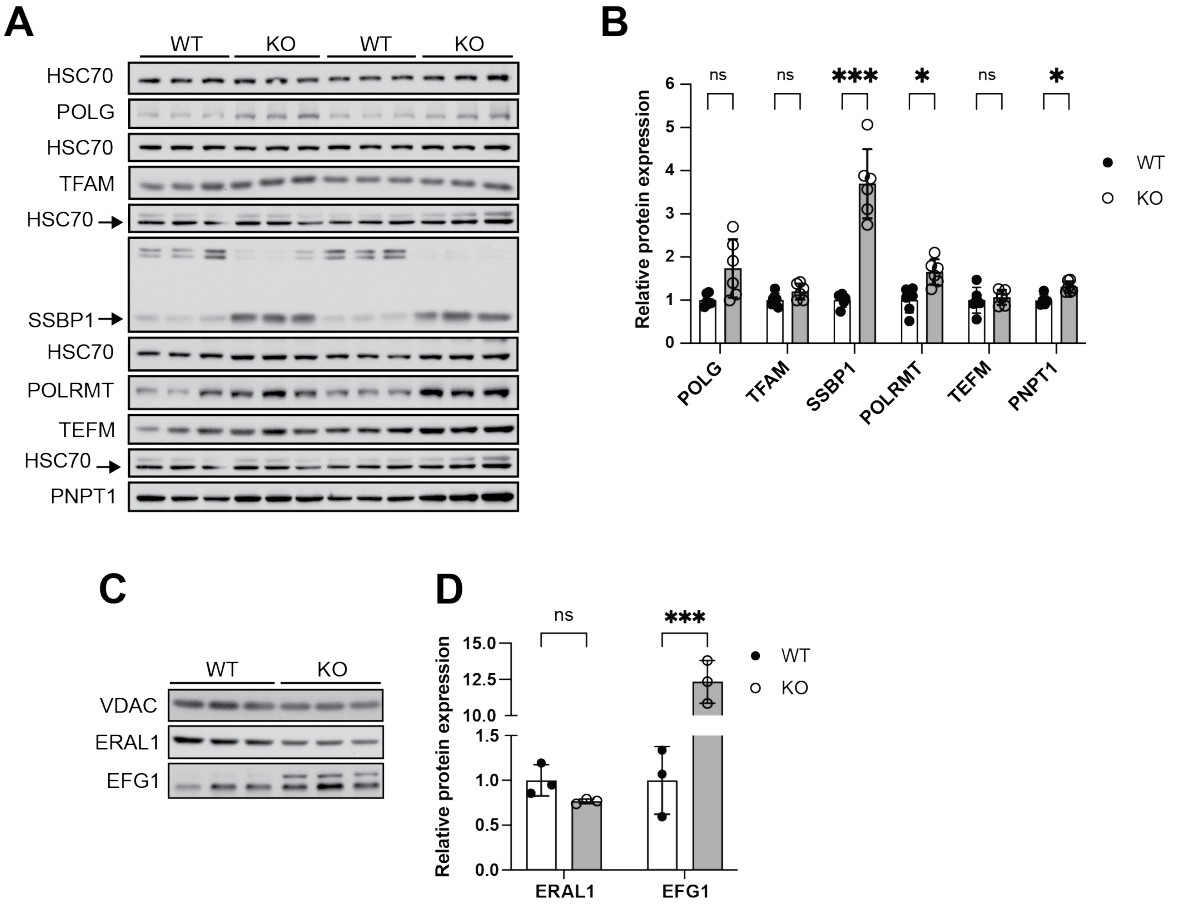


Figure 3.18 | Loss of LONP1 lead to a general surge of proteins involved in mitochondrial gene expression at 8 weeks of age.

A) Immunoblot analysis of proteins in the whole heart lysate; HSC70 was used as a loading control. B) Protein quantification of the immunoblot in A); n = 6. C) Immunoblot analysis and D) quantification of proteins in isolated mitochondria; VDAC was used as a loading control; n = 3. E) Heatmaps of *Z*-scores of log_2-transformed LFQ intensities and the respective log_2 fold changes of significantly altered proteins in the LONP1 KO; n = 4.
**p* < 0.05, ****p* < 0.001, ns = no statistical difference. Values are means ± SD.

levels were increased by 1.7- and 3.6-times, respectively (Figure 3.18 A, B). Other upregulated proteins include PNPT1 (1.6-times increase) (Figure 3.18 A, B) which is involved in decay of mtRNA, and EFG1 (12.3-times increase), a translation elongation factor (Figure 3.18 C, D).

A proteomic analysis confirmed an overall increase in enzymes participating in mitochondrial gene expression. Most notably a transcription factor TFB2M (8.4-times increase), NSUN4 (16.6-times increase) which is involved in processing of mt-rRNA, and a translation factor NOA1 (8.35-times increase). These proteins are one of the most upregulated proteins in the proteomic dataset (**Error! Reference source not found.**). Surprisingly, no changes in TFAM were detected in the western blot whereas proteomics showed a significantly decreased protein steady-state levels. TFAM was already shown to be a LONP1 substrate (Matsushima et al., 2010). Another decreased protein is a translation factor TUFM. The increase in EFG1 was much more moderate in the proteomic dataset than in the western blot and SSBP1 was not detected at all.

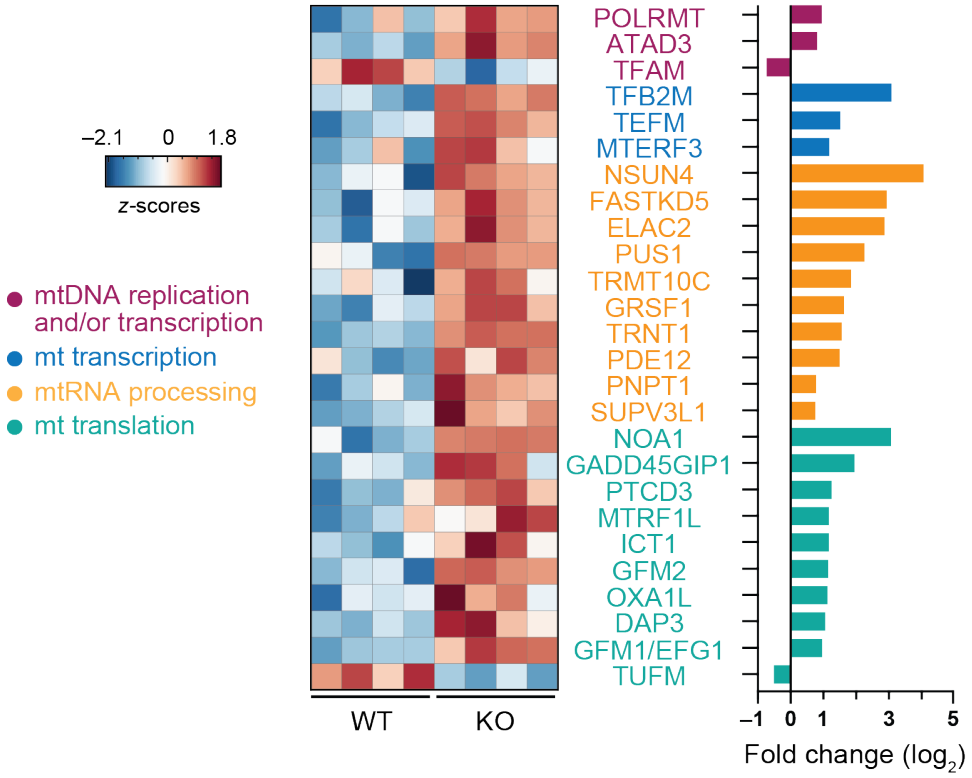


Figure 3.19 | Loss of LONP1 lead to a general surge of proteins involved in mitochondrial gene expression at 8 weeks of age.

Heatmaps of *Z*-scores of log_2-transformed LFQ intensities and the respective log_2 fold changes of significantly altered proteins in the LONP1 KO; n = 4.

The increase of POLRMT and SSBP1 was validated also in the 20-week-old heart lysates (Figure 3.20 A, B) as well as in the aged heart lysates (Figure 3.20 C). Peculiarly, contrary to the proteomic data, there was a significant decline in the amount of TFB2M protein on the western blot at 20 weeks of age and the decline is notable already in the 8-week-old samples (Figure 3.20 A).

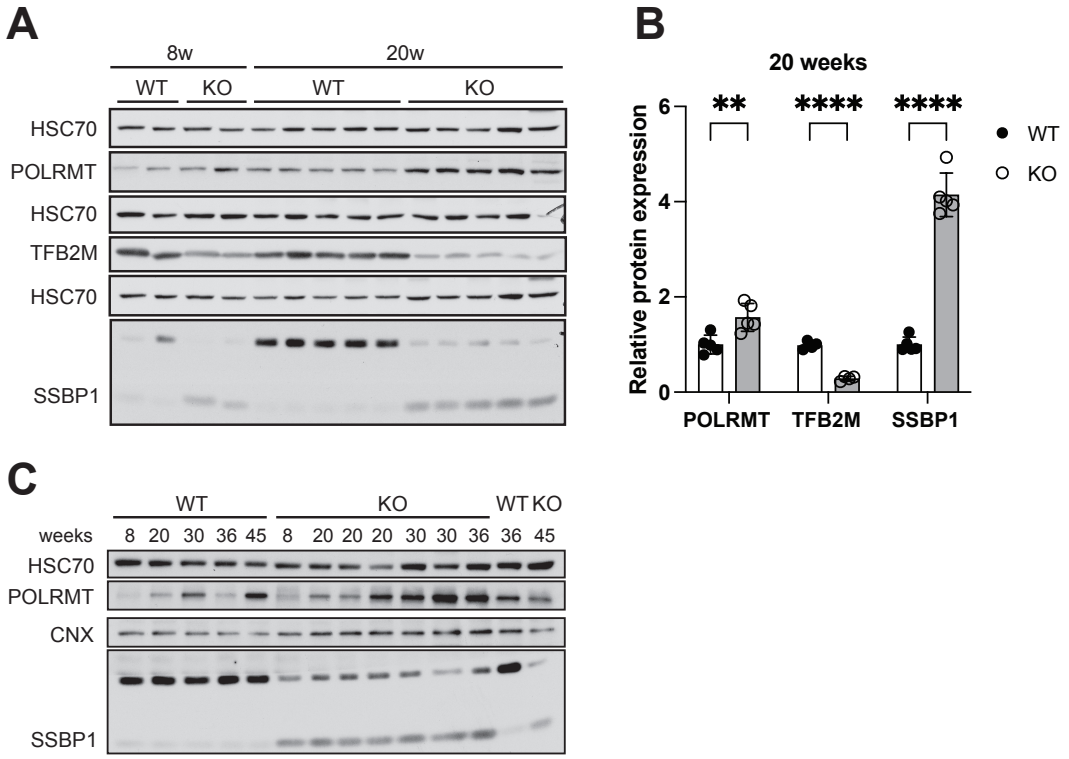


Figure 3.20 | Detected changes in proteins involved in mitochondrial gene expression at 20 weeks of age

A) Immunoblot analysis of proteins in the whole heart lysate; HSC70 was used as a loading control. B) Protein quantification of the immunoblot in A); n = 4–5. C) Immunoblot analysis of proteins in the whole heart lysate – a comparison to terminal mice.
**p < 0.01, ****p < 0.0001. Values are means ± SD.

3.5.1 A cell model with siRNA-mediated knockdown of *Lonp1* does not phenocopy LONP1 deficiency *in vivo*

To further address mechanisms that cause changes observed *in vivo*, we tried to develop a functional cell model with LONP1 depletion. No mammalian cell model of a full depletion of LONP1 has been reported in the literature so far. As our own efforts to obtain a full depletion of LONP1 in mammalian cells were unsuccessful, a model with a transient knockdown of LONP1 was generated using RNA interference (Figure 3.21). Wild type mouse embryonic fibroblasts (MEFs) were transfected with two different

Lonp1 siRNAs for 48 hours and then harvested and analysed. *Lonp1* siRNA-1 reduced LONP1 levels to 17.7% and *Lonp1* siRNA-2 to 33.5%.

The RNAi model did not phenocopy the mouse model – changes in the analysed proteins are summarized in the Table 3.1. Only POLRMT and NDUSF3 repeated the phenomena observed in the previous models, the other changes remain inconclusive when taking all three models into the account.

Table 3.1 | Heart KO and cell *Lonp1* siRNA comparison

protein	**heart WB** Figure **3.7** Figure 3.18	**heart proteomics** **Error! Reference source not found.** Figure 3.24	***Lonp1* siRNA-2** Figure 3.21
POLG	*1,737*	–	*0,733*
SSBP1	3,697	–	0,652
TWNK	–	–	0,565
POLRMT	1,653	1,926	1,517
ERAL1	*0,766*	–	0,446
LRPPRC	–	*0,978*	0,405
EFG1	12,330	1,936	*0,944*
NDUFS3	0,448	0,685	0,372
UQCRC1	*0,647*	0,710	*0,944*
ATP5A1	–	0,834	*0,969*

Fold changes in protein expression. In *grey* – non-significant change; "–" – protein was not tested/detected.

From the available data, the *Lonp1* siRNA models have a different phenotype than our *in vivo* model probably because cell models lack the complexity and specificity of a tissue. The cells are also not as affected since they still express a small quantity of the functioning protease. The *Lonp1* siRNA model is therefore not a suitable model to study the molecular mechanisms of LONP1.

All our efforts to develop a cell model with a complete depletion of LONP1 were futile. Other possible choices are patient fibroblasts with LONP1 mutations (Besse et al., 2020, Peter et al., 2018) or cell models with hypomorphic mutations (Pollecker et al., 2021).

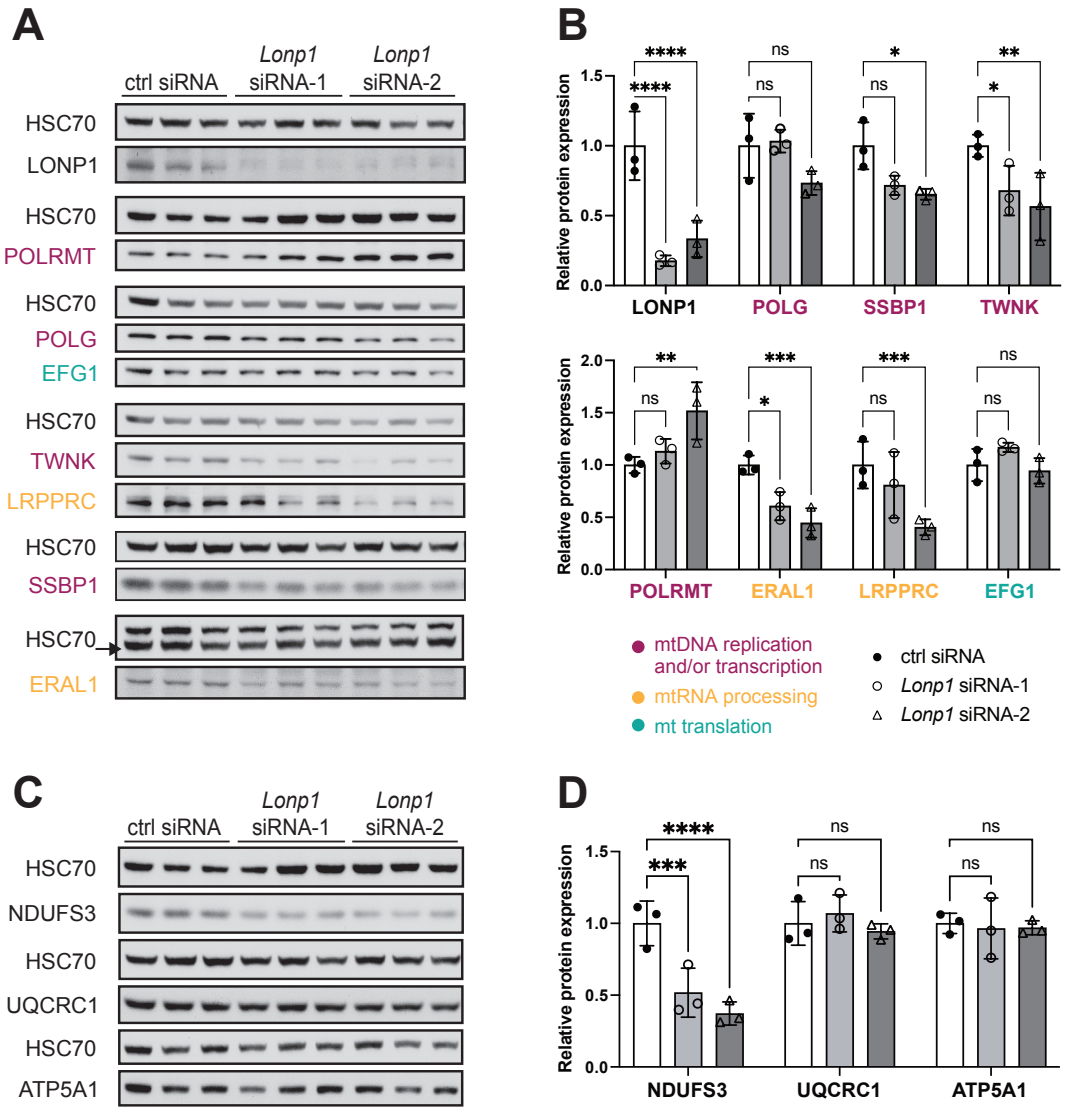


Figure 3.21 | Lonp1 KD in cells does not phenocopy the mouse model

A) Immunoblot analysis of proteins in the cell lysate; HSC70 was used as a loading control. B) Protein quantification of the immunoblot in A); n = 3. C) Immunoblot analysis and D) protein quantification of OXPHOS proteins in the cell lysate; HSC70 was used as a loading control; n = 3.

*p < 0.05, **p < 0.01, ***p < 0.001, ****p < 0.0001, ns = no statistical significance. Values are means ± SD.

3.5.3 RNAseq analysis revealed a transcriptional regulation of the observed changes on the protein level

Sequencing of heart mRNA at 8 weeks of age revealed 4032 significantly changed mRNAs out of which 2322 were upregulated and 1710 downregulated in the KO heart (Figure 3.22 A). As for nuclear encoded mitochondrial mRNAs, 464 were significantly changed out of which 165 were upregulated and 299 downregulated.

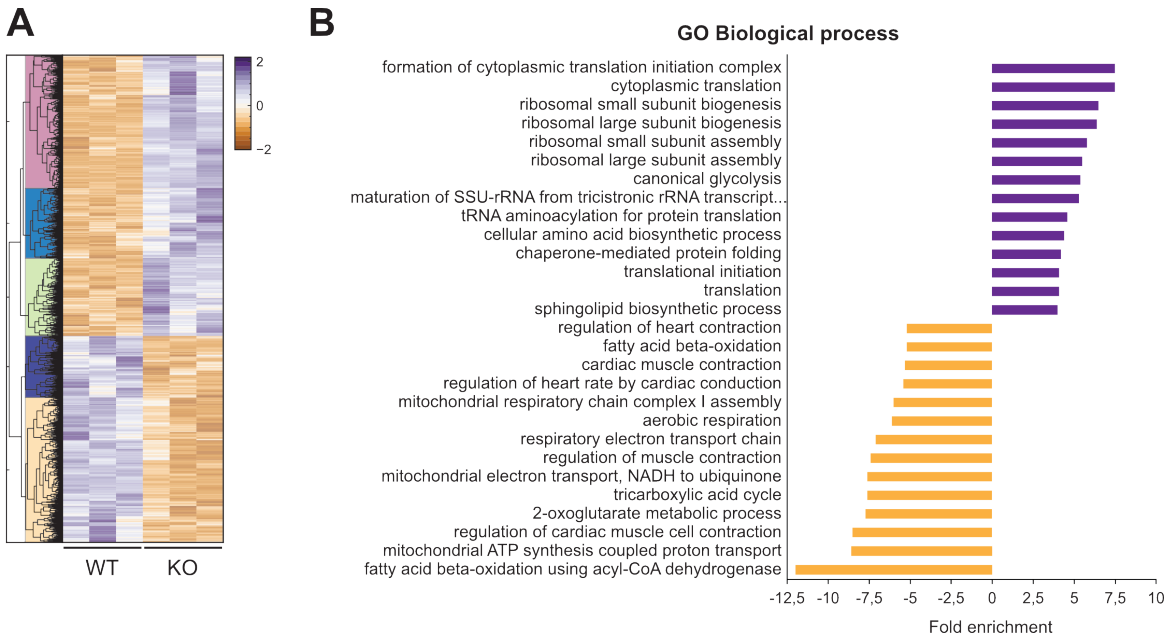


Figure 3.22 | A general overview of the LONP1 KO heart transcriptome at 8 weeks of age

A) Hierarchical clustering of *Z*-scores of $\log_2$-transformed LFQ intensities of significant changes (4032 mRNAs); n = 3. B) Gene ontology (GO) enrichment for biological processes of the significantly changed transcripts.

The analysis of enrichment for GOBP terms very much mirrored the proteomic enrichment analysis which implies that all these enriched processes are changed also on transcriptional level and the alterations are not only post-translational (Figure 3.22 B). Again, the most significantly upregulated terms turned out to be cytosolic translation pathways. In addition to the proteomics data, the analysis also hinted at systemic changes in metabolism. It is also important to note that pathways responsible for heart muscle function are shown to be also downregulated.

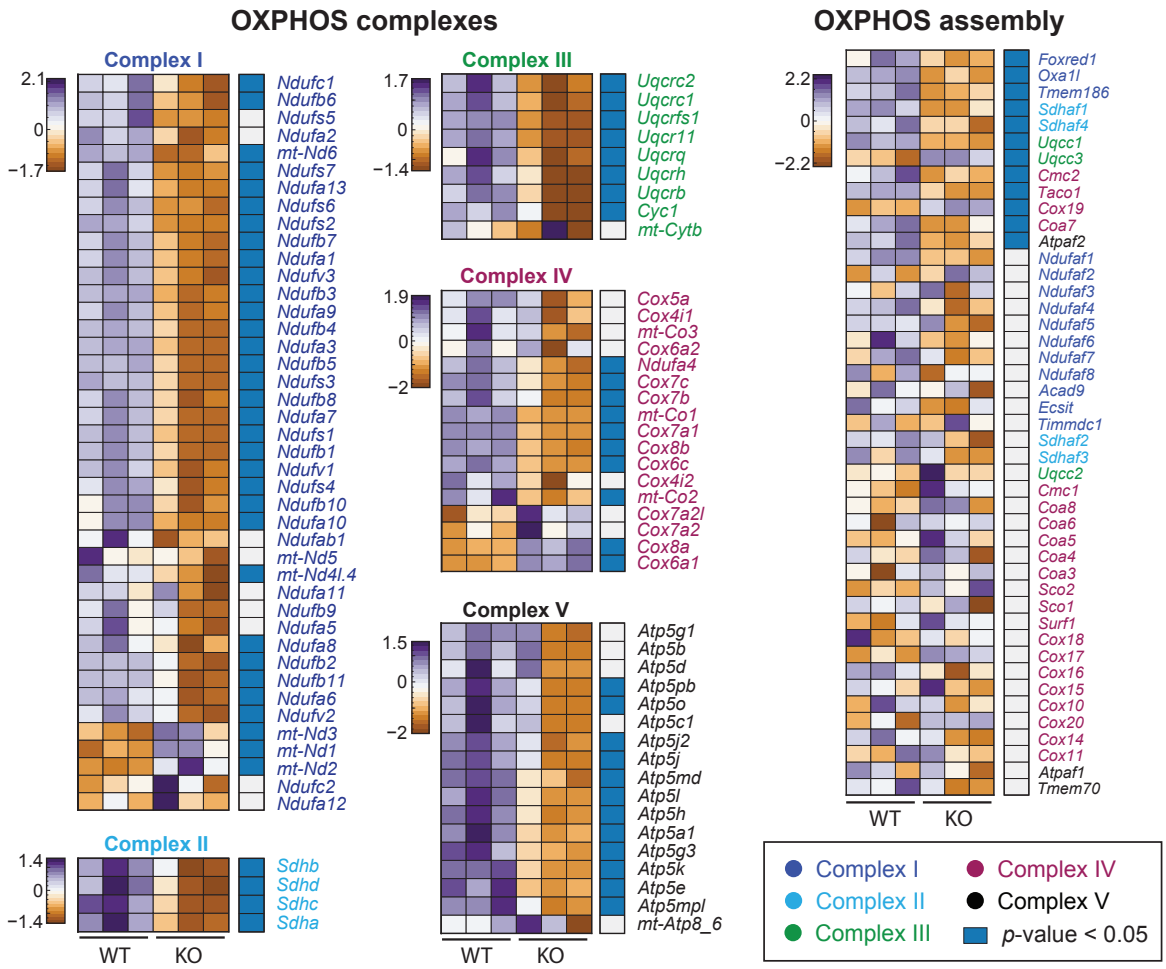


Figure 3.23 | Transcriptomics reveal a decline of OXPHOS subunits already on the transcript level.

Heatmaps of *Z*-scores of $\log_2$-transformed LFQ intensities of all detected OXPHOS subunits and their assembly factors; n = 3.

As for OXPHOS, there is a clear decrease in the synthesis of nuclear encoded OXPHOS subunits (Figure 3.22 B and Figure 3.23) which might explain the observed decrease in the protein levels. Peculiarly, CII is also affected albeit the mRNA deficiency is not translated into the protein levels (Figure 1.12).

It is still reasonable to hypothesize that LONP1 is important for OXPHOS stability, and it is probably involved post-translationally, as additionally to the loss of mRNA, there is a greater decline in the protein steady-state levels (Figure 3.24). Only 12 of the assembly factors were affected, but interestingly most of their mRNA steady state levels were reduced, although on the protein level it is quite the opposite (Figure 1.12 and Figure 3.24).

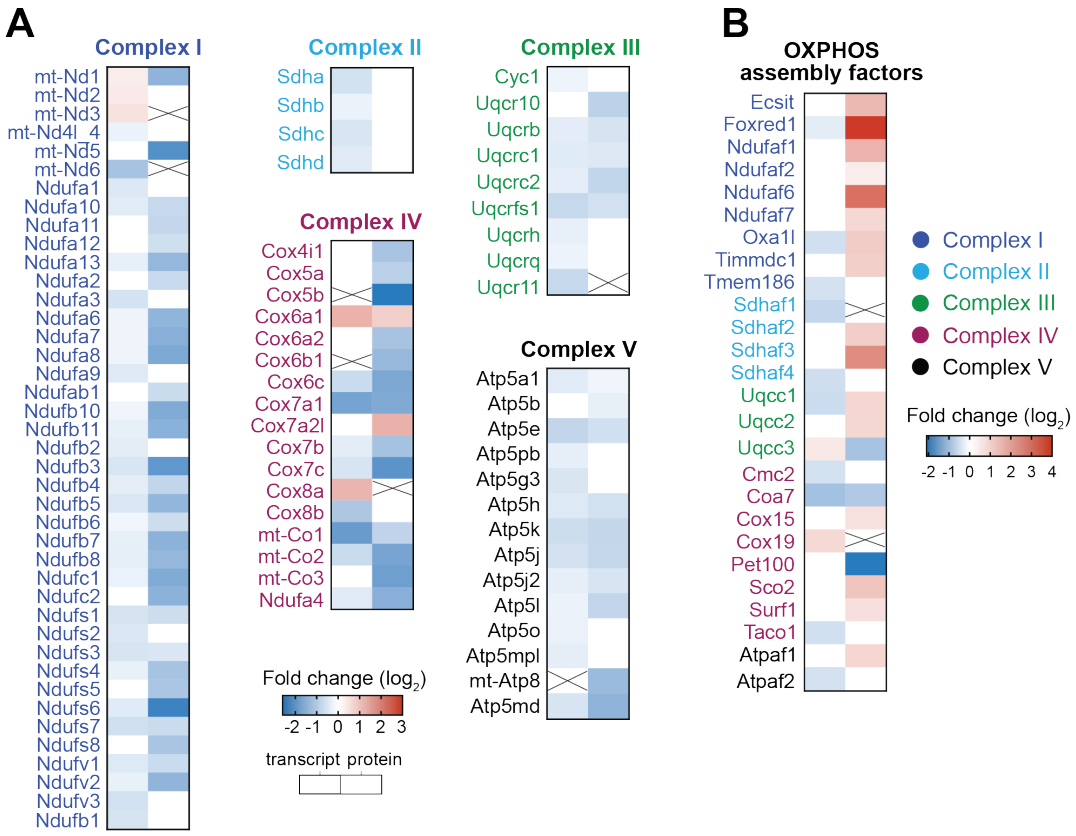


Figure 3.24 | OXPHOS subunits are more affected on the protein level

Heatmaps representing statistically significant log_2 fold changes on transcript (n = 3) and/or protein level (n = 4) of OXPHOS subunits A) and their assembly factors B). White rectangles represent non-significant change, crossed rectangles represent genes that were not detected in the respective dataset. The data plotted in this chart can be found in the **Table 6.2**.

3.5.3.1 Global changes

To obtain a detailed assessment of what drove the complex global changes in the KO heart, we compared the transcriptome and proteome. From 3044 common genes, 848 were significantly changed in both datasets. Out of these genes, 545 were upregulated on both mRNA and protein level while 207 genes were both downregulated (Figure 3.25 A). Unsurprisingly, the most upregulated genes in both datasets represented stress responses, especially ISR (mostly cellular amino acid biosynthesis). Among the least expressed genes were *Synpo2*, *Tmod4,* and *Myot* which are all associated with the cytoskeleton in muscle, and *Ces1d* – a major lipase in the white adipose tissue.

In addition to the aforementioned conclusions from the individual GOBP enrichment analysis, the combined datasets also confirm rewiring of metabolism in the KO heart. The metabolism seems to be fuelled mainly by glycolysis and lipid

biosynthesis while β-oxidation and TCA cycle belong to the pathways that are the most downregulated (Figure 3.25 B).

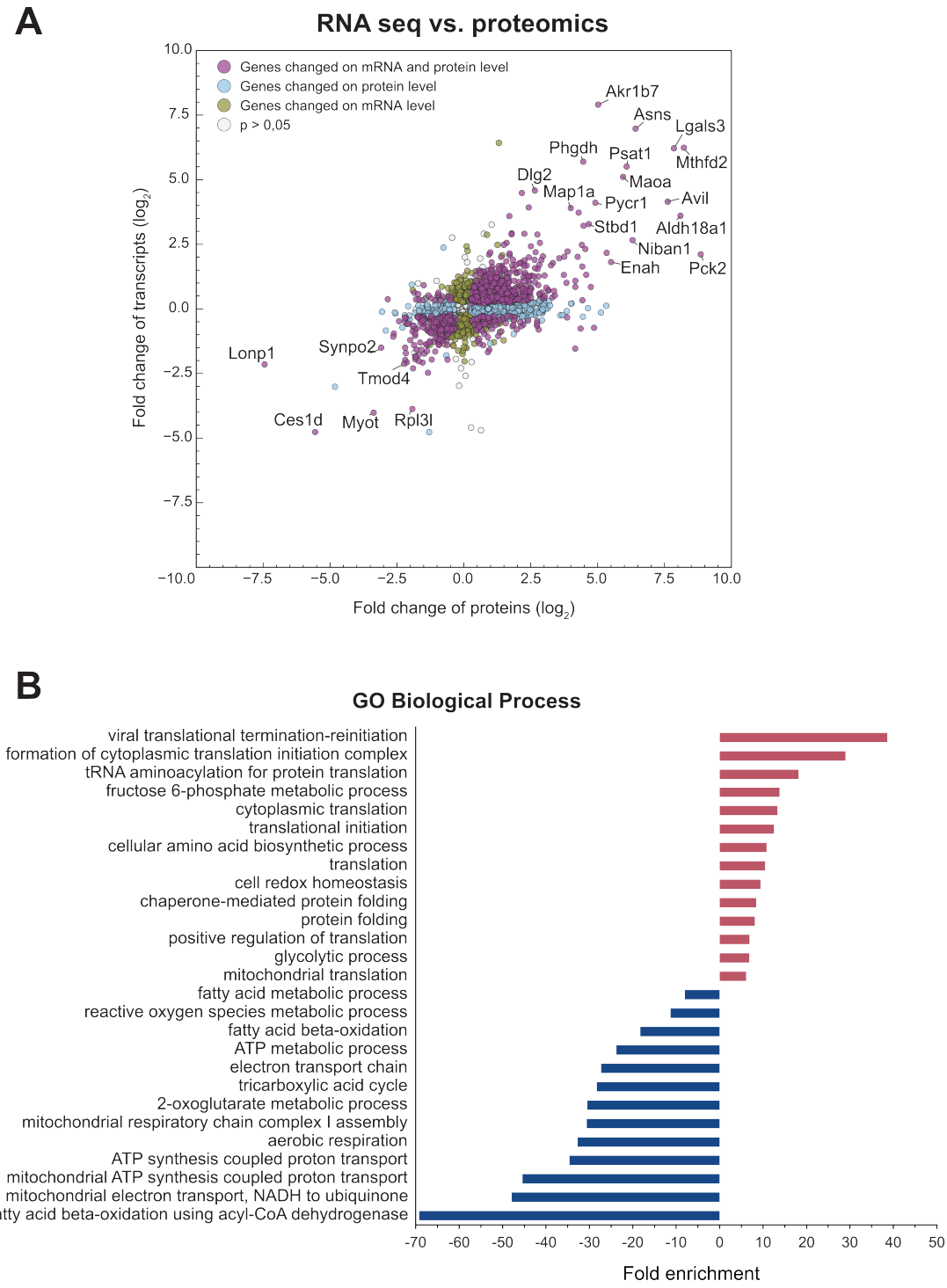


Figure 3.25 | Comparison of the proteomic and transcriptomic datasets from the 8-week-old hearts.

A) A volcano plot – log_2 fold changes of transcripts on Y axis, log_2 fold changes of proteins on X axis. 3044 genes plotted in total. B) GO enrichment for biological processes of genes that are significantly both up- or downregulated on mRNA and protein level to assess systemic changes in expression.

3.5.3.2 Mitochondrially encoded RNAs

Sequencing mtRNAs revealed an interesting finding where different mt genes were affected differently but the changes were not uniform or tied to a specific mtDNA region (Figure 3.26 A). In agreement with the increased levels of mtLSU proteins, the steady-state levels of 16S rRNA (*mt-Rnr2*) were upregulated by 127%. Surprisingly, the steady-state levels of 12S rRNA (*mt-Rnr1*) were decreased to 27% of the WT level. As for the protein-coding mt-mRNAs, only *mt-Nd5* (CI), *mt-Cytb* (CIII), *mt-Co3* (CIV), and *mt-Atp8_6* (CV) levels were not significantly changed. Strangely, the mRNA levels of *mt-Nd1*, *mt-Nd2,* and *mt-Nd3* (CI) were increased by ~1.3-times, whereas *mt-Nd4l_4*, *mt-Nd6* of CI, and *mt-Co1*, *mt-Co2* of CIV were reduced to 79-26% of the WT mt-mRNAs. Overall, given the very different changes in mtRNA levels, which are not reflected in mt-protein levels (Figure 3.26 B), there is probably a very complex level of regulation of mitochondrial gene expression by LONP1.

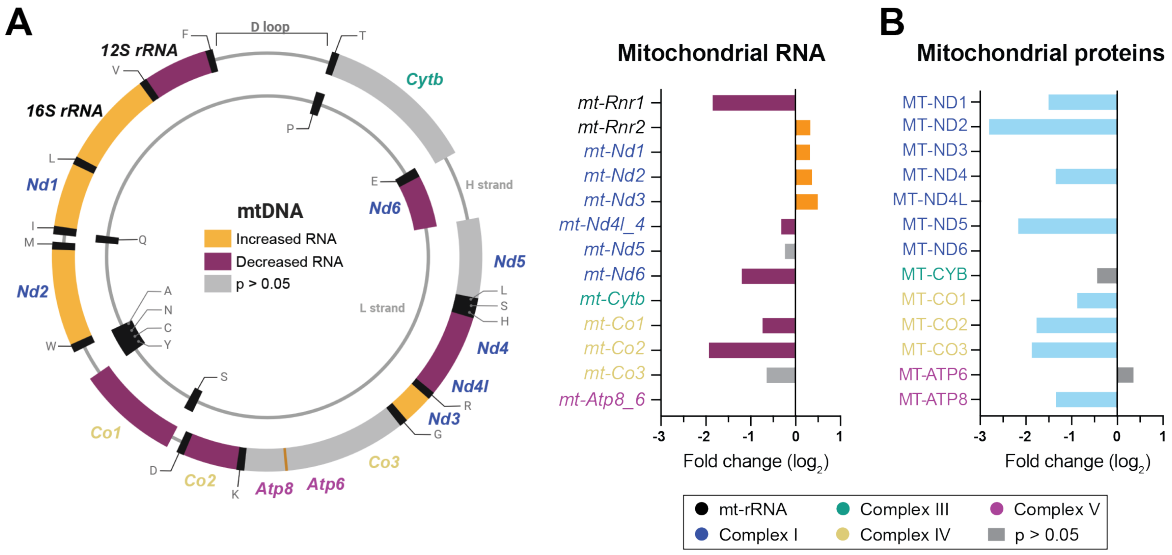


Figure 3.26 | Comparison of changes of mitochondrially encoded genes on transcript and protein level

A) On the left: A scheme of mtDNA including colour-coded changes of the transcripts; on the right: transcriptomic log_2 fold changes; n = 3. B) Proteomic log_2 fold changes; n = 4. Statistically non-significant changes are represented by empty fields or grey colour.

The comparative analysis was applied also on the enzymes involved in mitochondrial gene expression. In total, 160 genes covering the entire pathway were analysed. Generally, the loss of LONP1 affected the whole pathway – 126 genes were changed on the mRNA and/or the protein level (Figure 3.27). The changes occurred mainly on the protein level where 112 proteins were altered. Interestingly, a decrease in protein levels was observed only in 3 of them – TFAM, TUFM, and NDUFAB1. The transcriptome was changed to a lesser degree and the alterations were more diverse. Majority of the transcriptomic changes occurred in the genes encoding for enzymes that process mtRNA and in mitoribosomal transcripts.

Regarding the mitoribosomal subunits, although a few transcripts were decreased, almost all the significantly affected subunits increased on the protein level. That further supports the theory of LONP1 being involved in the assembly and stability of the 55S mitoribosome as the subunits seem to accumulate and their surge is most probably not a response to the cellular needs.

Essentially, those genes that were not regulated transcriptionally, but accumulated on a protein level could be candidates for LONP1 *bona fide* substrates.

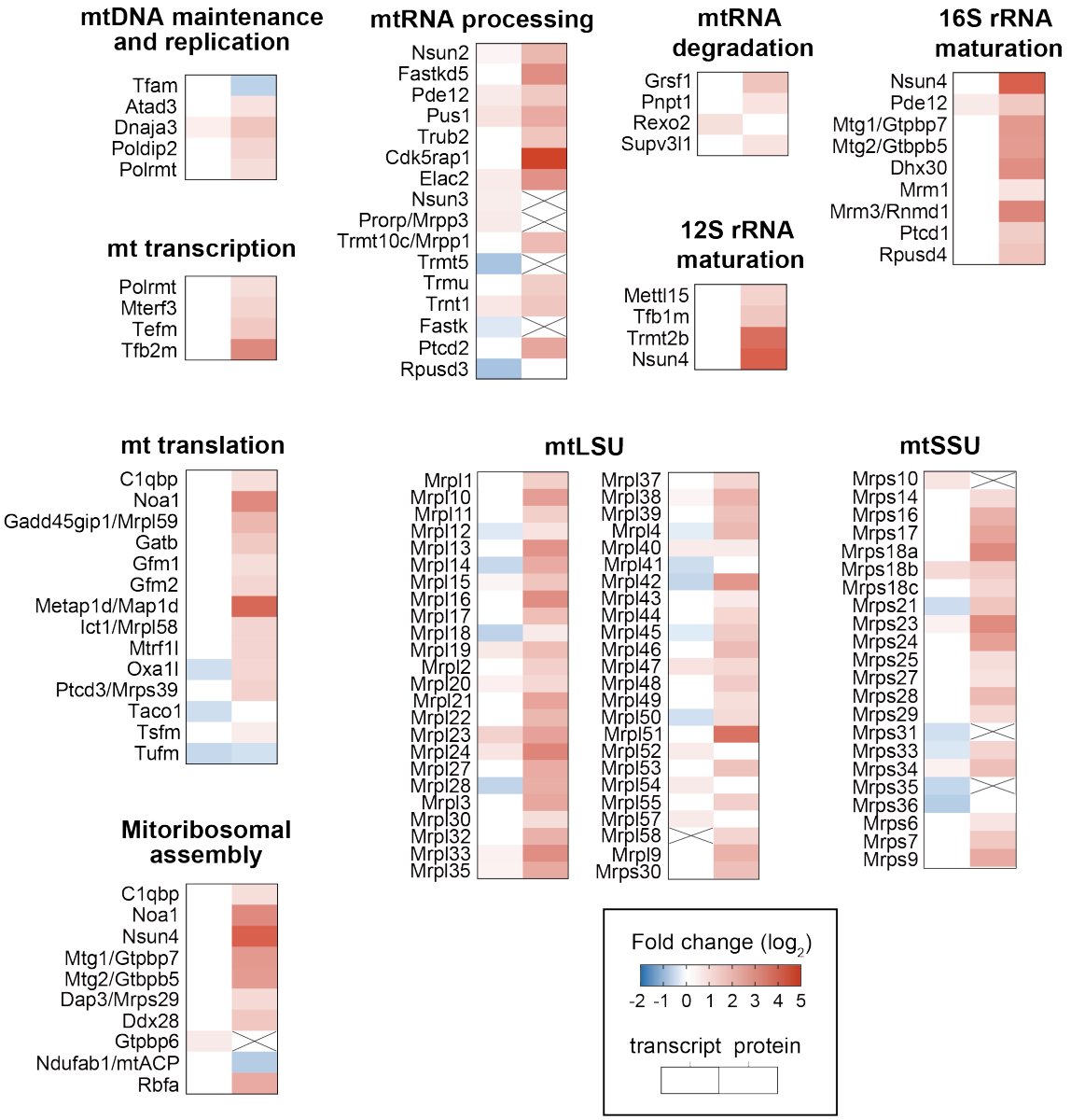


Figure 3.27 | Comparison of changes of genes in mitochondrial gene expression machinery on transcript and protein level

Heatmaps representing statistically significant $\log_2$ fold changes on transcript (left column; n = 3) and/or protein (right column; n = 4) levels. Genes are categorized according to their involvement in individual processes. White rectangles represent non-significant change, crossed rectangles represent genes that were not detected in the respective dataset. The plotted data can be found in the supplementary **Table 6.1.**

3.6 Investigating the insoluble proteins in LONP1 KO

The investigation of the mitochondrial ultrastructure led to a detection of the electron dense occlusions in the TEM images (Figure 3.6 A). Considering that these mitochondria lacked the LONP1 protease, it is possible that these occlusions are aggregated proteins. To determine whether the KO cardiac mitochondria contain insoluble proteins, crude mitochondria freshly isolated from 8-week-old hearts were treated with 0.5% Triton-X and centrifuged at 125 000 × *g* to pellet proteins that were not solubilized by the detergent. The total lysate (input) and the insoluble fraction (pellet) were sent to a proteomic analysis. In total, 1208 proteins were detected, 710 were mitochondrial (Figure 3.28 A). It is not surprising that protein levels are overall increased in the KO input when compared to the WT input. As a control whether the isolation of the insoluble proteins was successful, the WT pellet was correlated with the WT input (Figure 3.28 B). Only two proteins were significantly enriched in the WT pellet fraction, while 522 proteins were more present in the WT input fraction. This shows that majority of the proteins in the WT remained soluble.

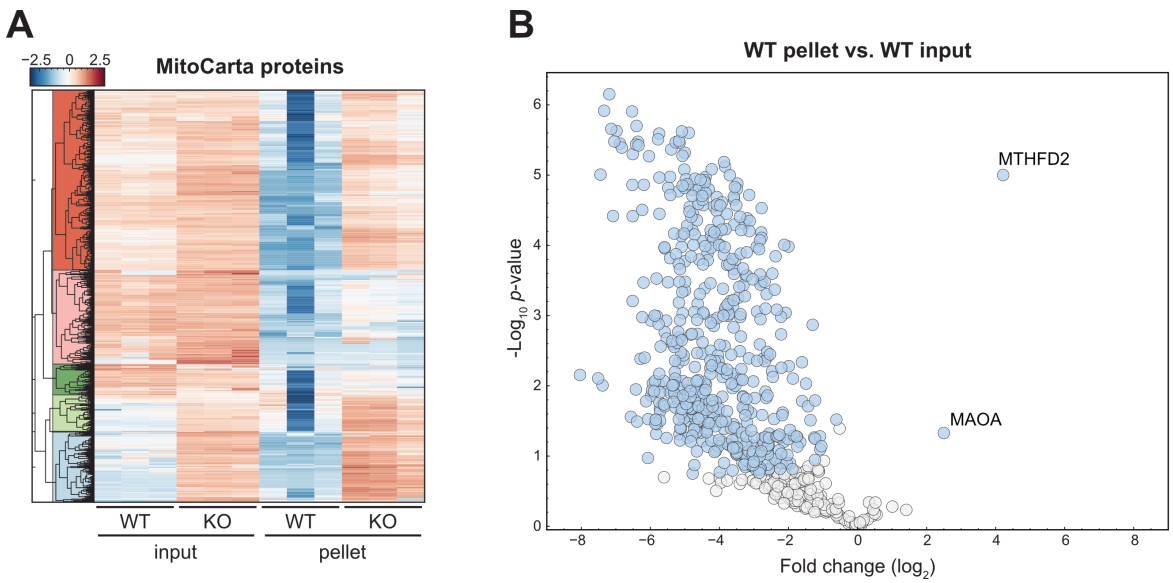


Figure 3.28 | A proteomic analysis of insoluble proteins in the LONP1 KO cardiac mitochondria

A) Hierarchical clustering of *Z*-scores of log_2-transformed LFQ intensities of 710 mitochondrial proteins treated by 0.5% Triton-X (input). Proteins not dissolved by the detergent were pelleted by ultracentrifugation (pellet); n = 3. B) A volcano plot comparing WT mitochondrial proteins from the pellet and the input. Only 2 proteins were significantly enriched in the WT pellet, the majority of proteins (708) remained soluble.

To pool the insoluble proteins that were enriched in the KO pellet, the KO pellet was first compared to WT pellet. Out of 531 significantly changed proteins, only one protein was significantly decreased in the KO pellet (Figure 3.29 A). Next, the enrichment of proteins in KO pellet in comparison to the KO input were analysed (Figure 3.29 B). There, 461 proteins were significantly changed and 121 were increased in the KO pellet. To make sure only the most insoluble proteins will be inspected, both datasets were matched together to filter out the proteins most enriched in the KO pellet (Figure 3.29 C).

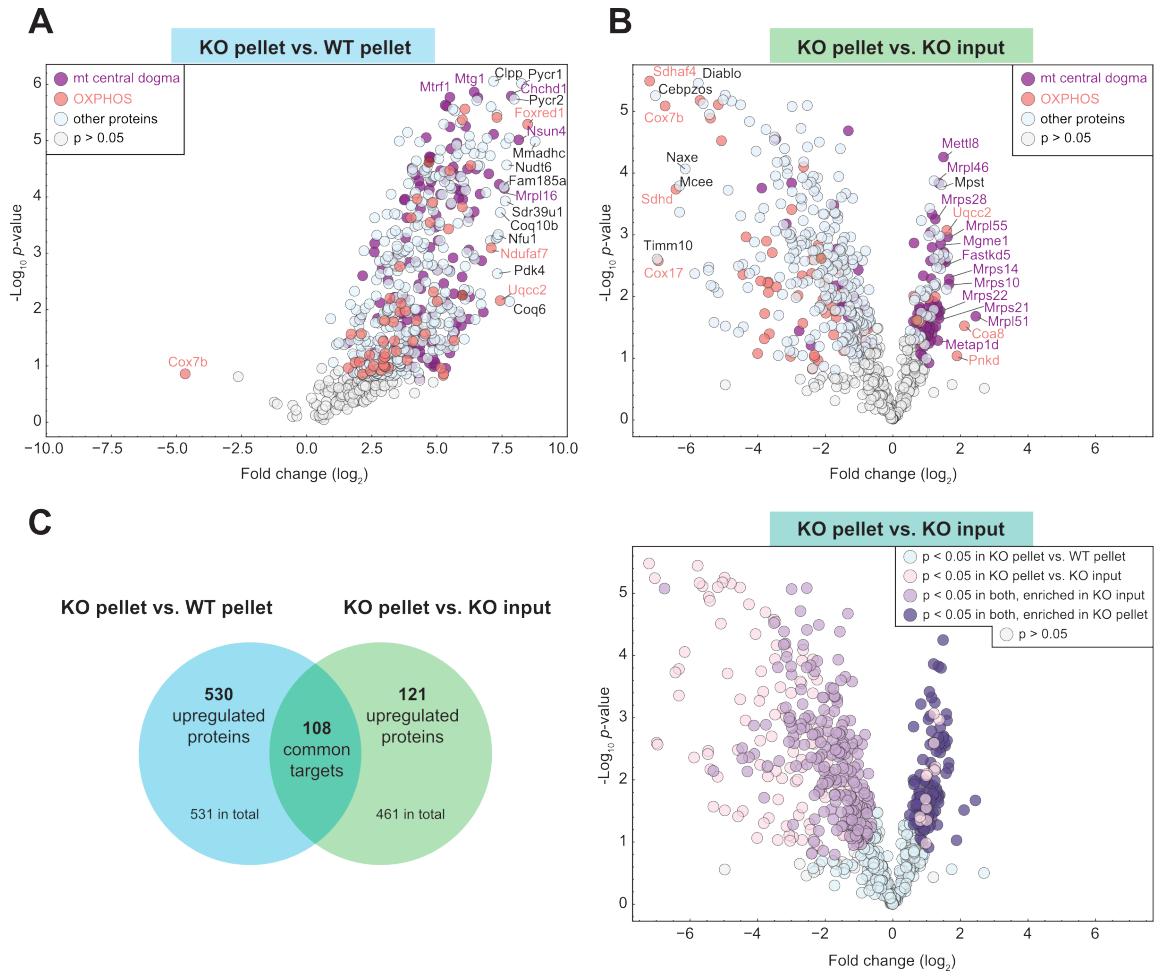


Figure 3.29 | Pooling the most interesting insoluble targets

A) A volcano plot representing the comparison of the insoluble fractions (WT and KO pellet), where 530 proteins were significantly enriched in the KO pellet. B) A volcano plot representing the comparison of KO pellet vs. KO input, where 121 proteins were enriched in the KO pellet. C) On the right: A volcano plot representing the comparison of KO pellet vs. KO input overlayed with the enrichment of the KO pellet from A) – only 108 proteins were enriched in the KO pellet in both of these datasets. On the left: A summary.

In the end, these two datasets contained 108 common targets which were sorted according to the MitoCarta 3.0 pathways (Figure 3.30). Most of these targets are enzymes involved in the mitochondrial central dogma with mtLSU and mtSSU subunits being the most prominent protein groups. Other targets included proteins involved in

mitochondrial metabolic pathways, protein import and homeostasis, and also OXPHOS proteins.

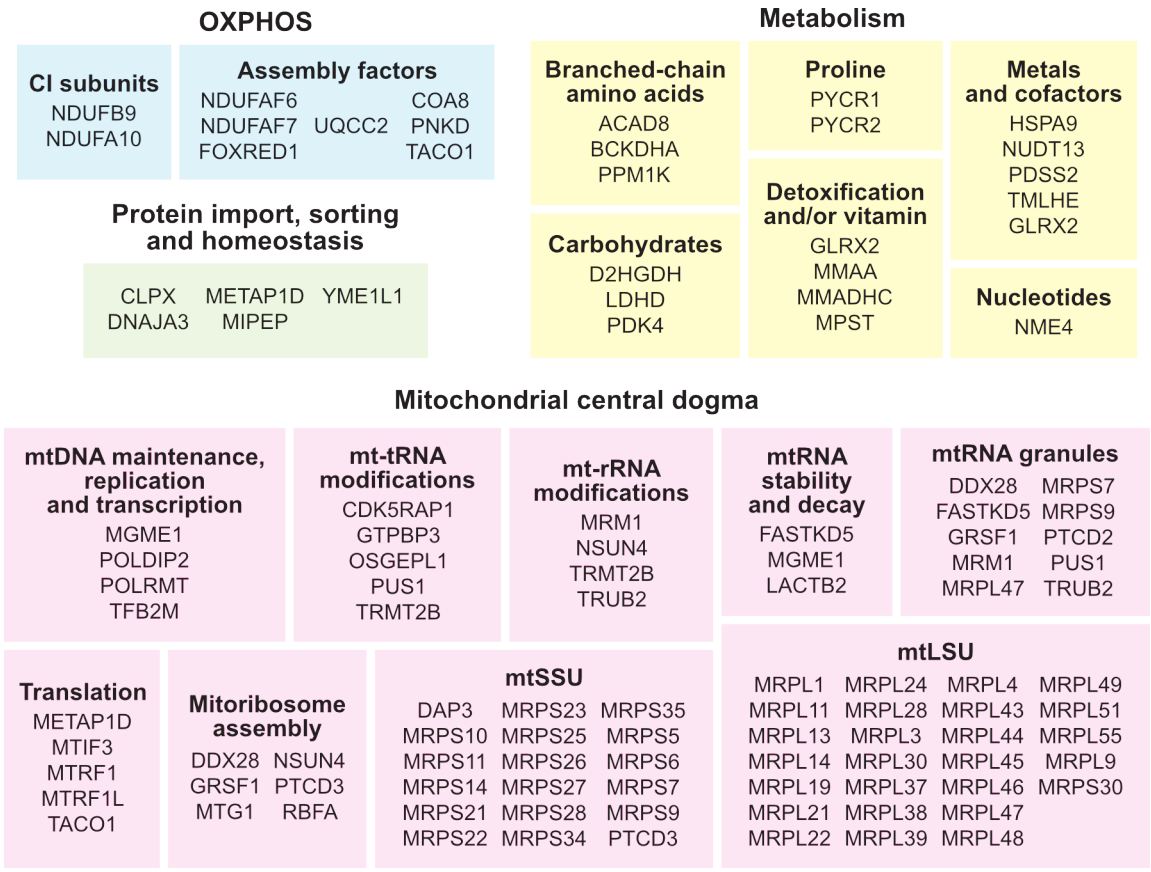


Figure 3.30 | All 108 targets identified in the proteomic analysis of the insoluble mitochondrial proteins

The proteins are categorized according to the MitoPathways defined in MitoCarta 3.0. The data for this chart can be found in the supplementary **Table 6.3**.

3.6.1.1 Comparative analysis

In the search of LONP1 substrates, the proteomic and transcriptomic datasets were matched and screened for those genes that were not changed on the transcript level but have accumulated on the protein level (Figure 3.31 A). This comparison yielded 184 targets that were consequently correlated to the 108 insoluble proteins enriching the KO pellet. These two datasets narrowed the list of the promising substrates to 54 proteins (Figure 3.31 B). As seen on the list, most of these targets are the proteins involved in the mitochondrial central dogma, which highly implicates LONP1 as an important regulator of the mitochondrial gene expression. However, whether these proteins are LONP1 targets and the mechanism of the possible regulation the mitochondrial gene expression by LONP1 remain to be elucidated.

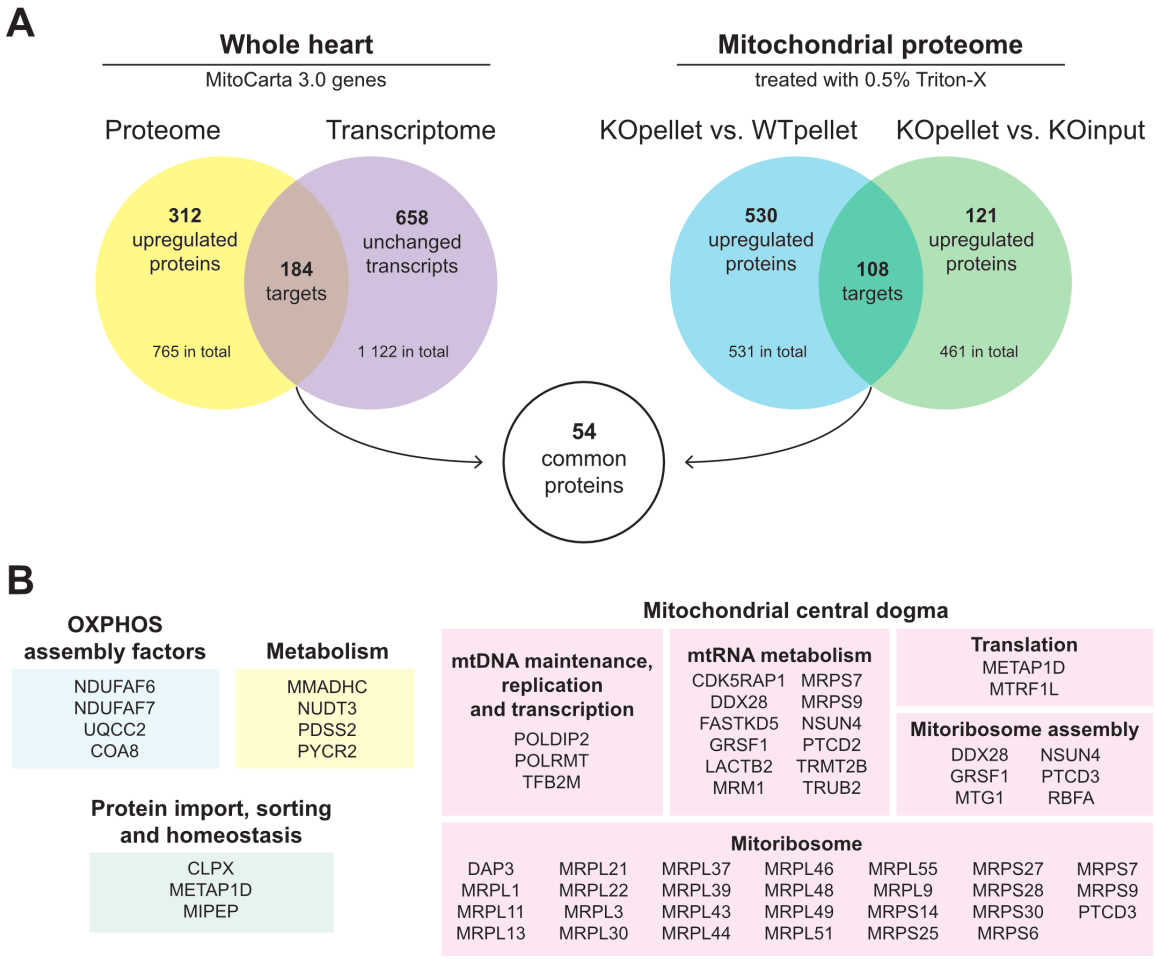


Figure 3.31 | An OMICS approach to identify the most interesting candidates for LONP1 substrates

A) A summary of the comparative approach. 184 mitochondrial targets from the comparison of the heart proteome and transcriptome were correlated to the previously described list of 108 insoluble proteins. That revealed 54 proteins common for both of these datasets. These proteins are listed in B) and are categorized according to the MitoPathways defined in MitoCarta 3.0. The data for this chart can be found in the supplementary **Table 6.4**.

4 Discussion

This project studied LONP1 and its function in the mammalian mitochondria. The goals were to establish a model for LONP1 deficiency, and to describe the roles of LONP1 in OXPHOS, in protein quality control, and mainly in mitochondrial gene expression.

We confirmed that *Lonp1* is an essential gene as the knockout-first embryos died at E8.5, which was previously reported in mice deficient for *Lonp1* (Quiros et al., 2014). Embryonic lethality around E8.5 and before E10.5 has been shown for multiple mouse models with severely disrupted mitochondrial gene expression caused by a whole-body depletion of the respective gene (Table 4.1).

Table 4.1 | Mouse models of mitochondrial gene expression.

gene	function	mean survival	reference
Tfam	mtDNA packaging, transcription factor	20 days	(Wang et al., 1999)
Elac2	Phosphodiesterase, tRNA maturation	4 weeks	(Siira et al., 2018)
Polrmt	RNA polymerase	6 weeks	(Kuhl et al., 2016)
Dars2	Asp-tRNA ligase	7 weeks	(Dogan et al., 2014)
Tefm	Transcription elongation factor	9 weeks	(Jiang et al., 2019)
Ptcd1	16S rRNA stability, processing, mtLSU biogenesis	10 weeks	(Perks et al., 2017)
Mrpp3	Endonucleolytic cleavage of tRNAs at their 5'-end	11 weeks	(Rackham et al., 2016)
Lrpprc	mRNA stability	16 weeks	(Ruzzenente et al., 2012)
Ssbp1	Single-strand-binding protein	18 weeks	(Jiang et al., 2021)
Mterf3	Transcription termination factor	18 weeks	(Park et al., 2007)
Twnk	mtDNA helicase	19 weeks	(Milenkovic et al., 2013)
Tfb1m	Dimethylation of 12S rRNA	24 weeks	(Metodiev et al., 2009)
Mterf4	Maturation of mtLSU	24 weeks	(Camara et al., 2011)
Nsun4	Methylation of 12S rRNA, maturation of mtLSU	25 weeks	(Metodiev et al., 2014)
Mtif3	Translation initiation factor	25 weeks	(Rudler et al., 2019)

Listed are essential genes that were depleted in heart and skeletal muscle-specific conditional knockout mice.

We then generated a conditional knockout mouse using a Cre recombinase under the control of muscle creatinine kinase (CKMM) promoter. This promoter becomes active after E13 (Li et al., 2000).We showed that loss of LONP1 in the heart and

skeletal muscle leads to a dilated cardiomyopathy, a body weight loss observed already at 8 weeks of age, and a decreased heart weight at 20 weeks of age. That is an unexpected discovery. An enlarged heart causing an increased heart weight to body weight ratio is the hallmark of dilated cardiomyopathy caused by the tissue-specific disruption of mitochondrial gene expression. The models and their life expectancies are listed in the Table 4.1.

The KO animals have a shortened lifespan – most animals must be humanely sacrificed at ~22–23 weeks (median survival = 30 weeks) due to ethical reasons. At the end point, the KO mice suffered from a significant weight loss which was caused by a probable loss of muscle mass and fat. These observations might be the symptoms of cachexia, which is defined by a weight loss, a depletion of adipose tissue and is sometimes accompanied by a muscle waste (sarcopenia) (Molinari et al., 2016, von Haehling et al., 2017). For comparison, the lifespans of the other heart models range from 20 days (*Tfam*) to 25 weeks (*Nsun4*) (Table 4.1).

Previous experience with CKMM driven Cre recombination showed delayed depletion of respective proteins in skeletal muscle comparing to heart (Wang et al., 1999). Therefore, we focused our initial studies on heart. The transcriptomic and proteomic analyses in the 8-week-old hearts revealed a global upregulation of proteins associated with stress responses – the most expressed proteins are the markers of the cellular amino acid biosynthesis and the integrated stress response (e.g., MTHFD2, ASNS, ALDH18A1, PCK2 (Forsström et al., 2019, Yu et al., 2021)), glycophagy – a specific form of autophagy (STBD1 (Koutsifeli et al., 2022)), chronic heart failure (LGALS3 (Sato et al., 2022)), and regulation of autophagy and apoptosis (NIBAN1 (Diana and Carvalheira, 2022)). The presence of the integrated stress response and inhibition of the cytoplasmic translation was also confirmed by immunoblot experiments. The gene ontology analysis of upregulated proteins further showed an enrichment in pathways involved in cytoplasmic and mitochondrial translation, but also pathways associated with proteotoxic stress – cell redox homeostasis and protein folding.

On the contrary, the most downregulated proteins are associated with cytoskeleton in the muscle (TMOD4, MYOT (Ochala et al., 2009, Almenar-Queralt et al., 1999)) and lipid metabolism (CES1D (Li et al., 2022)). The GO analysis of the downregulated proteins identified tricarboxylic acid cycle (TCA), fatty acid β-oxidation (FAO), and OXPHOS to be the most downregulated pathways in the LONP1 KO heart. Downregulating of these pathways together with the upregulated steady state levels of PCK2 and glycolytic proteins indicate a metabolic switch in the LONP1 KO heart.

4.1 LONP1 in OXPHOS

We showed that absence of LONP1 resulted in an overall loss of OXPHOS proteins that contain mitochondrially encoded subunits, especially CI and CIV. This loss was proportionally reflected in the amounts of assembled complexes. It also led to an accumulation of a CV subcomplex which is probably the free F1 stalk in the BN-PAGE analysis. The free F1 stalk was observed repeatedly in the models with an impaired

mitochondrial gene expression – Lon KD in *Drosophila* (Pareek et al., 2018) and also mouse models TFB1M KO (Metodiev et al., 2009), LRPPRC KO (Ruzzenente et al., 2012), DARS2 KO (Dogan et al., 2014), or TWNK KO (Milenkovic et al., 2013). The accumulation of the F1 stalk is probably a stress response to the OXPHOS dysfunction. It is likely a newly synthesized subcomplex possibly to maintain the membrane potential. The OXPHOS impairment caused a decrease *in gel* activity of CI and CIV, and also a lower respiratory rate.

Interestingly, we also observed a global decline of the OXPHOS transcripts, although CI and CIV are more affected on the protein level. As for CIII and CV, the scale of changes on both transcriptional and protein levels is comparable. Surprisingly, there was also a significant decrease of all four CII transcripts despite the protein complex not being altered. This global effect does not apply to the steady-state levels of mitochondrially encoded transcripts – although 8 of the 13 mt-proteins were decreased, only 4 mt-mRNAs were also decreased, while 3 mt-mRNAs were upregulated. The observed mt-mRNA levels also do not translate to the *de novo* protein synthesis, which is overall only mildly decreased. It is seemingly only the proteins ND1, ND3, COX1, COX2, and COX3 which are less synthesized. This mild decrease in the translation is probably not the sole cause of the global loss of OXPHOS proteins. The only mitochondrial gene that was unaffected on both transcriptional and protein level, was *mt-Cyb*.

Many assembly factors are upregulated on the protein level which could be a compensatory mechanism for the OXPHOS depletion, but the lack of upregulated transcripts of these genes indicates that this is not a transcriptionally activated response. It is possible that the proteins simply accumulate because they are not being turned over by LONP1. For example, SDHAF2 (also known as SDH5) is degraded by LONP1 when not bound to SDHA (Bezawork-Geleta et al., 2014). There are also three assembly factors that are decreased on the protein level – UQCC3, COA7 and PET100. COA7 was shown to interact with LONP1 (Formosa et al., 2022). Here, it could be hypothesized that the chaperone-like activity of LONP1 might be needed to stabilize COA7.

As for the ways how LONP1 regulates OXPHOS subunits, there are a few examples from the literature. It has been shown that some OXPHOS proteins are degraded by Lon proteases. Yeast LONP1 homologue PIM1 degrades Atp1, Atp2 (α- and β-subunits of CV), Rip1, Qcr2 (Rieske and core protein 2 of CIII) (Bayot et al., 2010). It has been proposed that LONP1 could be involved in the regulation of Fe-S clusters. For example, SDHB, an Fe-S containing subunit of CII, was proposed as an LONP1 target upon loss of SDHAF1, an assembly factor of CII (Maio et al., 2016). As another example, LONP1 was shown to interact with NDUFS8, an Fe-S containing subunit of CI (Kao et al., 2015). Other bona fide OXPHOS targets include COX4i1 and COX5B in hypoxia after being phosphorylated by PKA (Sepuri et al., 2017, Fukuda et al., 2007). Beside directly turning over OXPHOS subunits, LONP1 has been shown to process newly imported OXPHOS proteins and promote their folding together with mtHSP70 (Zurita Rendon and Shoubridge, 2018, Shin et al., 2021a).

Catalytically inactive Lon promotes assembly with its chaperone-like activity as it was shown for CV in yeasts (Rep et al., 1996). Lon proteases might also indirectly determine OXPHOS levels by regulating key steps of mitochondrial gene expression. Pim1 proteolytic activity is required for translation of Cox1 possibly by processing precursors of translation proteins, or even RNA-binding proteins which block the mt-mRNAs from being translated (van Dyck et al., 1998). Pim1 targets mS38 (homolog of MRPS38) which facilitates translation of Cox1, Cox2 and Cox3 (Mays et al., 2019).

In our model, the decreased mRNA steady-state levels indicate an overall attenuated expression of nuclear encoded OXPHOS proteins. As shown in the GO terms enrichment analyses, LONP1 KO is undergoing a metabolic switch. The general downregulation of OXPHOS could be another branch of this switch which is a stress response to the respiratory dysfunction. That would also explain why we observe the CII transcript levels downregulated as well. However, this does not solely explain the even greater decline of OXPHOS protein levels. It is possible that due to the decreased expression of the mitochondrially encoded OXPHOS core subunits fewer complexes can be assembled in general. Furthermore, as CI and CIV were more affected than the other complexes, this indicates a specific role for LONP1. Besides the indicated roles in the regulation of OXPHOS translation and the chaperone-like function, LONP1 could be important for the turnover of OXPHOS assembly factors. This would mean that without LONP1 the complexes might be stabilized as assembly intermediates. As such, the intermediates might not be allowed to pass a quality control checkpoint and therefore they disassemble, and individual proteins are then degraded by other proteases.

4.2 LONP1 in mt gene expression

The defective OXPHOS and the mild reduction in mitochondrial translation in LONP1 KO was indicative of more disturbances in the mitochondrial gene expression machinery. Unlike the deletion of *pim1* in yeast (Suzuki et al., 1994), the loss of *Lonp1* in the mouse heart did not cause any changes in the mtDNA levels. However, it did result in a 1.5-times increase of the *de novo* mt-RNA synthesis. On the other hand, the de novo synthesis of mitochondrial proteins was downregulated.

Similarly, without changing the mtDNA/ncDNA ratio, the downregulation of *Lon* in *Drosophilae* led to a decrease in CI and CIV activity and a decrease in mitochondrial translation (Pareek et al., 2018). Pareek et al. also observed increased levels of steady-state levels of mtRNAs and a considerable amount of these mtRNAs sedimenting to the bottom fraction in a sucrose density fractionation without co-migrating with the 55S mitoribosome. They hypothesize that the mitochondrial translation is not efficient enough to process all the mtRNAs which results in the subsequent respiratory defect (Pareek et al., 2018).

4.2.1 LONP1 in mitoribosomal biogenesis

Seeing the translational defect and the respiratory deficiency in the LONP1 KO, we also analysed mitoribosomal proteins (MRPs). MRPs were part of a protein group that

was identified by the GO analysis as one of the most upregulated biological processes. There was a general upregulation of MRPs in the LONP1 KO heart detected in the immunoblots and in the proteomic analyses.

The accumulation of MRPs was described also in the following mouse heart models – LRPPRC (Ruzzenente et al., 2012), MTERF4 (Kuhl et al., 2017), and CLPP (Szczepanowska et al., 2016). Interestingly, absence of LONP1 increased mainly mtLSU subunits, while the other models experience a surge of mainly mtSSU subunits. Studies in yeasts have identified three PIM1 mitoribosomal substrates – Mrp20 (Bayot et al., 2010), Mrpl32 (Kunova et al., 2017), and mS8 (Mays et al., 2019). These proteins are the homologues of MRPL23, MRPL32, and MRPS38 (also known as AURKAIP1) in mammals. MRPS38 as a possible substrate implies that LONP1 could be also involved in the regulation of mtSSU. A co-immunoprecipitation study also showed LONP1 to be interacting with 11 mtLSU proteins (Zurita Rendon and Shoubridge, 2018). CLPP also allows for the efficient assembly of mtSSU by removing ERAL1, a 12S rRNA chaperone (Szczepanowska et al., 2016). Our data suggest that, similarly as CLPP, LONP1 could be regulating the assembly of mtLSU by targeting an assembly factor of mtLSU. It also proposes a possibility of two mitochondrial matrix proteases working together and complementing each other in the regulation of the mitoribosomal assembly.

Our analysis of the mitoribosomes demonstrated the majority of the MRPLs to be present in the 39S fractions, although a fully assembled mitoribosome is also detected. We observed a weak mtSSU band in the 28S fraction in the KO mitochondria. This band was not seen in the WT, but that is caused by the poorly performing mtSSU antibodies. However, proportionally this slight increase of mtSSU in the LONP1 KO also reflects the mild accumulation of mtSSU proteins observed in the proteomics. The transcriptomic analysis revealed a mild upregulation by 27% of the 16S rRNA which is in accordance with the increase of assembled mtLSU. Intriguingly, the 12S rRNA was reduced by 73%, but the 28S ribosome fraction was also increased. The accumulation of MRPs might be a mechanism to compensate for the impaired assembly and defective translation.

Most of the detected factors for 12S rRNA, 16S rRNA maturation and the assembly of mitoribosomes are accumulated on the protein level while not being changed on the transcript level. This could be one of the possible explanations as to why is the assembly impaired – perhaps the presence of any of these factors, if functional, could keep the mitoribosomal intermediates in immature conformations. Another possibility might be that all these factors are upregulated because mitoribosomal assembly is defective. It is possible that LONP1 regulates an important checkpoint in 39S assembly, where LONP1 assists the removal of a specific factor. When this does not happen, the mtLSU accumulates, but is not correctly assembled and cannot form proper fully assembled mitoribosome. Similar mechanism was observed for 28S/ERAL1 and CLPP (Szczepanowska et al., 2016).

Contrastingly, in a cell model with transient *Lonp1* silencing, the authors observed a different molecular phenotype (Zurita Rendon and Shoubridge, 2018). They reported

a progressive loss of mtDNA, a decrease of both 12S and 16S rRNA steady-state levels, and mainly, this transient depletion resulted in a decrease of MRPs and a partial loss of the fully assembled mitoribosome. The latter observation is in a direct opposition to our own observation. This discrepancy can be explained by the different complexity of used models. However, LONP1's importance for the stability and biogenesis of mitoribosomes is apparent.

4.2.2 LONP1 in RNA processing

Not only MRPs, but also other proteins contributing to mitochondrial gene expression were mostly upregulated in LONP1 KO mitochondria. The most notable increases detected by proteomics are CDK5RAP1 (25.41-times increase), NSUN4 (16.56-times), TRMT2B (13.18-times), METAP1D (14.72-times), and MRPL51 (12.38-times). As these proteins were not affected on the transcriptional level, they could be potential substrates of LONP1. CKD5RAP1 is a methylthiotransferase which introduces a 2-methylthio group into mt-tRNA^{Phe}, mt-tRNA^{Trp}, mt-tRNA^{Tyr}, and mt-tRNA^{Ser} in mammalian mitochondria (Wei et al., 2015). NSUN4 is an essential methyltransferase which coordinates mitoribosomal assembly by methylation of 12 rRNA, and in a complex with MTERF4 binds to an immature mtLSU at the late stage of the assembly and serves as a final checkpoint to ensure proper folding of the mtLSU intermediate (Metodiev et al., 2014, Cipullo et al., 2021, Cheng et al., 2021). TRMT2B is a dual specificity RNA methyltransferase which can modify not only 12S rRNA, but also a number of mt-tRNAs (Powell and Minczuk, 2020, Laptev et al., 2020). METAP1D is a methionyl aminopeptidase which removes N-terminal methionine from mitochondrial proteins (Serero et al., 2003). MRPL51 is a mtLSU protein which was shown to interact with OXA1L (Haque et al., 2010). It is hard to assume what consequences can the accumulation of the RNA transferases have. The study of the regulation of mtRNAs is a fast-growing field, but there is still a lot to uncover (e.g., the physiological roles of the mtRNA modifications (Bohnsack and Sloan, 2018)). It is possible, that we are observing an increase of the 28S and 39S mitoribosomes, but not an increase in the 55S monosome, because these modifications are stabilizing the late mitoribosomal assembly intermediates. Without a factor (e.g., a protease) to remove the acting enzymes, the mitoribosomal assembly might have difficulties to proceed, especially in the case of NSUN4 (Camara et al., 2011). The drastic increase in these possible LONP1 substrate could be also due to these substrates accumulating in insoluble aggregates. The aggregation could then impair their proper function, which would also lead to a translation defect.

4.2.3 LONP1 and TFAM

An unexpected discovery is the protein levels of TFAM, which were surprisingly not significantly changed in the immunoblot analysis. Furthermore, the protein levels were even decreased to ~60% of WT in the proteomic analysis, although the mRNA levels are unchanged. That is a puzzling observation as TFAM was shown to be a target of LONP1 in *in vitro* studies (Zhao et al., 2022, Zurita Rendon and Shoubridge, 2018,

Gibellini et al., 2014). When TFAM is not bound to mtDNA and is phosphorylated by PKA, it is then recognized by LONP1 (Matsushima et al., 2010, Lu et al., 2013). Moreover, some other studies also report downregulation of TFAM when LONP1 is depleted (Zhao et al., 2022, Zurita Rendon and Shoubridge, 2018, Gibellini et al., 2014). This might imply that there is another protease or mechanism that contributes to the turnover of TFAM.

It is widely accepted that TFAM levels correlate with mtDNA levels as TFAM packages mtDNA into nucleoids (Kukat et al., 2015). The TFAM:mtDNA ratio also directly influences the replication and transcription rates *in vitro* and *in vivo* (Matsushima et al., 2010, Bruser et al., 2021, Bonekamp et al., 2021). Indeed, it was shown that that high TFAM levels in the heart led to the increase of the mtDNA levels (Bonekamp et al., 2021). The authors propose that TFAM:mtDNA ratio is maintained to allow for a proper function of mitochondrial transcription (Bonekamp et al., 2021). Manipulating the expression of TFAM to control mtDNA copy number could provide a therapeutic tool to cure human mtDNA mutation diseases (Filograna et al., 2019). The authors demonstrated that increasing the mtDNA levels through manipulation of the TFAM levels can be beneficial. The increased mtDNA levels alleviated mitochondrial pathologies caused by a heteroplasmic mutation although the level of heteroplasmy did not change (Filograna et al., 2019). Another study demonstrated the importance of the absolute mtDNA copy number (Jiang et al., 2017). The mutator mice accumulate random mtDNA mutations throughout their life due to a mutation in POLGγ disrupting the proofreading ability of the exonuclease (Trifunovic et al., 2004). These mice age prematurely, and the males suffer from infertility (Trifunovic et al., 2004). In this study, overexpression of TFAM led to the increase of the mtDNA levels in the mutator mouse (Jiang et al., 2017). The increased mtDNA copy number not only partially rescued the mitochondrial pathologies, but it also cured the infertility in the male mice (Jiang et al., 2017). Because of the therapeutic potential of TFAM, it is important to also study the role of LONP1 in the regulation of TFAM.

In our model, TFAM did not accumulate, and its decrease also did not result in a downregulation of mtDNA levels. This raises a question whether there could be a different protein that is able to stabilize mtDNA as well, but under normal physiological conditions is being degraded by LONP1? Or perhaps is TFAM not depleted enough and is still able to maintain mtDNA? Is TFAM also a substrate of the other proteases that were shown to be upregulated as a response to the mitochondrial stress?

4.2.4 Conclusion of LONP1 in mt gene expression

In general, we think that LONP1 is fundamental to ensure the proper expression of mitochondrial genes. LONP1 seems to be especially important for the regulation of RNA-processing enzymes and mitoribosomal assembly. Because the RNA processing and mitoribosomal assembly are dysfunctional, the mitochondrial translation is inefficient. That leads to the respiratory defect. It is possible that the mitochondrial transcription is upregulated to compensate for the translational defect. However, we have not observed an increase of mtDNA copy numbers. This suggests that the

increase in *de novo* mtRNA synthesis is a result of the lack of regulation of this process. This is also supported by the steady-state levels of mtRNAs which are not generally upregulated. The diverse changes in the mtRNA levels could also indicate that the individual RNAs are processed by different transcription or processing factors which operate through different mechanisms. LONP1 could be responsible for the turnover of these factors or for aiding the function of these factors.

LONP1 depletion led to the accumulation of mtLSU proteins and also mtSSU proteins to a lesser extent. We also observed an increase in the 39S and 28S ribosome levels. It could be hypothesised that this increase is there to compensate for the dysfunctional translation. However, the surge of MRPs does not originate from an upregulated transcription of these genes. Although the individual mitoribosomal subunits accumulated, we have not observed increased levels of the fully assembled mitoribosome. It seems that there is a lack of a turnover of the MPRs. Although they seem to assemble into mtLSU and mtSSU, what we observe could be in fact late assembly intermediates which are stabilized by the upregulated assembly factors. As the assembly factors are not dissociated and degraded (by LONP1), the mitoribosomal subunits cannot finish the assembly. Furthermore, the fully assembled 55S ribosome is potentially functionally defective as the translation in the LONP1 KO is not efficient, which suggests a faulty quality control in the mitoribosomal assembly. It is also important to note that many if not the most of the MRPs and their assembly factors were detected in the insoluble pellets in the LONP1 KO mitochondria. This would probably deem them dysfunctional.

4.3 LONP1 in protein quality control

Transmission electron microscopy images revealed very defined electron dense occlusion in the LONP1 KO hearts. These occlusions of various definition were observed in other LON-deficient models (cells, heart and skeletal muscle, patient samples) as well (Suzuki et al., 1994, Zurita Rendon and Shoubridge, 2018, Hannah-Shmouni et al., 2019, Zhao et al., 2022). It has been proposed that these are misfolded proteins that aggregate due to the absence of LONP1. LONP1 was already shown to remove oxidatively damaged aconitase before it forms insoluble aggregates (Bota and Davies, 2002).

To test this, we lysed LONP1 mitochondria with 0.5% Triton-X and then pelleted the detergent-resistant proteins with an ultracentrifuge. These insoluble proteins and the total lysate were analysed with mass spectrophotometry. Out of 710 mitochondrial proteins, we have identified 108 insoluble proteins that were enriched in the LONP1 KO pellet when compared to the WT pellet, and at the same time they were also enriched in the KO pellet when compared to the KO input. Most of these targets were proteins of mitochondrial central dogma, but it was also proteins of various mitochondrial metabolic pathways (e.g., branched-chain amino acids, carbohydrate metabolism, etc.). We also detected proteins involved in OXPHOS and protein imports and homeostasis, including chaperones mt-HSP70 (also HSPA9) and CLPX.

Interestingly, there were 7 insoluble OXPHOS assembly factors and only 2 OXPHOS subunits (CI).

To narrow down the pool of possible LONP1 substrates, we combined these results with our data from the whole heart transcriptomics and proteomics, where we filtered only those mitochondrial targets that were not transcriptionally affected but were increased on the protein level. This yielded 54 proteins in total. Among these proteins, we also detected the 5 targets that were the most increased proteins of mitochondrial gene expression CDK5RAP1, NSUN4, METAP1D, TRMT2B, MRPL51.

This analysis has also revealed many mitoribosomal proteins to become insoluble, which could be one of the reasons why the mitochondrial translation is partially inhibited in the LONP1 KO mitochondria.

An intriguing finding is a detection of a lot of factors which form a mitochondrial RNA granule (MRG), e.g., DDX28, FASTKD5, GRFS1, MRM1, etc. (Figure 3.30) (Xavier and Martinou, 2021). MRGs are membraneless structures constituted of RNAs and RNA-binding proteins residing inside mitochondrial matrix. They have been associated with mtRNA processing and mitoribosomal biogenesis – they might compartmentalize these processes to increase their efficiency (Antonicka and Shoubridge, 2015). Physically, MRGs are soluble fluid condensates which are highly dynamic and can change their kinetics depending on their surroundings (Rey et al., 2020). However, condensate-forming proteins could be intrinsically disordered and binding of RNA was shown to change the folding properties of proteins (Alberti and Hyman, 2021). It is therefore very conceivable that MRGs are formed by misfolding-prone proteins which can aggregate and become insoluble. That would explain the presence of MRG proteins in the insoluble pellets in the LONP1 KO. It could also mean that not all these insoluble MRG proteins are necessarily LONP1 substrates. Nevertheless, LONP1 was reported to interact with TWNK and SSBP1, two nucleoid proteins that were shown to colocalise to MRGs as well. That creates an opportunity for LONP1 to also be present in MRGs and to regulate the MRG proteins locally.

4.4 Summary

LONP1 is a protein essential for the maintenance of mitochondrial biology. We have shown that the absence of LONP1 in the mouse heart leads to a premature death of the animal at ~22-23 weeks. The absence of LONP1 resulted in the accumulation of insoluble proteins (possibly protein aggregates) in the mitochondrial matrix. Moreover, the depletion of LONP1 also caused impaired mitochondrial gene expression as evidenced by the accumulation of the proteins involved in mitochondrial gene expression, increased *de novo* mtRNA synthesis yet dysfunctional mitochondrial translation. The dysfunctional translation is probably caused by the impaired mitoribosomal assembly, and it results in a malfunctioning respiratory chain. The proteins of mitochondrial gene expression were also found in the insoluble fractions in the LONP1 KO mitochondria which could be also responsible for their dysfunction. We have also described the importance of LONP1 in the regulation specific to CI and CIV as these two complexes were the most affected by the LONP1 depletion.

This study aimed to describe the consequences of the LONP1 depletion *in vivo*. In the future, it will be important to address the specific mechanisms of how LONP1 operates. In order to investigate that, there is a need for a reliable cell model of the LONP1 depletion. Furthermore, it is also important to find more LONP1 substrates as there has been only a handful of them described in literature so far. This would also help us understand the role of LONP1 in the maintenance of mitochondrial physiology in general.

5 References

AGARONYAN, K., MOROZOV, Y. I., ANIKIN, M. & TEMIAKOV, D. 2015. Mitochondrial biology. Replication-transcription switch in human mitochondria. *Science,* 347**,** 548-51.

AHOLA, S., RIVERA MEJIAS, P., HERMANS, S., CHANDRAGIRI, S., GIAVALISCO, P., NOLTE, H. & LANGER, T. 2022. OMA1-mediated integrated stress response protects against ferroptosis in mitochondrial cardiomyopathy. *Cell Metab,* 34**,** 1875-1891 e7.

ALBERTI, S. & HYMAN, A. A. 2021. Biomolecular condensates at the nexus of cellular stress, protein aggregation disease and ageing. *Nat Rev Mol Cell Biol,* 22**,** 196-213.

ALBERTS, B., JOHNSON, A., LEWIS, J., MORGAN, D., RAFF, M., ROBERTS, K. & WALTER, P. 2017. Molecular Biology of the Cell.

ALCAZAR-FABRA, M., RODRIGUEZ-SANCHEZ, F., TREVISSON, E. & BREA-CALVO, G. 2021. Primary Coenzyme Q deficiencies: A literature review and online platform of clinical features to uncover genotype-phenotype correlations. *Free Radic Biol Med,* 167**,** 141-180.

ALMENAR-QUERALT, A., LEE, A., CONLEY, C. A., DE POUPLANA, L. R. & FOWLER, V. M. 1999. Identification of a Novel Tropomodulin Isoform, Skeletal Tropomodulin, That Caps Actin Filament Pointed Ends in Fast Skeletal Muscle. *Journal of Biological Chemistry,* 274**,** 28466-28475.

ANDERSON, S., BARRELL BG, D. B. M. H. C. A. R. D. J. E. I. C. N. D. P. R. B. A. S. F. S. P. H., BANKIER, A. T., BARRELL, B. G., DE BRUIJN, M. H. L., COULSON, A. R., DROUIN, J., EPERON, I. C., NIERLICH, D. P., ROE, B. A., SANGER, F., SCHREIER, P. H., SMITH, A. J. H., STADEN, R. & YOUNG, I. G. 1981. Sequence and organization of the human mitochondrial genome.

ANTONICKA, H. & SHOUBRIDGE, E. A. 2015. Mitochondrial RNA Granules Are Centers for Posttranscriptional RNA Processing and Ribosome Biogenesis. *Cell Rep,* 10**,** 920-932.

BAYOT, A., GAREIL, M., ROGOWSKA-WRZESINSKA, A., ROEPSTORFF, P., FRIGUET, B. & BULTEAU, A. L. 2010. Identification of novel oxidized protein substrates and physiological partners of the mitochondrial ATP-dependent Lon-like protease Pim1. *J Biol Chem,* 285**,** 11445-57.

BENDER, T., LEIDHOLD, C., RUPPERT, T., FRANKEN, S. & VOOS, W. 2010. The role of protein quality control in mitochondrial protein homeostasis under oxidative stress. *Proteomics,* 10**,** 1426-43.

BENDER, T., LEWRENZ, I., FRANKEN, S., BAITZEL, C. & VOOS, W. 2011. Mitochondrial enzymes are protected from stress-induced aggregation by mitochondrial chaperones and the Pim1/LON protease. *Mol Biol Cell,* 22**,** 541-54.

BESSE, A., BREZAVAR, D., HANSON, J., LARSON, A. & BONNEN, P. E. 2020. LONP1 de novo dominant mutation causes mitochondrial encephalopathy with loss of LONP1 chaperone activity and excessive LONP1 proteolytic activity. *Mitochondrion,* 51**,** 68-78.

BEZAWORK-GELETA, A., BRODIE, E. J., DOUGAN, D. A. & TRUSCOTT, K. N. 2015. LON is the master protease that protects against protein aggregation in human mitochondria through direct degradation of misfolded proteins. *Sci Rep,* 5**,** 17397.

BEZAWORK-GELETA, A., SAIYED, T., DOUGAN, D. A. & TRUSCOTT, K. N. 2014. Mitochondrial matrix proteostasis is linked to hereditary paraganglioma: LON-

mediated turnover of the human flavinylation factor SDH5 is regulated by its interaction with SDHA. *FASEB J,* 28**,** 1794-804.
BHATTA, A., DIENEMANN, C., CRAMER, P. & HILLEN, H. S. 2021. Structural basis of RNA processing by human mitochondrial RNase P. *Nat Struct Mol Biol,* 28**,** 713-723.
BLUM, T. B., HAHN, A., MEIER, T., DAVIES, K. M. & KUHLBRANDT, W. 2019. Dimers of mitochondrial ATP synthase induce membrane curvature and self-assemble into rows. *Proc Natl Acad Sci U S A,* 116**,** 4250-4255.
BOEHM, E., ZAGANELLI, S., MAUNDRELL, K., JOURDAIN, A. A., THORE, S. & MARTINOU, J. C. 2017. FASTKD1 and FASTKD4 have opposite effects on expression of specific mitochondrial RNAs, depending upon their endonuclease-like RAP domain. *Nucleic Acids Res,* 45**,** 6135-6146.
BOGENHAGEN, D. F. 2012. Mitochondrial DNA nucleoid structure. *Biochim Biophys Acta,* 1819**,** 914-20.
BOHNSACK, M. T. & SLOAN, K. E. 2018. The mitochondrial epitranscriptome: the roles of RNA modifications in mitochondrial translation and human disease. *Cell Mol Life Sci,* 75**,** 241-260.
BONEKAMP, N. A., JIANG, M., MOTORI, E., GARCIA VILLEGAS, R., KOOLMEISTER, C., ATANASSOV, I., MESAROS, A., PARK, C. B. & LARSSON, N. G. 2021. High levels of TFAM repress mammalian mitochondrial DNA transcription in vivo. *Life Sci Alliance,* 4**,** e202101034.
BOROWSKI, L. S., DZIEMBOWSKI, A., HEJNOWICZ, M. S., STEPIEN, P. P. & SZCZESNY, R. J. 2013. Human mitochondrial RNA decay mediated by PNPase-hSuv3 complex takes place in distinct foci. *Nucleic Acids Res,* 41**,** 1223-40.
BOTA, D. A. & DAVIES, K. J. 2002. Lon protease preferentially degrades oxidized mitochondrial aconitase by an ATP-stimulated mechanism. *Nat Cell Biol,* 4**,** 674-80.
BOUDA, E., STAPON, A. & GARCIA-DIAZ, M. 2019. Mechanisms of mammalian mitochondrial transcription. *Protein Sci,* 28**,** 1594-1605.
BROWN, A., RATHORE, S., KIMANIUS, D., AIBARA, S., BAI, X. C., RORBACH, J., AMUNTS, A. & RAMAKRISHNAN, V. 2017. Structures of the human mitochondrial ribosome in native states of assembly. *Nat Struct Mol Biol,* 24**,** 866-869.
BRUSER, C., KELLER-FINDEISEN, J. & JAKOBS, S. 2021. The TFAM-to-mtDNA ratio defines inner-cellular nucleoid populations with distinct activity levels. *Cell Rep,* 37**,** 110000.
CAMARA, Y., ASIN-CAYUELA, J., PARK, C. B., METODIEV, M. D., SHI, Y., RUZZENENTE, B., KUKAT, C., HABERMANN, B., WIBOM, R., HULTENBY, K., FRANZ, T., ERDJUMENT-BROMAGE, H., TEMPST, P., HALLBERG, B. M., GUSTAFSSON, C. M. & LARSSON, N. G. 2011. MTERF4 regulates translation by targeting the methyltransferase NSUN4 to the mammalian mitochondrial ribosome. *Cell Metab,* 13**,** 527-39.
CARROLL, J., HE, J., DING, S., FEARNLEY, I. M. & WALKER, J. E. 2021. TMEM70 and TMEM242 help to assemble the rotor ring of human ATP synthase and interact with assembly factors for complex I. *Proc Natl Acad Sci U S A,* 118.
CHANG, D. D. & CLAYTON, D. A. 1985. Priming of human mitochondrial DNA replication occurs at the light-strand promoter. *Proc Natl Acad Sci U S A,* 82**,** 351-5.
CHANG, J. H. & TONG, L. 2012. Mitochondrial poly(A) polymerase and polyadenylation. *Biochim Biophys Acta,* 1819**,** 992-7.

CHARETTE, M. F., HENDERSON, G. W. & MARKOVITZ, A. 1981. ATP hydrolysis-dependent protease activity of the lon (capR) protein of Escherichia coli K-12. *Proc Natl Acad Sci U S A,* 78**,** 4728-32.
CHENG, C. W., KUO, C. Y., FAN, C. C., FANG, W. C., JIANG, S. S., LO, Y. K., WANG, T. Y., KAO, M. C. & LEE, A. Y. 2013. Overexpression of Lon contributes to survival and aggressive phenotype of cancer cells through mitochondrial complex I-mediated generation of reactive oxygen species. *Cell Death Dis,* 4**,** e681.
CHENG, I., MIKITA, N., FISHOVITZ, J., FRASE, H., WINTRODE, P. & LEE, I. 2012. Identification of a region in the N-terminus of Escherichia coli Lon that affects ATPase, substrate translocation and proteolytic activity. *J Mol Biol,* 418**,** 208-25.
CHENG, J., BERNINGHAUSEN, O. & BECKMANN, R. 2021. A distinct assembly pathway of the human 39S late pre-mitoribosome. *Nat Commun,* 12**,** 4544.
CHENG, X., KANKI, T., FUKUOH, A., OHGAKI, K., TAKEYA, R., AOKI, Y., HAMASAKI, N. & KANG, D. 2005. PDIP38 associates with proteins constituting the mitochondrial DNA nucleoid. *J Biochem,* 138**,** 673-8.
CHOMYN, A., CLEETER, M. W., RAGAN, C. I., RILEY, M., DOOLITTLE, R. F. & ATTARDI, G. 1986. URF6, last unidentified reading frame of human mtDNA, codes for an NADH dehydrogenase subunit. *Science,* 234**,** 614-8.
CHOMYN, A., MARIOTTINI, P., CLEETER, M. W., RAGAN, C. I., MATSUNO-YAGI, A., HATEFI, Y., DOOLITTLE, R. F. & ATTARDI, G. 1985. Six unidentified reading frames of human mitochondrial DNA encode components of the respiratory-chain NADH dehydrogenase. *Nature,* 314**,** 592-7.
CHUJO, T., OHIRA, T., SAKAGUCHI, Y., GOSHIMA, N., NOMURA, N., NAGAO, A. & SUZUKI, T. 2012. LRPPRC/SLIRP suppresses PNPase-mediated mRNA decay and promotes polyadenylation in human mitochondria. *Nucleic Acids Res,* 40**,** 8033-47.
CHUNG, C. H. & GOLDBERG, A. L. 1981. The product of the lon (capR) gene in Escherichia coli is the ATP-dependent protease, protease La. *Proc Natl Acad Sci U S A,* 78**,** 4931-5.
CIPULLO, M., GESE, G. V., KHAWAJA, A., HALLBERG, B. M. & RORBACH, J. 2021. Structural basis for late maturation steps of the human mitoribosomal large subunit. *Nat Commun,* 12**,** 3673.
COLOMBINI, M. 1989. Voltage gating in the mitochondrial channel, VDAC. *J Membr Biol,* 111**,** 103-11.
CREWE, C., SCHAFER, C., LEE, I., KINTER, M. & SZWEDA, L. I. 2017. Regulation of Pyruvate Dehydrogenase Kinase 4 in the Heart through Degradation by the Lon Protease in Response to Mitochondrial Substrate Availability. *J Biol Chem,* 292**,** 305-312.
D'SOUZA, A. R. & MINCZUK, M. 2018. Mitochondrial transcription and translation: overview. *Essays Biochem,* 62**,** 309-320.
DAVIES, K. M. & DAUM, B. 2013. Role of cryo-ET in membrane bioenergetics research. *Biochem Soc Trans,* 41**,** 1227-34.
DIANA, P. & CARVALHEIRA, G. M. G. 2022. NIBAN1, Exploring its Roles in Cell Survival Under Stress Context. *Front Cell Dev Biol,* 10**,** 867003.
DIKOGLU, E., ALFAIZ, A., GORNA, M., BERTOLA, D., CHAE, J. H., CHO, T. J., DERBENT, M., ALANAY, Y., GURAN, T., KIM, O. H., LLERENAR, J. C., JR., YAMAMOTO, G., SUPERTI-FURGA, G., REYMOND, A., XENARIOS, I., STEVENSON, B., CAMPOS-XAVIER, B., BONAFE, L., SUPERTI-FURGA, A.

& UNGER, S. 2015. Mutations in LONP1, a mitochondrial matrix protease, cause CODAS syndrome. *Am J Med Genet A,* 167**,** 1501-9.
DOGAN, S. A., PUJOL, C., MAITI, P., KUKAT, A., WANG, S., HERMANS, S., SENFT, K., WIBOM, R., RUGARLI, E. I. & TRIFUNOVIC, A. 2014. Tissue-specific loss of DARS2 activates stress responses independently of respiratory chain deficiency in the heart. *Cell Metab,* 19**,** 458-69.
DYMECKI, S. M. 1996. Flp recombinase promotes site-specific DNA recombination in embryonic stem cells and transgenic mice. *Proc Natl Acad Sci U S A,* 93**,** 6191-6.
ERJAVEC, N., BAYOT, A., GAREIL, M., CAMOUGRAND, N., NYSTROM, T., FRIGUET, B. & BULTEAU, A. L. 2013. Deletion of the mitochondrial Pim1/Lon protease in yeast results in accelerated aging and impairment of the proteasome. *Free Radic Biol Med,* 56**,** 9-16.
ERNSTER, L. & SCHATZ, G. 1981. Mitochondria: A historical review.
FALKENBERG, M. 2018. Mitochondrial DNA replication in mammalian cells: overview of the pathway. *Essays Biochem,* 62**,** 287-296.
FARGE, G. & FALKENBERG, M. 2019. Organization of DNA in Mammalian Mitochondria. *Int J Mol Sci,* 20.
FARR, C. L., WANG, Y. & KAGUNI, L. S. 1999. Functional interactions of mitochondrial DNA polymerase and single-stranded DNA-binding protein. Template-primer DNA binding and initiation and elongation of DNA strand synthesis. *J Biol Chem,* 274**,** 14779-85.
FESSLER, E., ECKL, E. M., SCHMITT, S., MANCILLA, I. A., MEYER-BENDER, M. F., HANF, M., PHILIPPOU-MASSIER, J., KREBS, S., ZISCHKA, H. & JAE, L. T. 2020. A pathway coordinated by DELE1 relays mitochondrial stress to the cytosol. *Nature,* 579**,** 433-437.
FIEDORCZUK, K., LETTS, J. A., DEGLIESPOSTI, G., KASZUBA, K., SKEHEL, M. & SAZANOV, L. A. 2016. Atomic structure of the entire mammalian mitochondrial complex I. *Nature,* 538**,** 406-410.
FILOGRANA, R., KOOLMEISTER, C., UPADHYAY, M., PAJAK, A., CLEMENTE, P., WIBOM, R., SIMARD, M. L., WREDENBERG, A., FREYER, C., STEWART, J. B. & LARSSON, N. G. 2019. Modulation of mtDNA copy number ameliorates the pathological consequences of a heteroplasmic mtDNA mutation in the mouse. *Sci Adv,* 5**,** eaav9824.
FORMOSA, L. E., MAGHOOL, S., SHARPE, A. J., RELJIC, B., MUELLNER-WONG, L., STROUD, D. A., RYAN, M. T. & MAHER, M. J. 2022. Mitochondrial COA7 is a heme-binding protein with disulfide reductase activity, which acts in the early stages of complex IV assembly. *Proceedings of the National Academy of Sciences,* 119**,** e2110357119.
FORMOSA, L. E., MUELLNER-WONG, L., RELJIC, B., SHARPE, A. J., JACKSON, T. D., BEILHARZ, T. H., STOJANOVSKI, D., LAZAROU, M., STROUD, D. A. & RYAN, M. T. 2020. Dissecting the Roles of Mitochondrial Complex I Intermediate Assembly Complex Factors in the Biogenesis of Complex I. *Cell Rep,* 31**,** 107541.
FORSSTRÖM, S., JACKSON, C. B., CARROLL, C. J., KURONEN, M., PIRINEN, E., PRADHAN, S., MARMYLEVA, A., AURANEN, M., KLEINE, I.-M., KHAN, N. A., ROIVAINEN, A., MARJAMÄKI, P., LILJENBÄCK, H., WANG, L., BATTERSBY, B. J., RICHTER, U., VELAGAPUDI, V., NIKKANEN, J., EURO, L. & SUOMALAINEN, A. 2019. Fibroblast Growth Factor 21 Drives Dynamics of Local and Systemic Stress Responses in Mitochondrial Myopathy with mtDNA Deletions. *Cell Metabolism,* 30**,** 1040-1054.e7.

FU, G. K. & MARKOVITZ, D. M. 1998. The human LON protease binds to mitochondrial promoters in a single-stranded, site-specific, strand-specific manner. *Biochemistry,* 37**,** 1905-9.
FU, G. K., SMITH, M. J. & MARKOVITZ, D. M. 1997. Bacterial protease Lon is a site-specific DNA-binding protein. *J Biol Chem,* 272**,** 534-8.
FUKUDA, R., ZHANG, H., KIM, J. W., SHIMODA, L., DANG, C. V. & SEMENZA, G. L. 2007. HIF-1 regulates cytochrome oxidase subunits to optimize efficiency of respiration in hypoxic cells. *Cell,* 129**,** 111-22.
GIBELLINI, L., PINTI, M., BORALDI, F., GIORGIO, V., BERNARDI, P., BARTOLOMEO, R., NASI, M., DE BIASI, S., MISSIROLI, S., CARNEVALE, G., LOSI, L., TESEI, A., PINTON, P., QUAGLINO, D. & COSSARIZZA, A. 2014. Silencing of mitochondrial Lon protease deeply impairs mitochondrial proteome and function in colon cancer cells. *FASEB J,* 28**,** 5122-35.
GÖKE, A., SCHROTT, S., MIZRAK, A., BELYY, V., OSMAN, C. & WALTER, P. 2020. Mrx6 regulates mitochondrial DNA copy number in Saccharomyces cerevisiae by engaging the evolutionarily conserved Lon protease Pim1. *Mol Biol Cell,* 31**,** 527-545.
GRANOT, Z., KOBILER, O., MELAMED-BOOK, N., EIMERL, S., BAHAT, A., LU, B., BRAUN, S., MAURIZI, M. R., SUZUKI, C. K., OPPENHEIM, A. B. & ORLY, J. 2007. Turnover of mitochondrial steroidogenic acute regulatory (StAR) protein by Lon protease: the unexpected effect of proteasome inhibitors. *Mol Endocrinol,* 21**,** 2164-77.
GRAY, H. & WONG, T. W. 1992. Purification and identification of subunit structure of the human mitochondrial DNA polymerase. *J Biol Chem,* 267**,** 5835-41.
GREENLEAF, A. L., KELLY, J. L. & LEHMAN, I. R. 1986. Yeast RPO41 gene product is required for transcription and maintenance of the mitochondrial genome. *Proc Natl Acad Sci U S A,* 83**,** 3391-4.
GROSS, M. H. & KONIECZNY, I. 2020. Polyphosphate induces the proteolysis of ADP-bound fraction of initiator to inhibit DNA replication initiation upon stress in Escherichia coli. *Nucleic Acids Res,* 48**,** 5457-5466.
GU, J., WU, M., GUO, R., YAN, K., LEI, J., GAO, N. & YANG, M. 2016. The architecture of the mammalian respirasome. *Nature,* 537**,** 639-43.
GUERRERO-CASTILLO, S., BAERTLING, F., KOWNATZKI, D., WESSELS, H. J., ARNOLD, S., BRANDT, U. & NIJTMANS, L. 2017. The Assembly Pathway of Mitochondrial Respiratory Chain Complex I. *Cell Metab,* 25**,** 128-139.
GUILLON, B., BULTEAU, A. L., WATTENHOFER-DONZE, M., SCHMUCKER, S., FRIGUET, B., PUCCIO, H., DRAPIER, J. C. & BOUTON, C. 2009. Frataxin deficiency causes upregulation of mitochondrial Lon and ClpP proteases and severe loss of mitochondrial Fe-S proteins. *FEBS J,* 276**,** 1036-47.
GUO, R., ZONG, S., WU, M., GU, J. & YANG, M. 2017. Architecture of Human Mitochondrial Respiratory Megacomplex I(2)III(2)IV(2). *Cell,* 170**,** 1247-1257 e12.
GUO, X., AVILES, G., LIU, Y., TIAN, R., UNGER, B. A., LIN, Y. T., WIITA, A. P., XU, K., CORREIA, M. A. & KAMPMANN, M. 2020. Mitochondrial stress is relayed to the cytosol by an OMA1-DELE1-HRI pathway. *Nature,* 579**,** 427-432.
GUR, E. 2013. The Lon AAA+ protease. *Subcell Biochem,* 66**,** 35-51.
GUR, E. & SAUER, R. T. 2008. Recognition of misfolded proteins by Lon, a AAA(+) protease. *Genes Dev,* 22**,** 2267-77.
GUSTAFSSON, C. M., FALKENBERG, M. & LARSSON, N. G. 2016. Maintenance and Expression of Mammalian Mitochondrial DNA. *Annu Rev Biochem,* 85**,** 133-60.

GUSTCHINA, A., LI, M., ANDRIANOVA, A. G., KUDZHAEV, A. M., LOUNTOS, G. T., SEKULA, B., CHERRY, S., TROPEA, J. E., SMIRNOV, I. V., WLODAWER, A. & ROTANOVA, T. V. 2022. Unique Structural Fold of LonBA Protease from Bacillus subtilis, a Member of a Newly Identified Subfamily of Lon Proteases. *Int J Mol Sci,* 23.

HAAG, S., SLOAN, K. E., RANJAN, N., WARDA, A. S., KRETSCHMER, J., BLESSING, C., HUBNER, B., SEIKOWSKI, J., DENNERLEIN, S., REHLING, P., RODNINA, M. V., HOBARTNER, C. & BOHNSACK, M. T. 2016. NSUN3 and ABH1 modify the wobble position of mt-tRNAMet to expand codon recognition in mitochondrial translation. *EMBO J,* 35**,** 2104-2119.

HANNAH-SHMOUNI, F., MACNEIL, L., BRADY, L., NILSSON, M. I. & TARNOPOLSKY, M. 2019. Expanding the Clinical Spectrum of LONP1-Related Mitochondrial Cytopathy. *Front Neurol,* 10**,** 981.

HAO, H. X., KHALIMONCHUK, O., SCHRADERS, M., DEPHOURE, N., BAYLEY, J. P., KUNST, H., DEVILEE, P., CREMERS, C. W., SCHIFFMAN, J. D., BENTZ, B. G., GYGI, S. P., WINGE, D. R., KREMER, H. & RUTTER, J. 2009. SDH5, a gene required for flavination of succinate dehydrogenase, is mutated in paraganglioma. *Science,* 325**,** 1139-42.

HAQUE, M. E., ELMORE, K. B., TRIPATHY, A., KOC, H., KOC, E. C. & SPREMULLI, L. L. 2010. Properties of the C-terminal tail of human mitochondrial inner membrane protein Oxa1L and its interactions with mammalian mitochondrial ribosomes. *J Biol Chem,* 285**,** 28353-62.

HARMEL, J., RUZZENENTE, B., TERZIOGLU, M., SPAHR, H., FALKENBERG, M. & LARSSON, N. G. 2013. The leucine-rich pentatricopeptide repeat-containing protein (LRPPRC) does not activate transcription in mammalian mitochondria. *J Biol Chem,* 288**,** 15510-9.

HILLEN, H. S., MOROZOV, Y. I., SARFALLAH, A., TEMIAKOV, D. & CRAMER, P. 2017. Structural Basis of Mitochondrial Transcription Initiation. *Cell,* 171**,** 1072-1081 e10.

HOLZMANN, J., FRANK, P., LOFFLER, E., BENNETT, K. L., GERNER, C. & ROSSMANITH, W. 2008. RNase P without RNA: identification and functional reconstitution of the human mitochondrial tRNA processing enzyme. *Cell,* 135**,** 462-74.

HOU, T., ZHANG, R., JIAN, C., DING, W., WANG, Y., LING, S., MA, Q., HU, X., CHENG, H. & WANG, X. 2019. NDUFAB1 confers cardio-protection by enhancing mitochondrial bioenergetics through coordination of respiratory complex and supercomplex assembly. *Cell Res,* 29**,** 754-766.

HOWARD-FLANDERS, P., SIMSON, E. & THERIOT, L. 1964. A LOCUS THAT CONTROLS FILAMENT FORMATION AND SENSITIVITY TO RADIATION IN ESCHERICHIA COLI K-12. *Genetics,* 49**,** 237-246.

IKON, N. & RYAN, R. O. 2017. Cardiolipin and mitochondrial cristae organization. *Biochim Biophys Acta Biomembr,* 1859**,** 1156-1163.

INATOMI, T., MATSUDA, S., ISHIUCHI, T., DO, Y., NAKAYAMA, M., ABE, S., KASHO, K., WANROOIJ, S., NAKADA, K., ICHIYANAGI, K., SASAKI, H., YASUKAWA, T. & KANG, D. 2022. TFB2M and POLRMT are essential for mammalian mitochondrial DNA replication. *Biochim Biophys Acta Mol Cell Res,* 1869**,** 119167.

IOVINE, J. C., CLAYPOOL, S. M. & ALDER, N. N. 2021. Mitochondrial compartmentalization: emerging themes in structure and function. *Trends Biochem Sci,* 46**,** 902-917.

JIANG, M., KAUPPILA, T. E. S., MOTORI, E., LI, X., ATANASSOV, I., FOLZ-DONAHUE, K., BONEKAMP, N. A., ALBARRAN-GUTIERREZ, S., STEWART, J. B. & LARSSON, N. G. 2017. Increased Total mtDNA Copy Number Cures Male Infertility Despite Unaltered mtDNA Mutation Load. *Cell Metab,* 26**,** 429-436 e4.

JIANG, M., XIE, X., ZHU, X., JIANG, S., MILENKOVIC, D., MISIC, J., SHI, Y., TANDUKAR, N., LI, X., ATANASSOV, I., JENNINGER, L., HOBERG, E., ALBARRAN-GUTIERREZ, S., SZILAGYI, Z., MACAO, B., SIIRA, S. J., CARELLI, V., GRIFFITH, J. D., GUSTAFSSON, C. M., NICHOLLS, T. J., FILIPOVSKA, A., LARSSON, N. G. & FALKENBERG, M. 2021. The mitochondrial single-stranded DNA binding protein is essential for initiation of mtDNA replication. *Sci Adv,* 7**,** eabf8631.

JIANG, S., KOOLMEISTER, C., MISIC, J., SIIRA, S., KUHL, I., SILVA RAMOS, E., MIRANDA, M., JIANG, M., POSSE, V., LYTOVCHENKO, O., ATANASSOV, I., SCHOBER, F. A., WIBOM, R., HULTENBY, K., MILENKOVIC, D., GUSTAFSSON, C. M., FILIPOVSKA, A. & LARSSON, N. G. 2019. TEFM regulates both transcription elongation and RNA processing in mitochondria. *EMBO Rep,* 20**,** e48101.

JIN, S. M., LAZAROU, M., WANG, C., KANE, L. A., NARENDRA, D. P. & YOULE, R. J. 2010. Mitochondrial membrane potential regulates PINK1 import and proteolytic destabilization by PARL. *J Cell Biol,* 191**,** 933-42.

JONAS, K., LIU, J., CHIEN, P. & LAUB, M. T. 2013. Proteotoxic stress induces a cell-cycle arrest by stimulating Lon to degrade the replication initiator DnaA. *Cell,* 154**,** 623-36.

JONES, A. J., BLAZA, J. N., VARGHESE, F. & HIRST, J. 2017. Respiratory Complex I in Bos taurus and Paracoccus denitrificans Pumps Four Protons across the Membrane for Every NADH Oxidized. *J Biol Chem,* 292**,** 4987-4995.

JOURDAIN, A. A., KOPPEN, M., RODLEY, C. D., MAUNDRELL, K., GUEGUEN, N., REYNIER, P., GUARAS, A. M., ENRIQUEZ, J. A., ANDERSON, P., SIMARRO, M. & MARTINOU, J. C. 2015. A mitochondria-specific isoform of FASTK is present in mitochondrial RNA granules and regulates gene expression and function. *Cell Rep,* 10**,** 1110-21.

KANG, S. G., DIMITROVA, M. N., ORTEGA, J., GINSBURG, A. & MAURIZI, M. R. 2005. Human mitochondrial ClpP is a stable heptamer that assembles into a tetradecamer in the presence of ClpX. *J Biol Chem,* 280**,** 35424-32.

KAO, T. Y., CHIU, Y. C., FANG, W. C., CHENG, C. W., KUO, C. Y., JUAN, H. F., WU, S. H. & LEE, A. Y. 2015. Mitochondrial Lon regulates apoptosis through the association with Hsp60-mtHsp70 complex. *Cell Death Dis,* 6**,** e1642.

KARLOWICZ, A., WEGRZYN, K., GROSS, M., KACZYNSKA, D., ROPELEWSKA, M., SIEMIATKOWSKA, M., BUJNICKI, J. M. & KONIECZNY, I. 2017. Defining the crucial domain and amino acid residues in bacterial Lon protease for DNA binding and processing of DNA-interacting substrates. *J Biol Chem,* 292**,** 7507-7518.

KELLY, J. L., GREENLEAF, A. L. & LEHMAN, I. R. 1986. Isolation of the nuclear gene encoding a subunit of the yeast mitochondrial RNA polymerase. *J Biol Chem,* 261**,** 10348-51.

KEREICHE, S., KOVACIK, L., BEDNAR, J., PEVALA, V., KUNOVA, N., ONDROVICOVA, G., BAUER, J., AMBRO, L., BELLOVA, J., KUTEJOVA, E. & RASKA, I. 2016. The N-terminal domain plays a crucial role in the structure of a full-length human mitochondrial Lon protease. *Sci Rep,* 6**,** 33631.

KILBERG, M. S., BALASUBRAMANIAN, M., FU, L. & SHAN, J. 2012. The transcription factor network associated with the amino acid response in mammalian cells. *Adv Nutr,* 3**,** 295-306.

KIM, H. J. & BARRIENTOS, A. 2018. MTG1 couples mitoribosome large subunit assembly with intersubunit bridge formation. *Nucleic Acids Res,* 46**,** 8435-8453.

KITA, K., SUZUKI, T. & OCHI, T. 2012. Diphenylarsinic acid promotes degradation of glutaminase C by mitochondrial Lon protease. *J Biol Chem,* 287**,** 18163-72.

KOLANCZYK, M., PECH, M., ZEMOJTEL, T., YAMAMOTO, H., MIKULA, I., CALVARUSO, M. A., VAN DEN BRAND, M., RICHTER, R., FISCHER, B., RITZ, A., KOSSLER, N., THURISCH, B., SPOERLE, R., SMEITINK, J., KORNAK, U., CHAN, D., VINGRON, M., MARTASEK, P., LIGHTOWLERS, R. N., NIJTMANS, L., SCHUELKE, M., NIERHAUS, K. H. & MUNDLOS, S. 2011. NOA1 is an essential GTPase required for mitochondrial protein synthesis. *Mol Biol Cell,* 22**,** 1-11.

KONOVALOVA, S. & TYYNISMAA, H. 2013. Mitochondrial aminoacyl-tRNA synthetases in human disease. *Mol Genet Metab,* 108**,** 206-11.

KOPPEN, M., METODIEV, M. D., CASARI, G., RUGARLI, E. I. & LANGER, T. 2007. Variable and tissue-specific subunit composition of mitochondrial m-AAA protease complexes linked to hereditary spastic paraplegia. *Mol Cell Biol,* 27**,** 758-67.

KORHONEN, J. A., GASPARI, M. & FALKENBERG, M. 2003. TWINKLE Has 5' -> 3' DNA helicase activity and is specifically stimulated by mitochondrial single-stranded DNA-binding protein. *J Biol Chem,* 278**,** 48627-32.

KOUTSIFELI, P., VARMA, U., DANIELS, L. J., ANNANDALE, M., LI, X., NEALE, J. P. H., HAYES, S., WEEKS, K. L., JAMES, S., DELBRIDGE, L. M. D. & MELLOR, K. M. 2022. Glycogen-autophagy: Molecular machinery and cellular mechanisms of glycophagy. *Journal of Biological Chemistry,* 298**,** 102093.

KUHL, I., MIRANDA, M., ATANASSOV, I., KUZNETSOVA, I., HINZE, Y., MOURIER, A., FILIPOVSKA, A. & LARSSON, N. G. 2017. Transcriptomic and proteomic landscape of mitochondrial dysfunction reveals secondary coenzyme Q deficiency in mammals. *Elife,* 6.

KÜHL, I., MIRANDA, M., POSSE, V., MILENKOVIC, D., MOURIER, A., SIIRA, S. J., BONEKAMP, N. A., NEUMANN, U., FILIPOVSKA, A., POLOSA, P. L., GUSTAFSSON, C. M. & LARSSON, N.-G. 2016. POLRMT regulates the switch between replication primer formation and gene expression of mammalian mtDNA. *Science advances,* 2**,** e1600963-e1600963.

KUHL, I., MIRANDA, M., POSSE, V., MILENKOVIC, D., MOURIER, A., SIIRA, S. J., BONEKAMP, N. A., NEUMANN, U., FILIPOVSKA, A., POLOSA, P. L., GUSTAFSSON, C. M. & LARSSON, N. G. 2016. POLRMT regulates the switch between replication primer formation and gene expression of mammalian mtDNA. *Sci Adv,* 2**,** e1600963.

KUKAT, C., DAVIES, K. M., WURM, C. A., SPAHR, H., BONEKAMP, N. A., KUHL, I., JOOS, F., POLOSA, P. L., PARK, C. B., POSSE, V., FALKENBERG, M., JAKOBS, S., KUHLBRANDT, W. & LARSSON, N. G. 2015. Cross-strand binding of TFAM to a single mtDNA molecule forms the mitochondrial nucleoid. *Proc Natl Acad Sci U S A,* 112**,** 11288-93.

KUKAT, C., WURM, C. A., SPAHR, H., FALKENBERG, M., LARSSON, N. G. & JAKOBS, S. 2011. Super-resolution microscopy reveals that mammalian mitochondrial nucleoids have a uniform size and frequently contain a single copy of mtDNA. *Proc Natl Acad Sci U S A,* 108**,** 13534-9.

KUMARAN, N. & MUNAVAR, M. H. 2019. Suppression of Deltalon phenotypes in Escherichia coli by N-terminal DnaK peptides. *J Basic Microbiol,* 59**,** 302-313.
KUMARAN, N. A. M., KARTHIK, M., KUMAR, V., JEBASINGH, T. & MUNAVAR, M. H. 2020. Two new mutations in dnaJ suppress DNA damage hypersensitivity and capsule overproduction phenotypes of Deltalon mutant of Escherichia coli by modulating the expression of clpYQ (hslUV) and rcsA genes. *Gene,* 726**,** 144135.
KUMMER, E. & BAN, N. 2021. Mechanisms and regulation of protein synthesis in mitochondria. *Nat Rev Mol Cell Biol,* 22**,** 307-325.
KUNOVA, N., ONDROVICOVA, G., BAUER, J. A., BELLOVA, J., AMBRO, L., MARTINAKOVA, L., KOTRASOVA, V., KUTEJOVA, E. & PEVALA, V. 2017. The role of Lon-mediated proteolysis in the dynamics of mitochondrial nucleic acid-protein complexes. *Sci Rep,* 7**,** 631.
KURODA, A., NOMURA, K., OHTOMO, R., KATO, J., IKEDA, T., TAKIGUCHI, N., OHTAKE, H. & KORNBERG, A. 2001. Role of inorganic polyphosphate in promoting ribosomal protein degradation by the Lon protease in E. coli. *Science,* 293**,** 705-8.
KUTEJOVA, E., DURCOVA, G., SUROVKOVA, E. & KUZELA, S. 1993. Yeast mitochondrial ATP-dependent protease: purification and comparison with the homologous rat enzyme and the bacterial ATP-dependent protease La. *FEBS Lett,* 329**,** 47-50.
LAGOUGE, M., MOURIER, A., LEE, H. J., SPAHR, H., WAI, T., KUKAT, C., SILVA RAMOS, E., MOTORI, E., BUSCH, J. D., SIIRA, S., GERMAN MOUSE CLINIC, C., KREMMER, E., FILIPOVSKA, A. & LARSSON, N. G. 2015. SLIRP Regulates the Rate of Mitochondrial Protein Synthesis and Protects LRPPRC from Degradation. *PLoS Genet,* 11**,** e1005423.
LAPTEV, I., SHVETSOVA, E., LEVITSKII, S., SEREBRYAKOVA, M., RUBTSOVA, M., BOGDANOV, A., KAMENSKI, P., SERGIEV, P. & DONTSOVA, O. 2020. Mouse Trmt2B protein is a dual specific mitochondrial metyltransferase responsible for m(5)U formation in both tRNA and rRNA. *RNA Biol,* 17**,** 441-450.
LARSSON, N. G., WANG, J., WILHELMSSON, H., OLDFORS, A., RUSTIN, P., LEWANDOSKI, M., BARSH, G. S. & CLAYTON, D. A. 1998. Mitochondrial transcription factor A is necessary for mtDNA maintenance and embryogenesis in mice. *Nat Genet,* 18**,** 231-6.
LAVDOVSKAIA, E., DENKS, K., NADLER, F., STEUBE, E., LINDEN, A., URLAUB, H., RODNINA, M. V. & RICHTER-DENNERLEIN, R. 2020. Dual function of GTPBP6 in biogenesis and recycling of human mitochondrial ribosomes. *Nucleic Acids Res,* 48**,** 12929-12942.
LETTS, J. A., FIEDORCZUK, K., DEGLIESPOSTI, G., SKEHEL, M. & SAZANOV, L. A. 2019. Structures of Respiratory Supercomplex I+III(2) Reveal Functional and Conformational Crosstalk. *Mol Cell,* 75**,** 1131-1146 e6.
LETTS, J. A., FIEDORCZUK, K. & SAZANOV, L. A. 2016. The architecture of respiratory supercomplexes. *Nature,* 537**,** 644-648.
LI, G., LI, X., YANG, L., WANG, S., DAI, Y., FEKRY, B., VEILLON, L., TAN, L., BERDEAUX, R., ECKEL-MAHAN, K., LORENZI, P. L., ZHAO, Z., LEHNER, R. & SUN, K. 2022. Adipose tissue–specific ablation of Ces1d causes metabolic dysregulation in mice. *Life Science Alliance,* 5**,** e202101209.
LI, H., WANG, J., WILHELMSSON, H., HANSSON, A., THOREN, P., DUFFY, J., RUSTIN, P. & LARSSON, N. G. 2000. Genetic modification of survival in tissue-

specific knockout mice with mitochondrial cardiomyopathy. *Proc Natl Acad Sci U S A,* 97**,** 3467-72.
LIU, T., LU, B., LEE, I., ONDROVICOVA, G., KUTEJOVA, E. & SUZUKI, C. K. 2004. DNA and RNA binding by the mitochondrial lon protease is regulated by nucleotide and protein substrate. *J Biol Chem,* 279**,** 13902-10.
LOPEZ SANCHEZ, M. I. G., KRUGER, A., SHIRIAEV, D. I., LIU, Y. & RORBACH, J. 2021. Human Mitoribosome Biogenesis and Its Emerging Links to Disease. *Int J Mol Sci,* 22**,** 3827.
LU, B., LEE, J., NIE, X., LI, M., MOROZOV, Y. I., VENKATESH, S., BOGENHAGEN, D. F., TEMIAKOV, D. & SUZUKI, C. K. 2013. Phosphorylation of human TFAM in mitochondria impairs DNA binding and promotes degradation by the AAA+ Lon protease. *Mol Cell,* 49**,** 121-32.
LU, B., YADAV, S., SHAH, P. G., LIU, T., TIAN, B., PUKSZTA, S., VILLALUNA, N., KUTEJOVA, E., NEWLON, C. S., SANTOS, J. H. & SUZUKI, C. K. 2007. Roles for the human ATP-dependent Lon protease in mitochondrial DNA maintenance. *J Biol Chem,* 282**,** 17363-74.
LUPAS, A. N. & MARTIN, J. 2002. AAA proteins. *Curr Opin Struct Biol,* 12**,** 746-53.
MAIO, N., GHEZZI, D., VERRIGNI, D., RIZZA, T., BERTINI, E., MARTINELLI, D., ZEVIANI, M., SINGH, A., CARROZZO, R. & ROUAULT, T. A. 2016. Disease-Causing SDHAF1 Mutations Impair Transfer of Fe-S Clusters to SDHB. *Cell Metab,* 23**,** 292-302.
MAITI, P., ANTONICKA, H., GINGRAS, A. C., SHOUBRIDGE, E. A. & BARRIENTOS, A. 2020. Human GTPBP5 (MTG2) fuels mitoribosome large subunit maturation by facilitating 16S rRNA methylation. *Nucleic Acids Res,* 48**,** 7924-7943.
MARTIN, W. F., GARG, S. & ZIMORSKI, V. 2015. Endosymbiotic theories for eukaryote origin. *Philos Trans R Soc Lond B Biol Sci,* 370**,** 20140330.
MATIC, S., JIANG, M., NICHOLLS, T. J., UHLER, J. P., DIRKSEN-SCHWANENLAND, C., POLOSA, P. L., SIMARD, M. L., LI, X., ATANASSOV, I., RACKHAM, O., FILIPOVSKA, A., STEWART, J. B., FALKENBERG, M., LARSSON, N. G. & MILENKOVIC, D. 2018. Mice lacking the mitochondrial exonuclease MGME1 accumulate mtDNA deletions without developing progeria. *Nat Commun,* 9**,** 1202.
MATSUSHIMA, Y., GOTO, Y. & KAGUNI, L. S. 2010. Mitochondrial Lon protease regulates mitochondrial DNA copy number and transcription by selective degradation of mitochondrial transcription factor A (TFAM). *Proc Natl Acad Sci U S A,* 107**,** 18410-5.
MATSUSHIMA, Y., TAKAHASHI, K., YUE, S., FUJIYOSHI, Y., YOSHIOKA, H., AIHARA, M., SETOYAMA, D., UCHIUMI, T., FUKUCHI, S. & KANG, D. 2021. Mitochondrial Lon protease is a gatekeeper for proteins newly imported into the matrix. *Commun Biol,* 4**,** 974.
MAYS, J. N., CAMACHO-VILLASANA, Y., GARCIA-VILLEGAS, R., PEREZ-MARTINEZ, X., BARRIENTOS, A. & FONTANESI, F. 2019. The mitoribosome-specific protein mS38 is preferentially required for synthesis of cytochrome c oxidase subunits. *Nucleic Acids Res,* 47**,** 5746-5760.
MERCER, R., TIM, NEPH, S., DINGER, E., MARCEL, CRAWFORD, J., SMITH, A., MARTIN, SHEARWOOD, J., ANNE-MARIE, HAUGEN, E., BRACKEN, P., CAMERON, RACKHAM, O., STAMATOYANNOPOULOS, A., JOHN, FILIPOVSKA, A. & MATTICK, S., JOHN 2011. The Human Mitochondrial Transcriptome. *Cell,* 146**,** 645-658.
METODIEV, M. D., LESKO, N., PARK, C. B., CAMARA, Y., SHI, Y., WIBOM, R., HULTENBY, K., GUSTAFSSON, C. M. & LARSSON, N. G. 2009. Methylation

of 12S rRNA is necessary for in vivo stability of the small subunit of the mammalian mitochondrial ribosome. *Cell Metab,* 9**,** 386-97.

METODIEV, M. D., SPAHR, H., LOGUERCIO POLOSA, P., MEHARG, C., BECKER, C., ALTMUELLER, J., HABERMANN, B., LARSSON, N. G. & RUZZENENTE, B. 2014. NSUN4 is a dual function mitochondrial protein required for both methylation of 12S rRNA and coordination of mitoribosomal assembly. *PLoS Genet,* 10**,** e1004110.

MILENKOVIC, D., MATIC, S., KUHL, I., RUZZENENTE, B., FREYER, C., JEMT, E., PARK, C. B., FALKENBERG, M. & LARSSON, N. G. 2013. TWINKLE is an essential mitochondrial helicase required for synthesis of nascent D-loop strands and complete mtDNA replication. *Hum Mol Genet,* 22**,** 1983-93.

MINCZUK, M., HE, J., DUCH, A. M., ETTEMA, T. J., CHLEBOWSKI, A., DZIONEK, K., NIJTMANS, L. G., HUYNEN, M. A. & HOLT, I. J. 2011. TEFM (c17orf42) is necessary for transcription of human mtDNA. *Nucleic Acids Res,* 39**,** 4284-99.

MITCHELL, P. 1976. Possible molecular mechanisms of the protonmotive function of cytochrome systems. *J Theor Biol,* 62**,** 327-67.

MIZUSAWA, S. & GOTTESMAN, S. 1983. Protein degradation in Escherichia coli: the lon gene controls the stability of sulA protein. *Proc Natl Acad Sci U S A,* 80**,** 358-62.

MNATSAKANYAN, N., LLAGUNO, M. C., YANG, Y., YAN, Y., WEBER, J., SIGWORTH, F. J. & JONAS, E. A. 2019. A mitochondrial megachannel resides in monomeric F(1)F(O) ATP synthase. *Nat Commun,* 10**,** 5823.

MOLINARI, F., MALARA, N., MOLLACE, V., ROSANO, G. & FERRARO, E. 2016. Animal models of cardiac cachexia. *Int J Cardiol,* 219**,** 105-10.

MONTOYA, J., CHRISTIANSON, T., LEVENS, D., RABINOWITZ, M. & ATTARDI, G. 1982. Identification of initiation sites for heavy-strand and light-strand transcription in human mitochondrial DNA. *Proc Natl Acad Sci U S A,* 79**,** 7195-9.

MOOSAVI, B., BERRY, E. A., ZHU, X. L., YANG, W. C. & YANG, G. F. 2019. The assembly of succinate dehydrogenase: a key enzyme in bioenergetics. *Cell Mol Life Sci,* 76**,** 4023-4042.

NAGAIKE, T., SUZUKI, T., KATOH, T. & UEDA, T. 2005. Human mitochondrial mRNAs are stabilized with polyadenylation regulated by mitochondria-specific poly(A) polymerase and polynucleotide phosphorylase. *J Biol Chem,* 280**,** 19721-7.

NAGAIKE, T., SUZUKI, T., TOMARI, Y., TAKEMOTO-HORI, C., NEGAYAMA, F., WATANABE, K. & UEDA, T. 2001. Identification and characterization of mammalian mitochondrial tRNA nucleotidyltransferases. *J Biol Chem,* 276**,** 40041-9.

NGO, H. B., LOVELY, G. A., PHILLIPS, R. & CHAN, D. C. 2014. Distinct structural features of TFAM drive mitochondrial DNA packaging versus transcriptional activation. *Nat Commun,* 5**,** 3077.

NIMMO, G. A. M., VENKATESH, S., PANDEY, A. K., MARSHALL, C. R., HAZRATI, L. N., BLASER, S., AHMED, S., CAMERON, J., SINGH, K., RAY, P. N., SUZUKI, C. K. & YOON, G. 2019. Bi-allelic mutations of LONP1 encoding the mitochondrial LonP1 protease cause pyruvate dehydrogenase deficiency and profound neurodegeneration with progressive cerebellar atrophy. *Hum Mol Genet,* 28**,** 290-306.

NISHII, W., SUZUKI, T., NAKADA, M., KIM, Y. T., MURAMATSU, T. & TAKAHASHI, K. 2005. Cleavage mechanism of ATP-dependent Lon protease toward ribosomal S2 protein. *FEBS Lett,* 579**,** 6846-50.

NOLTE, H., MACVICAR, T. D., TELLKAMP, F. & KRUGER, M. 2018. Instant Clue: A Software Suite for Interactive Data Visualization and Analysis. *Sci Rep,* 8**,** 12648.

NUNNARI, J. & SUOMALAINEN, A. 2012. Mitochondria: in sickness and in health. *Cell,* 148**,** 1145-59.

OCHALA, J., CARPÉN, O. & LARSSON, L. 2009. Maintenance of muscle mass, fiber size, and contractile function in mice lacking the Z-disc protein myotilin. *Upsala Journal of Medical Sciences,* 114**,** 235-241.

OHKUBO, A., VAN HAUTE, L., RUDLER, D. L., STENTENBACH, M., STEINER, F. A., RACKHAM, O., MINCZUK, M., FILIPOVSKA, A. & MARTINOU, J. C. 2021. The FASTK family proteins fine-tune mitochondrial RNA processing. *PLoS Genet,* 17**,** e1009873.

OJALA, D., MONTOYA, J. & ATTARDI, G. 1981. tRNA punctuation model of RNA processing in human mitochondria. *Nature,* 290**,** 470-4.

PAREEK, G., THOMAS, R. E., VINCOW, E. S., MORRIS, D. R. & PALLANCK, L. J. 2018. Lon protease inactivation in Drosophila causes unfolded protein stress and inhibition of mitochondrial translation. *Cell Death Discov,* 4**,** 51.

PARK, C. B., ASIN-CAYUELA, J., CAMARA, Y., SHI, Y., PELLEGRINI, M., GASPARI, M., WIBOM, R., HULTENBY, K., ERDJUMENT-BROMAGE, H., TEMPST, P., FALKENBERG, M., GUSTAFSSON, C. M. & LARSSON, N. G. 2007. MTERF3 is a negative regulator of mammalian mtDNA transcription. *Cell,* 130**,** 273-85.

PAUL, M. F., ALUSHIN, G. M., BARROS, M. H., RAK, M. & TZAGOLOFF, A. 2012. The putative GTPase encoded by MTG3 functions in a novel pathway for regulating assembly of the small subunit of yeast mitochondrial ribosomes. *J Biol Chem,* 287**,** 24346-55.

PERKS, K. L., FERREIRA, N., RICHMAN, T. R., ERMER, J. A., KUZNETSOVA, I., SHEARWOOD, A. J., LEE, R. G., VIOLA, H. M., JOHNSTONE, V. P. A., MATTHEWS, V., HOOL, L. C., RACKHAM, O. & FILIPOVSKA, A. 2017. Adult-onset obesity is triggered by impaired mitochondrial gene expression. *Sci Adv,* 3**,** e1700677.

PETER, B., WADDINGTON, C. L., OLAHOVA, M., SOMMERVILLE, E. W., HOPTON, S., PYLE, A., CHAMPION, M., OHLSON, M., SIIBAK, T., CHRZANOWSKA-LIGHTOWLERS, Z. M. A., TAYLOR, R. W., FALKENBERG, M. & LIGHTOWLERS, R. N. 2018. Defective mitochondrial protease LonP1 can cause classical mitochondrial disease. *Hum Mol Genet,* 27**,** 1743-1753.

PHILLIPS, T. A., VANBOGELEN, R. A. & NEIDHARDT, F. C. 1984. lon gene product of Escherichia coli is a heat-shock protein. *J Bacteriol,* 159**,** 283-7.

PIETRAS, Z., WOJCIK, M. A., BOROWSKI, L. S., SZEWCZYK, M., KULINSKI, T. M., CYSEWSKI, D., STEPIEN, P. P., DZIEMBOWSKI, A. & SZCZESNY, R. J. 2018. Controlling the mitochondrial antisense - role of the SUV3-PNPase complex and its co-factor GRSF1 in mitochondrial RNA surveillance. *Mol Cell Oncol,* 5**,** e1516452.

PINKE, G., ZHOU, L. & SAZANOV, L. A. 2020. Cryo-EM structure of the entire mammalian F-type ATP synthase. *Nat Struct Mol Biol,* 27**,** 1077-1085.

POLIANSKYTE, Z., PEITSARO, N., DAPKUNAS, A., LIOBIKAS, J., SOLIYMANI, R., LALOWSKI, M., SPEER, O., SEITSONEN, J., BUTCHER, S., CEREGHETTI, G. M., LINDER, M. D., MERCKEL, M., THOMPSON, J. & ERIKSSON, O. 2009. LACTB is a filament-forming protein localized in mitochondria. *Proc Natl Acad Sci U S A,* 106**,** 18960-5.

POLLECKER, K., SYLVESTER, M. & VOOS, W. 2021. Proteomic analysis demonstrates the role of the quality control protease LONP1 in mitochondrial protein aggregation. *J Biol Chem,* 297**,** 101134.
POMATTO, L. C., RAYNES, R. & DAVIES, K. J. 2017. The peroxisomal Lon protease LonP2 in aging and disease: functions and comparisons with mitochondrial Lon protease LonP1. *Biol Rev Camb Philos Soc,* 92**,** 739-753.
POPOW, J., ALLEAUME, A. M., CURK, T., SCHWARZL, T., SAUER, S. & HENTZE, M. W. 2015. FASTKD2 is an RNA-binding protein required for mitochondrial RNA processing and translation. *RNA,* 21**,** 1873-84.
POSSE, V. & GUSTAFSSON, C. M. 2017. Human Mitochondrial Transcription Factor B2 Is Required for Promoter Melting during Initiation of Transcription. *J Biol Chem,* 292**,** 2637-2645.
POSSE, V., SHAHZAD, S., FALKENBERG, M., HALLBERG, B. M. & GUSTAFSSON, C. M. 2015. TEFM is a potent stimulator of mitochondrial transcription elongation in vitro. *Nucleic Acids Res,* 43**,** 2615-24.
POWELL, C. A. & MINCZUK, M. 2020. TRMT2B is responsible for both tRNA and rRNA m(5)U-methylation in human mitochondria. *RNA Biol,* 17**,** 451-462.
PROTASONI, M., PEREZ-PEREZ, R., LOBO-JARNE, T., HARBOUR, M. E., DING, S., PENAS, A., DIAZ, F., MORAES, C. T., FEARNLEY, I. M., ZEVIANI, M., UGALDE, C. & FERNANDEZ-VIZARRA, E. 2020. Respiratory supercomplexes act as a platform for complex III-mediated maturation of human mitochondrial complexes I and IV. *EMBO J,* 39**,** e102817.
PROTASONI, M. & ZEVIANI, M. 2021. Mitochondrial Structure and Bioenergetics in Normal and Disease Conditions. *International Journal of Molecular Sciences,* 22**,** 586.
PUCHADES, C., RAMPELLO, A. J., SHIN, M., GIULIANO, C. J., WISEMAN, R. L., GLYNN, S. E. & LANDER, G. C. 2017. Structure of the mitochondrial inner membrane AAA+ protease YME1 gives insight into substrate processing. *Science,* 358.
QUIROS, P. M., ESPANOL, Y., ACIN-PEREZ, R., RODRIGUEZ, F., BARCENA, C., WATANABE, K., CALVO, E., LOUREIRO, M., FERNANDEZ-GARCIA, M. S., FUEYO, A., VAZQUEZ, J., ENRIQUEZ, J. A. & LOPEZ-OTIN, C. 2014. ATP-dependent Lon protease controls tumor bioenergetics by reprogramming mitochondrial activity. *Cell Rep,* 8**,** 542-56.
QUIROS, P. M., GOYAL, A., JHA, P. & AUWERX, J. 2017. Analysis of mtDNA/nDNA Ratio in Mice. *Curr Protoc Mouse Biol,* 7**,** 47-54.
RACKHAM, O., BUSCH, J. D., MATIC, S., SIIRA, S. J., KUZNETSOVA, I., ATANASSOV, I., ERMER, J. A., SHEARWOOD, A. M., RICHMAN, T. R., STEWART, J. B., MOURIER, A., MILENKOVIC, D., LARSSON, N. G. & FILIPOVSKA, A. 2016. Hierarchical RNA Processing Is Required for Mitochondrial Ribosome Assembly. *Cell Rep,* 16**,** 1874-90.
RACKHAM, O. & FILIPOVSKA, A. 2022. Organization and expression of the mammalian mitochondrial genome. *Nat Rev Genet,* 23**,** 606-623.
RAJALA, N., HENSEN, F., WESSELS, H. J., IVES, D., GLOERICH, J. & SPELBRINK, J. N. 2015. Whole cell formaldehyde cross-linking simplifies purification of mitochondrial nucleoids and associated proteins involved in mitochondrial gene expression. *PLoS One,* 10**,** e0116726.
RASHEED, M. & TARJAN, G. 2018. Succinate Dehydrogenase Complex: An Updated Review. *Arch Pathol Lab Med,* 142**,** 1564-1570.
RATH, S., SHARMA, R., GUPTA, R., AST, T., CHAN, C., DURHAM, T. J., GOODMAN, R. P., GRABAREK, Z., HAAS, M. E., HUNG, W. H. W., JOSHI, P. R.,

JOURDAIN, A. A., KIM, S. H., KOTRYS, A. V., LAM, S. S., MCCOY, J. G., MEISEL, J. D., MIRANDA, M., PANDA, A., PATGIRI, A., ROGERS, R., SADRE, S., SHAH, H., SKINNER, O. S., TO, T. L., WALKER, M. A., WANG, H., WARD, P. S., WENGROD, J., YUAN, C. C., CALVO, S. E. & MOOTHA, V. K. 2021. MitoCarta3.0: an updated mitochondrial proteome now with sub-organelle localization and pathway annotations. *Nucleic Acids Res,* 49**,** D1541-D1547.

REP, M., VAN DIJL, J. M., SUDA, K., SCHATZ, G., GRIVELL, L. A. & SUZUKI, C. K. 1996. Promotion of mitochondrial membrane complex assembly by a proteolytically inactive yeast Lon. *Science,* 274**,** 103-6.

REY, T., ZAGANELLI, S., CUILLERY, E., VARTHOLOMAIOU, E., CROISIER, M., MARTINOU, J. C. & MANLEY, S. 2020. Mitochondrial RNA granules are fluid condensates positioned by membrane dynamics. *Nat Cell Biol,* 22**,** 1180-1186.

RICHTER-DENNERLEIN, R., OELJEKLAUS, S., LORENZI, I., RONSOR, C., BARETH, B., SCHENDZIELORZ, A. B., WANG, C., WARSCHEID, B., REHLING, P. & DENNERLEIN, S. 2016. Mitochondrial Protein Synthesis Adapts to Influx of Nuclear-Encoded Protein. *Cell,* 167**,** 471-483 e10.

RIGAS, S., DARAS, G., LAXA, M., MARATHIAS, N., FASSEAS, C., SWEETLOVE, L. J. & HATZOPOULOS, P. 2009. Role of Lon1 protease in post-germinative growth and maintenance of mitochondrial function in Arabidopsis thaliana. *New Phytol,* 181**,** 588-600.

ROBBERSON, D. L., KASAMATSU, H. & VINOGRAD, J. 1972. Replication of mitochondrial DNA. Circular replicative intermediates in mouse L cells. *Proc Natl Acad Sci U S A,* 69**,** 737-41.

ROBERTSON, G. T., KOVACH, M. E., ALLEN, C. A., FICHT, T. A. & ROOP, R. M., 2ND 2000. The Brucella abortus Lon functions as a generalized stress response protease and is required for wild-type virulence in BALB/c mice. *Mol Microbiol,* 35**,** 577-88.

RORBACH, J., NICHOLLS, T. J. & MINCZUK, M. 2011. PDE12 removes mitochondrial RNA poly(A) tails and controls translation in human mitochondria. *Nucleic Acids Res,* 39**,** 7750-63.

ROSEN, R., BIRAN, D., GUR, E., BECHER, D., HECKER, M. & RON, E. Z. 2002. Protein aggregation in Escherichia coli: role of proteases. *FEMS Microbiol Lett,* 207**,** 9-12.

RUDLER, D. L., HUGHES, L. A., PERKS, K. L., RICHMAN, T. R., KUZNETSOVA, I., ERMER, J. A., ABUDULAI, L. N., SHEARWOOD, A. J., VIOLA, H. M., HOOL, L. C., SIIRA, S. J., RACKHAM, O. & FILIPOVSKA, A. 2019. Fidelity of translation initiation is required for coordinated respiratory complex assembly. *Sci Adv,* 5**,** eaay2118.

RUZZENENTE, B., METODIEV, M. D., WREDENBERG, A., BRATIC, A., PARK, C. B., CAMARA, Y., MILENKOVIC, D., ZICKERMANN, V., WIBOM, R., HULTENBY, K., ERDJUMENT-BROMAGE, H., TEMPST, P., BRANDT, U., STEWART, J. B., GUSTAFSSON, C. M. & LARSSON, N. G. 2012. LRPPRC is necessary for polyadenylation and coordination of translation of mitochondrial mRNAs. *EMBO J,* 31**,** 443-56.

SAMHITA, L., RAVAL, P. K. & AGASHE, D. 2020. Global mistranslation increases cell survival under stress in Escherichia coli. *PLoS Genet,* 16**,** e1008654.

SANCHEZ, M. I., MERCER, T. R., DAVIES, S. M., SHEARWOOD, A. M., NYGARD, K. K., RICHMAN, T. R., MATTICK, J. S., RACKHAM, O. & FILIPOVSKA, A. 2011. RNA processing in human mitochondria. *Cell Cycle,* 10**,** 2904-16.

SASARMAN, F., BRUNEL-GUITTON, C., ANTONICKA, H., WAI, T., SHOUBRIDGE, E. A. & CONSORTIUM, L. 2010. LRPPRC and SLIRP interact in a

ribonucleoprotein complex that regulates posttranscriptional gene expression in mitochondria. *Mol Biol Cell,* 21**,** 1315-23.
SATO, R., VATIC, M., DA FONSECA, G. W. P. & VON HAEHLING, S. 2022. Sarcopenia and Frailty in Heart Failure: Is There a Biomarker Signature? *Current Heart Failure Reports,* 19**,** 400-411.
SCHAGGER, H. & PFEIFFER, K. 2000. Supercomplexes in the respiratory chains of yeast and mammalian mitochondria. *EMBO J,* 19**,** 1777-83.
SCHINDELIN, J., ARGANDA-CARRERAS, I., FRISE, E., KAYNIG, V., LONGAIR, M., PIETZSCH, T., PREIBISCH, S., RUEDEN, C., SAALFELD, S., SCHMID, B., TINEVEZ, J. Y., WHITE, D. J., HARTENSTEIN, V., ELICEIRI, K., TOMANCAK, P. & CARDONA, A. 2012. Fiji: an open-source platform for biological-image analysis. *Nat Methods,* 9**,** 676-82.
SEPURI, N. B. V., ANGIREDDY, R., SRINIVASAN, S., GUHA, M., SPEAR, J., LU, B., ANANDATHEERTHAVARADA, H. K., SUZUKI, C. K. & AVADHANI, N. G. 2017. Mitochondrial LON protease-dependent degradation of cytochrome c oxidase subunits under hypoxia and myocardial ischemia. *Biochim Biophys Acta Bioenerg,* 1858**,** 519-528.
SERERO, A., GIGLIONE, C., SARDINI, A., MARTINEZ-SANZ, J. & MEINNEL, T. 2003. An unusual peptide deformylase features in the human mitochondrial N-terminal methionine excision pathway. *J Biol Chem,* 278**,** 52953-63.
SHI, Y., DIERCKX, A., WANROOIJ, P. H., WANROOIJ, S., LARSSON, N. G., WILHELMSSON, L. M., FALKENBERG, M. & GUSTAFSSON, C. M. 2012. Mammalian transcription factor A is a core component of the mitochondrial transcription machinery. *Proc Natl Acad Sci U S A,* 109**,** 16510-5.
SHIN, C. S., MENG, S., GARBIS, S. D., MORADIAN, A., TAYLOR, R. W., SWEREDOSKI, M. J., LOMENICK, B. & CHAN, D. C. 2021a. LONP1 and mtHSP70 cooperate to promote mitochondrial protein folding. *Nat Commun,* 12**,** 265.
SHIN, M., WATSON, E. R., SONG, A. S., MINDREBO, J. T., NOVICK, S. J., GRIFFIN, P. R., WISEMAN, R. L. & LANDER, G. C. 2021b. Structures of the human LONP1 protease reveal regulatory steps involved in protease activation. *Nat Commun,* 12**,** 3239.
SIGNES, A. & FERNANDEZ-VIZARRA, E. 2018. Assembly of mammalian oxidative phosphorylation complexes I-V and supercomplexes. *Essays Biochem,* 62**,** 255-270.
SIIRA, S. J., ROSSETTI, G., RICHMAN, T. R., PERKS, K., ERMER, J. A., KUZNETSOVA, I., HUGHES, L., SHEARWOOD, A. J., VIOLA, H. M., HOOL, L. C., RACKHAM, O. & FILIPOVSKA, A. 2018. Concerted regulation of mitochondrial and nuclear non-coding RNAs by a dual-targeted RNase Z. *EMBO Rep,* 19**,** e46198.
SIIRA, S. J., SPAHR, H., SHEARWOOD, A. J., RUZZENENTE, B., LARSSON, N. G., RACKHAM, O. & FILIPOVSKA, A. 2017. LRPPRC-mediated folding of the mitochondrial transcriptome. *Nat Commun,* 8**,** 1532.
SILVA-PINHEIRO, P., PARDO-HERNANDEZ, C., REYES, A., TILOKANI, L., MISHRA, A., CERUTTI, R., LI, S., ROZSIVALOVA, D. H., VALENZUELA, S., DOGAN, S. A., PETER, B., FERNANDEZ-SILVA, P., TRIFUNOVIC, A., PRUDENT, J., MINCZUK, M., BINDOFF, L., MACAO, B., ZEVIANI, M., FALKENBERG, M. & VISCOMI, C. 2021. DNA polymerase gamma mutations that impair holoenzyme stability cause catalytic subunit depletion. *Nucleic Acids Res,* 49**,** 5230-5248.

SKARNES, W. C., ROSEN, B., WEST, A. P., KOUTSOURAKIS, M., BUSHELL, W., IYER, V., MUJICA, A. O., THOMAS, M., HARROW, J., COX, T., JACKSON, D., SEVERIN, J., BIGGS, P., FU, J., NEFEDOV, M., DE JONG, P. J., STEWART, A. F. & BRADLEY, A. 2011. A conditional knockout resource for the genome-wide study of mouse gene function. *Nature,* 474**,** 337-42.

SNYDER, C. H., MERBITZ-ZAHRADNIK, T., LINK, T. A. & TRUMPOWER, B. L. 1999. Role of the Rieske iron-sulfur protein midpoint potential in the protonmotive Q-cycle mechanism of the cytochrome bc1 complex. *J Bioenerg Biomembr,* 31**,** 235-42.

SPELBRINK, J. N., LI, F. Y., TIRANTI, V., NIKALI, K., YUAN, Q. P., TARIQ, M., WANROOIJ, S., GARRIDO, N., COMI, G., MORANDI, L., SANTORO, L., TOSCANO, A., FABRIZI, G. M., SOMER, H., CROXEN, R., BEESON, D., POULTON, J., SUOMALAINEN, A., JACOBS, H. T., ZEVIANI, M. & LARSSON, C. 2001. Human mitochondrial DNA deletions associated with mutations in the gene encoding Twinkle, a phage T7 gene 4-like protein localized in mitochondria. *Nat Genet,* 28**,** 223-31.

SPIKES, T. E., MONTGOMERY, M. G. & WALKER, J. E. 2020. Structure of the dimeric ATP synthase from bovine mitochondria. *Proc Natl Acad Sci U S A,* 117**,** 23519-23526.

STAHLBERG, H., KUTEJOVA, E., SUDA, K., WOLPENSINGER, B., LUSTIG, A., SCHATZ, G., ENGEL, A. & SUZUKI, C. K. 1999. Mitochondrial Lon of Saccharomyces cerevisiae is a ring-shaped protease with seven flexible subunits. *Proceedings of the National Academy of Sciences of the United States of America,* 96**,** 6787-6790.

STRAUSS, K. A., JINKS, R. N., PUFFENBERGER, E. G., VENKATESH, S., SINGH, K., CHENG, I., MIKITA, N., THILAGAVATHI, J., LEE, J., SARAFIANOS, S., BENKERT, A., KOEHLER, A., ZHU, A., TROVILLION, V., MCGLINCY, M., MORLET, T., DEARDORFF, M., INNES, A. M., PRASAD, C., CHUDLEY, A. E., LEE, I. N. & SUZUKI, C. K. 2015. CODAS syndrome is associated with mutations of LONP1, encoding mitochondrial AAA+ Lon protease. *Am J Hum Genet,* 96**,** 121-35.

STROUD, D. A., SURGENOR, E. E., FORMOSA, L. E., RELJIC, B., FRAZIER, A. E., DIBLEY, M. G., OSELLAME, L. D., STAIT, T., BEILHARZ, T. H., THORBURN, D. R., SALIM, A. & RYAN, M. T. 2016. Accessory subunits are integral for assembly and function of human mitochondrial complex I. *Nature,* 538**,** 123-126.

SUZUKI, C. K., SUDA, K., WANG, N. & SCHATZ, G. 1994. Requirement for the yeast gene LON in intramitochondrial proteolysis and maintenance of respiration. *Science,* 264**,** 273-6.

SUZUKI, T., YASHIRO, Y., KIKUCHI, I., ISHIGAMI, Y., SAITO, H., MATSUZAWA, I., OKADA, S., MITO, M., IWASAKI, S., MA, D., ZHAO, X., ASANO, K., LIN, H., KIRINO, Y., SAKAGUCHI, Y. & SUZUKI, T. 2020. Complete chemical structures of human mitochondrial tRNAs. *Nat Commun,* 11**,** 4269.

SWAMY, K. H. & GOLDBERG, A. L. 1981. E. coli contains eight soluble proteolytic activities, one being ATP dependent. *Nature,* 292**,** 652-4.

SZCZEPANOWSKA, K., MAITI, P., KUKAT, A., HOFSETZ, E., NOLTE, H., SENFT, K., BECKER, C., RUZZENENTE, B., HORNIG-DO, H. T., WIBOM, R., WIESNER, R. J., KRUGER, M. & TRIFUNOVIC, A. 2016. CLPP coordinates mitoribosomal assembly through the regulation of ERAL1 levels. *EMBO J,* 35**,** 2566-2583.

SZCZEPANOWSKA, K. & TRIFUNOVIC, A. 2022. Mitochondrial matrix proteases: quality control and beyond. *FEBS J,* 289**,** 7128-7146.

SZEWCZYK, M., MALIK, D., BOROWSKI, L. S., CZARNOMSKA, S. D., KOTRYS, A. V., KLOSOWSKA-KOSICKA, K., NOWOTNY, M. & SZCZESNY, R. J. 2020. Human REXO2 controls short mitochondrial RNAs generated by mtRNA processing and decay machinery to prevent accumulation of double-stranded RNA. *Nucleic Acids Res,* 48**,** 5572-5590.

TAN, B. G., MUTTI, C. D., SHI, Y., XIE, X., ZHU, X., SILVA-PINHEIRO, P., MENGER, K. E., DIAZ-MALDONADO, H., WEI, W., NICHOLLS, T. J., CHINNERY, P. F., MINCZUK, M., FALKENBERG, M. & GUSTAFSSON, C. M. 2022. The human mitochondrial genome contains a second light strand promoter. *Mol Cell,* 82**,** 3646-3660 e9.

TERZIOGLU, M., RUZZENENTE, B., HARMEL, J., MOURIER, A., JEMT, E., LOPEZ, M. D., KUKAT, C., STEWART, J. B., WIBOM, R., MEHARG, C., HABERMANN, B., FALKENBERG, M., GUSTAFSSON, C. M., PARK, C. B. & LARSSON, N. G. 2013. MTERF1 binds mtDNA to prevent transcriptional interference at the light-strand promoter but is dispensable for rRNA gene transcription regulation. *Cell Metab,* 17**,** 618-26.

TIAN, Q., LI, T., HOU, W., ZHENG, J., SCHRUM, L. W. & BONKOVSKY, H. L. 2011. Lon peptidase 1 (LONP1)-dependent breakdown of mitochondrial 5-aminolevulinic acid synthase protein by heme in human liver cells. *J Biol Chem,* 286**,** 26424-30.

TIMON-GOMEZ, A., NYVLTOVA, E., ABRIATA, L. A., VILA, A. J., HOSLER, J. & BARRIENTOS, A. 2018. Mitochondrial cytochrome c oxidase biogenesis: Recent developments. *Semin Cell Dev Biol,* 76**,** 163-178.

TIRANTI, V., BARAT-GUERIDE, B., BIJL, J., DIDONATO, S. & ZEVIANI, M. 1991. A full-length cDNA encoding a mitochondrial DNA-specific single-stranded DNA binding protein from Xenopus laevis. *Nucleic Acids Res,* 19**,** 4291.

TORRES-CABASSA, A. S. & GOTTESMAN, S. 1987. Capsule synthesis in Escherichia coli K-12 is regulated by proteolysis. *J Bacteriol,* 169**,** 981-9.

TRIFUNOVIC, A., WREDENBERG, A., FALKENBERG, M., SPELBRINK, J. N., ROVIO, A. T., BRUDER, C. E., BOHLOOLY, Y. M., GIDLOF, S., OLDFORS, A., WIBOM, R., TORNELL, J., JACOBS, H. T. & LARSSON, N. G. 2004. Premature ageing in mice expressing defective mitochondrial DNA polymerase. *Nature,* 429**,** 417-23.

VAN DYCK, L., NEUPERT, W. & LANGER, T. 1998. The ATP-dependent PIM1 protease is required for the expression of intron-containing genes in mitochondria. *Genes Dev,* 12**,** 1515-24.

VAN DYCK, L., PEARCE, D. A. & SHERMAN, F. 1994. PIM1 encodes a mitochondrial ATP-dependent protease that is required for mitochondrial function in the yeast Saccharomyces cerevisiae. *Journal of Biological Chemistry,* 269**,** 238-42.

VANDE WALLE, L., WIRAWAN, E., LAMKANFI, M., FESTJENS, N., VERSPURTEN, J., SAELENS, X., VANDEN BERGHE, T. & VANDENABEELE, P. 2010. The mitochondrial serine protease HtrA2/Omi cleaves RIP1 during apoptosis of Ba/F3 cells induced by growth factor withdrawal. *Cell Res,* 20**,** 421-33.

VENKATESH, S., LEE, J., SINGH, K., LEE, I. & SUZUKI, C. K. 2012. Multitasking in the mitochondrion by the ATP-dependent Lon protease.

VERCELLINO, I. & SAZANOV, L. A. 2021. Structure and assembly of the mammalian mitochondrial supercomplex CIII(2)CIV. *Nature,* 598**,** 364-367.

VERCELLINO, I. & SAZANOV, L. A. 2022. The assembly, regulation and function of the mitochondrial respiratory chain. *Nat Rev Mol Cell Biol,* 23**,** 141-161.

VIDONI, S., HARBOUR, M. E., GUERRERO-CASTILLO, S., SIGNES, A., DING, S., FEARNLEY, I. M., TAYLOR, R. W., TIRANTI, V., ARNOLD, S., FERNANDEZ-VIZARRA, E. & ZEVIANI, M. 2017. MR-1S Interacts with PET100 and PET117 in Module-Based Assembly of Human Cytochrome c Oxidase. *Cell Rep,* 18**,** 1727-1738.

VILARDO, E., NACHBAGAUER, C., BUZET, A., TASCHNER, A., HOLZMANN, J. & ROSSMANITH, W. 2012. A subcomplex of human mitochondrial RNase P is a bifunctional methyltransferase--extensive moonlighting in mitochondrial tRNA biogenesis. *Nucleic Acids Res,* 40**,** 11583-93.

VON HAEHLING, S., EBNER, N., DOS SANTOS, M. R., SPRINGER, J. & ANKER, S. D. 2017. Muscle wasting and cachexia in heart failure: mechanisms and therapies. *Nat Rev Cardiol,* 14**,** 323-341.

VOOS, W. 2013. Chaperone-protease networks in mitochondrial protein homeostasis. *Biochim Biophys Acta,* 1833**,** 388-99.

VOOS, W., JAWOREK, W., WILKENING, A. & BRUDEREK, M. 2016. Protein quality control at the mitochondrion. *Essays Biochem,* 60**,** 213-225.

WAGNER, I., ARLT, H., VAN DYCK, L., LANGER, T. & NEUPERT, W. 1994. Molecular chaperones cooperate with PIM1 protease in the degradation of misfolded proteins in mitochondria. *EMBO J,* 13**,** 5135-45.

WAGNER, I., VAN DYCK, L., SAVEL'EV, A. S., NEUPERT, W. & LANGER, T. 1997. Autocatalytic processing of the ATP-dependent PIM1 protease: crucial function of a pro-region for sorting to mitochondria. *EMBO J,* 16**,** 7317-25.

WAI, T., SAITA, S., NOLTE, H., MULLER, S., KONIG, T., RICHTER-DENNERLEIN, R., SPRENGER, H. G., MADRENAS, J., MUHLMEISTER, M., BRANDT, U., KRUGER, M. & LANGER, T. 2016. The membrane scaffold SLP2 anchors a proteolytic hub in mitochondria containing PARL and the i-AAA protease YME1L. *EMBO Rep,* 17**,** 1844-1856.

WANG, J., WILHELMSSON, H., GRAFF, C., LI, H., OLDFORS, A., RUSTIN, P., BRUNING, J. C., KAHN, C. R., CLAYTON, D. A., BARSH, G. S., THOREN, P. & LARSSON, N. G. 1999. Dilated cardiomyopathy and atrioventricular conduction blocks induced by heart-specific inactivation of mitochondrial DNA gene expression. *Nat Genet,* 21**,** 133-7.

WANG, N., GOTTESMAN, S., WILLINGHAM, M. C., GOTTESMAN, M. M. & MAURIZI, M. R. 1993. A human mitochondrial ATP-dependent protease that is highly homologous to bacterial Lon protease. *Proc Natl Acad Sci U S A,* 90**,** 11247-51.

WANG, Y. & HEKIMI, S. 2016. Understanding Ubiquinone. *Trends Cell Biol,* 26**,** 367-378.

WEI, F. Y., ZHOU, B., SUZUKI, T., MIYATA, K., UJIHARA, Y., HORIGUCHI, H., TAKAHASHI, N., XIE, P., MICHIUE, H., FUJIMURA, A., KAITSUKA, T., MATSUI, H., KOGA, Y., MOHRI, S., SUZUKI, T., OIKE, Y. & TOMIZAWA, K. 2015. Cdk5rap1-mediated 2-methylthio modification of mitochondrial tRNAs governs protein translation and contributes to myopathy in mice and humans. *Cell Metab,* 21**,** 428-42.

WIEDEMANN, N., FRAZIER, A. E. & PFANNER, N. 2004. The Protein Import Machinery of Mitochondria. *Journal of Biological Chemistry,* 279**,** 14473-14476.

WLODAWER, A., SEKULA, B., GUSTCHINA, A. & ROTANOVA, T. V. 2022. Structure and the Mode of Activity of Lon Proteases from Diverse Organisms. *J Mol Biol,* 434**,** 167504.

WU, S. B., MA, Y. S., WU, Y. T., CHEN, Y. C. & WEI, Y. H. Mitochondrial DNA mutation-elicited oxidative stress, oxidative damage, and altered gene expression in cultured cells of patients with MERRF syndrome. 2010. 256-266.
XAVIER, V. J. & MARTINOU, J. C. 2021. RNA Granules in the Mitochondria and Their Organization under Mitochondrial Stresses. *Int J Mol Sci,* 22**,** 9502.
XIA, D., ESSER, L., TANG, W. K., ZHOU, F., ZHOU, Y., YU, L. & YU, C. A. 2013. Structural analysis of cytochrome bc1 complexes: implications to the mechanism of function. *Biochim Biophys Acta,* 1827**,** 1278-94.
YANG, J., SONG, A. S., WISEMAN, R. L. & LANDER, G. C. 2022. Cryo-EM structure of hexameric yeast Lon protease (PIM1) highlights the importance of conserved structural elements. *J Biol Chem,* 298**,** 101694.
YANG, Z., WANG, L., YANG, C., PU, S., GUO, Z., WU, Q., ZHOU, Z. & ZHAO, H. 2021. Mitochondrial Membrane Remodeling. *Front Bioeng Biotechnol,* 9**,** 786806.
YOSHINO, K., MUNAKATA, H., KUGE, O., ITO, A. & OGISHIMA, T. 2007. Haeme-regulated degradation of delta-aminolevulinate synthase 1 in rat liver mitochondria. *J Biochem,* 142**,** 453-8.
YU, S., MENG, S., XIANG, M. & MA, H. 2021. Phosphoenolpyruvate carboxykinase in cell metabolism: Roles and mechanisms beyond gluconeogenesis. *Mol Metab,* 53**,** 101257.
ZEHNBAUER, B. A., FOLEY, E. C., HENDERSON, G. W. & MARKOVITZ, A. 1981. Identification and purification of the Lon+ (capR+) gene product, a DNA-binding protein. *Proc Natl Acad Sci U S A,* 78**,** 2043-7.
ZEINERT, R. D., BANIASADI, H., TU, B. P. & CHIEN, P. 2020. The Lon Protease Links Nucleotide Metabolism with Proteotoxic Stress. *Mol Cell,* 79**,** 758-767 e6.
ZHANG, D., KEILTY, D., ZHANG, Z. F. & CHIAN, R. C. 2017. Mitochondria in oocyte aging: current understanding. *Facts Views Vis Obgyn,* 9**,** 29-38.
ZHAO, K., HUANG, X., ZHAO, W., LU, B. & YANG, Z. 2022. LONP1-mediated mitochondrial quality control safeguards metabolic shifts in heart development. *Development,* 149.
ZHU, J., VINOTHKUMAR, K. R. & HIRST, J. 2016. Structure of mammalian respiratory complex I. *Nature,* 536**,** 354-358.
ZHU, X., XIE, X., DAS, H., TAN, B. G., SHI, Y., AL-BEHADILI, A., PETER, B., MOTORI, E., VALENZUELA, S., POSSE, V., GUSTAFSSON, C. M., HALLBERG, B. M. & FALKENBERG, M. 2022. Non-coding 7S RNA inhibits transcription via mitochondrial RNA polymerase dimerization. *Cell,* 185**,** 2309-2323 e24.
ZIMORSKI, V., KU, C., MARTIN, W. F. & GOULD, S. B. 2014. Endosymbiotic theory for organelle origins.
ZURITA RENDON, O. & SHOUBRIDGE, E. A. 2018. LONP1 Is Required for Maturation of a Subset of Mitochondrial Proteins, and Its Loss Elicits an Integrated Stress Response. *Mol Cell Biol,* 38.

6 Supplementary data

Table 6.1 | Supplementary table for the Figure 3.27

Gene name	Transcriptome			Proteome		
	log fold change	padj	padj < 0.05	log fold change	q-value	q-value < 0.05
Atad3	0.206	0.232	-	0.806	0.001	+
C1qbp	0.168	0.545	-	0.909	0.004	+
Dap3/Mrps29	-0.123	0.468	-	1.052	0.004	+
Ddx28	0.508	0.057	-	1.536	0.007	+
Dhx30	-0.121	0.697	-	2.968	0.000	+
Dnaja3	0.492	0.000	+	1.591	0.000	+
Elac2	0.556	0.003	+	2.866	0.001	+
Fastk	-0.375	0.002	+			NA
Fastkd5	0.199	0.494	-	2.936	0.002	+
Gadd45gip1/Mrpl59	-0.086	0.652	-	1.949	0.007	+
Gatb	0.402	0.098	-	1.490	0.004	+
Gfm1	-0.122	0.394	-	0.953	0.000	+
Gfm2	-0.104	0.605	-	1.147	0.001	+
Grsf1	-0.002	0.960	-	1.623	0.001	+
Gtpbp6	0.598	0.046	+			NA
Metap1d/Map1d	-0.082	0.665	-	3.876	0.001	+
Mettl15	0.314	0.430	-	1.209	0.018	+
Mrm1	-0.259	0.454	-	0.741	0.036	+
Mrm3/Rnmd1	0.016	0.991	-	3.155	0.001	+
Mrpl1	-0.008	1.000	-	1.335	0.000	+
Mrpl10	0.127	0.454	-	2.571	0.006	+
Mrpl11	-0.218	0.318	-	1.331	0.003	+
Mrpl12	-0.358	0.024	+	0.777	0.018	+
Mrpl13	0.217	0.241	-	2.820	0.000	+
Mrpl14	-0.608	0.016	+	2.247	0.000	+
Mrpl15	0.313	0.039	+	1.591	0.000	+
Mrpl16	-0.161	0.443	-	2.957	0.000	+
Mrpl17	-0.165	0.478	-	1.759	0.000	+
Mrpl18	-0.707	0.000	+	0.620	0.027	+
Mrpl19	0.637	0.000	+	1.757	0.001	+
Mrpl2	-0.082	0.624	-	1.285	0.009	+
Mrpl20	0.461	0.010	+	1.085	0.005	+
Mrpl21	0.286	0.143	-	2.453	0.000	+

Mrpl22	-0.011	0.958	-	1.936	0.000	+
Mrpl23	1.271	0.027	+	2.481	0.000	+
Mrpl24	0.717	0.000	+	3.183	0.000	+
Mrpl27	0.222	0.388	-	2.220	0.000	+
Mrpl28	-0.671	0.000	+	2.168	0.000	+
Mrpl3	-0.231	0.113	-	2.355	0.001	+
Mrpl30	-0.208	0.169	-	0.945	0.003	+
Mrpl32	0.285	0.210	-	2.083	0.041	+
Mrpl33	0.432	0.007	+	2.967	0.003	+
Mrpl35	0.411	0.016	+	2.300	0.000	+
Mrpl37	-0.223	0.194	-	1.143	0.000	+
Mrpl38	0.347	0.025	+	2.047	0.001	+
Mrpl39	-0.087	0.658	-	1.715	0.001	+
Mrpl4	-0.312	0.036	+	1.899	0.000	+
Mrpl40	0.544	0.005	+	0.601	0.003	+
Mrpl41	-0.545	0.006	+	0.562	0.192	-
Mrpl42	-0.653	0.000	+	2.757	0.005	+
Mrpl43	0.119	0.557	-	0.606	0.005	+
Mrpl44	-0.140	0.428	-	1.133	0.003	+
Mrpl45	-0.349	0.042	+	1.469	0.001	+
Mrpl46	-0.217	0.405	-	1.816	0.000	+
Mrpl47	0.749	0.000	+	1.089	0.000	+
Mrpl48	0.043	0.873	-	1.408	0.001	+
Mrpl49	-0.287	0.139	-	0.900	0.037	+
Mrpl50	-0.513	0.001	+	0.965	0.029	+
Mrpl51	-0.246	0.054	-	3.626	0.001	+
Mrpl52	0.551	0.009	+			NA
Mrpl53	0.141	0.450	-	1.632	0.001	+
Mrpl54	0.565	0.001	+	0.960	0.061	-
Mrpl55	-0.216	0.202	-	1.288	0.002	+
Mrpl57	0.569	0.004	+	0.073	0.918	-
Mrpl58	0.012	0.908	-	1.163	0.009	+
Mrpl9	-0.167	0.345	-	2.074	0.000	+
Mrps10	0.732	0.000	+	0.333	0.193	-
Mrps14	0.090	0.691	-	0.966	0.011	+
Mrps16	0.023	0.875	-	2.089	0.002	+
Mrps17	0.258	0.196	-	2.491	0.000	+
Mrps18a	0.255	0.187	-	3.044	0.003	+
Mrps18b	1.021	0.000	+	1.437	0.000	+
Mrps18c	0.454	0.061	-	1.142	0.037	+

Mrps21	-0.556	0.000	+	1.592	0.000	+
Mrps23	0.429	0.003	+	3.022	0.000	+
Mrps24	-0.067	0.792	-	2.556	0.000	+
Mrps25	-0.082	0.757	-	0.930	0.006	+
Mrps27	-0.166	0.428	-	0.794	0.017	+
Mrps28	-0.146	0.483	-	1.874	0.000	+
Mrps30	0.363	0.057	-	1.719	0.002	+
Mrps31	-0.495	0.002	+	0.614	0.090	-
Mrps33	-0.382	0.032	+	1.171	0.004	+
Mrps34	0.427	0.024	+	1.718	0.000	+
Mrps35	-0.658	0.001	+	0.256	0.424	-
Mrps36	-0.781	0.000	+	-0.481	0.170	-
Mrps6	0.142	0.668	-	0.718	0.046	+
Mrps7	-0.245	0.146	-	1.516	0.001	+
Mrps9	-0.243	0.122	-	2.249	0.000	+
Mterf3	-0.029	0.856	-	1.176	0.019	+
Mtg1/Gtpbp7	-0.247	0.452	-	2.703	0.000	+
Mtg2/Gtbpb5	-0.213	0.401	-	2.643	0.000	+
Mtrf1l	-0.058	0.932	-	1.165	0.023	+
Ndufab1/mtACP	-0.260	0.056	-	-0.772	0.022	+
Noa1	0.213	0.525	-	3.062	0.000	+
Nsun2	0.345	0.019	+	1.941	0.002	+
Nsun3	0.534	0.047	+			NA
Nsun4	0.215	0.273	-	4.053	0.002	+
Oxa1l	-0.519	0.000	+	1.123	0.016	+
Pde12	0.619	0.006	+	1.491	0.003	+
Pnpt1	0.161	0.435	-	0.780	0.007	+
Polrmt	-0.031	0.883	-	0.946	0.011	+
Prorp/Mrpp3	0.592	0.033	+			NA
Ptcd1	-0.040	0.931	-	1.378	0.045	+
Ptcd2	-0.146	0.569	-	2.386	0.014	+
Ptcd3/Mrps39	-0.042	0.792	-	1.249	0.003	+
Pus1	0.802	0.001	+	2.255	0.002	+
Rexo2	0.859	0.000	+	2.154	0.062	-
Rpusd3	-0.901	0.044	+	1.371	0.104	-
Rpusd4	-0.319	0.364	-	1.605	0.006	+
Supv3l1	-0.177	0.410	-	0.758	0.004	+
Taco1	-0.527	0.002	+	0.352	0.069	-
Tefm	-0.008	0.922	-	1.516	0.001	+
Tfam	-0.349	0.330	-	-0.721	0.008	+

Tfb1m	-0.262	0.470	-	1.549	0.010	+
Tfb2m	0.021	0.960	-	3.078	0.000	+
Trmt10c/Mrpp1	-0.045	0.889	-	1.845	0.020	+
Trmt2b	-0.236	0.155	-	3.716	0.000	+
Trmt5	-0.892	3.99E-06	+			NA
Trmu	0.090	0.826	-	1.373	0.004	+
Trnt1	0.669	0.000	+	1.554	0.000	+
Trub2	0.221	0.326	-	1.602	0.000	+
Tsfm	-0.218	0.359	-	0.535	0.041	+
Tufm	-0.626	0	+	-0.504	0.006	+

Table 6.2 | Supplementary table for the Figure 3.24

Gene name	Transcriptome			Proteome		
	log fold change	padj	padj < 0.05	log fold change	q-value	q-value < 0.05
mt-Nd1	0.333	0.001	+	-1.523	0.000	+
mt-Nd2	0.378	0.001	+	-2.820	0.044	+
mt-Nd3	0.508	0.001	+			NA
mt-Nd4l_4	-0.332	0.007	+			NA
mt-Nd5	-0.249	0.120	-	-2.181	0.001	+
mt-Nd6	-1.214	0.000	+			NA
Ndufa1	-0.498	0.000	+	-0.324	0.304	-
Ndufa10	-0.438	0.000	+	-0.837	0.004	+
Ndufa11	-0.091	0.571	-	-0.868	0.015	+
Ndufa12	0.129	0.478	-	-0.707	0.001	+
Ndufa13	-0.366	0.001	+	-1.453	0.000	+
Ndufa2	-0.233	0.057	-	-0.799	0.010	+
Ndufa3	-0.622	0.000	+	-0.441	0.144	-
Ndufa5	-0.220	0.123	-	-0.302	0.190	-
Ndufa6	-0.303	0.028	+	-1.494	0.000	+
Ndufa7	-0.300	0.017	+	-1.612	0.001	+
Ndufa8	-0.303	0.039	+	-1.712	0.000	+
Ndufa9	-0.466	0.000	+	-0.390	0.068	-
Ndufab1	-0.260	0.056	-	-0.772	0.022	+
Ndufb10	-0.271	0.024	+	-1.673	0.000	+
Ndufb11	-0.365	0.007	+	-1.578	0.002	+
Ndufb2	-0.409	0.012	+	-0.590	0.214	-
Ndufb3	-0.569	0.000	+	-2.051	0.000	+
Ndufb4	-0.406	0.006	+	-0.892	0.003	+
Ndufb5	-0.541	0.000	+	-1.462	0.000	+
Ndufb6	-0.261	0.038	+	-0.726	0.018	+
Ndufb7	-0.373	0.001	+	-1.557	0.000	+
Ndufb8	-0.376	0.001	+	-1.446	0.000	+
Ndufb9	-0.159	0.241	-	-0.030	0.870	-
Ndufc1	-0.340	0.014	+	-1.677	0.002	+
Ndufc2	0.044	0.782	-	-1.560	0.000	+
Ndufs1	-0.589	0.000	+	-0.733	0.001	+
Ndufs2	-0.538	0.000	+	-0.149	0.443	-
Ndufs3	-0.580	0.000	+	-0.547	0.030	+
Ndufs4	-0.351	0.009	+	-1.202	0.000	+

Ndufs5	-0.154	0.208	-	-1.155	0.009	+
Ndufs6	-0.473	0.000	+	-2.396	0.000	+
Ndufs7	-0.677	0.000	+	-0.767	0.005	+
Ndufs8	-0.218	0.113	-	-1.172	0.002	+
Ndufv1	-0.492	0.000	+	-0.775	0.001	+
Ndufv2	-0.353	0.019	+	-1.507	0.000	+
Ndufv3	-0.645	0.000	+	-1.166	0.071	-
Ndufb1	-0.597	0.000	+	-0.687	0.059	-
Sdha	-0.607	0.000	+	-0.099	0.481	-
Sdhb	-0.308	0.014	+	-0.030	0.784	-
Sdhc	-0.570	0.000	+	0.555	0.061	-
Sdhd	-0.430	0.001	+	-0.223	0.390	-
Cyc1	-0.294	0.022	+	-0.177	0.202	-
mt-Cytb	-0.014	0.865	-	-0.456	0.287	-
Uqcr10	-0.184	0.165	-	-0.954	0.023	+
Uqcrb	-0.419	0.000	+	-0.598	0.012	+
Uqcrc1	-0.477	0.000	+	-0.494	0.010	+
Uqcrc2	-0.390	0.000	+	-0.881	0.000	+
Uqcrfs1	-0.836	0.000	+	-0.674	0.006	+
Uqcrh	-0.369	0.004	+	-0.336	0.079	-
Uqcrq	-0.324	0.015	+	-0.483	0.062	-
Uqcr11	-0.824	0.000	+			NA
Cox4i1	-0.152	0.262	-	-1.154	0.000	+
Cox5a	-0.238	0.103	-	-0.943	0.002	+
Cox5b	-0.182	0.138	-	-2.529	0.000	+
Cox6a1	1.246	0.000	+	0.770	0.033	+
Cox6a2	-0.041	0.775	-	-1.178	0.004	+
Cox6b1	-0.131	0.397	-	-1.383	0.000	+
Cox6c	-0.762	0.000	+	-1.728	0.000	+
Cox7a1	-1.789	0.000	+	-1.676	0.002	+
Cox7a2	0.162	0.224	-	-0.154	0.570	-
Cox7a2l	0.165	0.185	-	1.256	0.005	+
Cox7b	-0.403	0.006	+	-1.221	0.002	+
Cox7c	-0.580	0.000	+	-2.096	0.001	+
Cox8a	1.197	0.000	+			NA
Cox8b	-1.120	0.000	+	-0.857	0.361	-
Mt-co1	-0.752	0.000	+	-0.891	0.011	+
Mt-co2	-1.950	0.000	+	-1.782	0.000	+
mt-Co3	-0.659	0.201	-	-1.885	0.004	+
Cox4i2	-0.238	0.103	-			NA

Ndufa4	-0.428	0.000	+	-1.587	0.000	+
Atp5a1	-0.420	0.000	+	-0.261	0.039	+
Atp5b	-0.146	0.290	-	-0.351	0.043	+
Atp5c1	-0.221	0.110	-	-0.009	0.951	-
Atp5d	-0.130	0.391	-	-0.276	0.212	-
Atp5e	-0.860	0.000	+	-0.652	0.016	+
Atp5pb	-0.367	0.007	+	0.182	0.351	-
Atp5g1	-0.181	0.194	-	-0.098	0.910	-
Atp5g3	-0.540	0.000	+	-0.098	0.910	-
Atp5h	-0.473	0.000	+	-0.657	0.004	+
Atp5k	-0.723	0.000	+	-0.847	0.007	+
Atp5j	-0.625	0.000	+	-0.824	0.005	+
Atp5j2	-0.365	0.007	+	-0.576	0.009	+
Atp5l	-0.313	0.002	+	-0.868	0.004	+
Atp5o	-0.314	0.018	+	-0.166	0.359	-
Dmac2l	-0.132	0.616	-	0.453	0.066	-
Atp5mpl	-0.381	0.004	+	0.591	0.698	-
mt-Atp6	-0.012	0.922	-	0.368	0.387	-
mt-Atp8	-0.012	0.922	-	-1.353	0.002	+
Atp5md	-0.581	0.000	+	-1.504	0.013	+
Ecsit	-0.119	0.453	-	1.515	0.000	+
Foxred1	-0.329	0.029	+	3.886	0.000	+
Ndufaf1	-0.267	0.138	-	1.626	0.001	+
Ndufaf2	0.212	0.544	-	0.424	0.040	+
Ndufaf3	0.035	0.963	-	0.265	0.344	-
Ndufaf4	-0.244	0.109	-	0.130	0.623	-
Ndufaf5	-0.112	0.723	-	-0.104	0.654	-
Ndufaf6	-0.440	0.168	-	2.943	0.001	+
Ndufaf7	-0.220	0.430	-	0.883	0.018	+
Oxa1l	-0.519	0.000	+	1.123	0.016	+
Timmdc1	0.043	0.855	-	1.067	0.023	+
Tmem186	-0.502	0.010	+	0.366	0.529	-
Sdhaf1	-0.683	0.016	+			NA
Sdhaf2	-0.156	0.435	-	1.082	0.021	+
Sdhaf3	-0.378	0.343	-	2.407	0.004	+
Sdhaf4	-0.554	0.035	+	-0.153	0.655	-
Uqcc1	-0.607	0.000	+	0.911	0.004	+
Uqcc2	0.081	0.712	-	0.889	0.008	+
Uqcc3	0.505	0.019	+	-0.953	0.039	+
Cmc1	0.418	0.256	-	0.423	0.723	-

Cmc2	-0.490	0.027	+	0.651	0.093	-
Coa5	0.131	0.379	-	1.419	0.114	-
Coa7	-1.000	0.001	+	-0.867	0.002	+
Cox15	-0.027	0.945	-	0.662	0.003	+
Cox17	0.251	0.064	-	0.186	0.472	-
Cox19	0.838	0.000	+			NA
Cox20	0.240	0.238	-	0.094	0.790	-
Pet100	-0.495	0.107	-	-2.043	0.006	+
Sco1	-0.061	0.750	-	-0.022	0.896	-
Sco2	0.381	0.189	-	1.281	0.001	+
Surf1	0.359	0.150	-	0.700	0.031	+
Taco1	-0.527	0.002	+	0.352	0.069	-
Atpaf1	-0.155	0.566	-	0.910	0.001	+
Atpaf2	-0.492	0.012	+	1.353	0.097	-

Table 6.3 | Supplementary table for the Figure 3.30

Gene name	KOpellet vs. WTpellet		KOpellet vs. KOinput	
	log fold change	q-value	log fold change	q-value
Acad8	5.403	0.005	0.753	0.011
Alkbh7	7.284	0.000	1.116	0.005
Bckdha	4.853	0.006	1.386	0.001
Cdk5rap1	6.110	0.000	1.512	0.001
Clpx	5.606	0.004	0.835	0.008
Coa8	4.249	0.000	2.115	0.004
Cryzl2	6.542	0.000	1.090	0.001
D2hgdh	6.768	0.000	1.614	0.001
Dap3	4.614	0.004	0.990	0.006
Ddx28	5.052	0.001	1.062	0.006
Dnaja3	3.882	0.000	0.838	0.001
Dnajc28	5.130	0.003	1.213	0.001
Fam185a	7.578	0.000	1.212	0.001
Fastkd5	3.784	0.000	1.558	0.001
Foxred1	8.491	0.000	1.035	0.004
Glrx2	5.913	0.000	1.294	0.001
Grsf1	5.691	0.004	0.990	0.004
Gtpbp3	5.633	0.000	0.900	0.007
Gtpbp6	6.120	0.000	0.962	0.004
Hspa9	5.099	0.002	0.506	0.048
Lactb2	5.509	0.000	1.109	0.001
Ldhd	6.680	0.002	0.814	0.004
Metap1d	6.443	0.000	1.328	0.008
Mettl8	5.328	0.000	1.494	0.000
Mgme1	5.773	0.000	1.410	0.001
Mipep	6.932	0.000	0.655	0.027
Mmaa	5.479	0.003	0.932	0.004
Mmadhc	8.780	0.000	1.584	0.001
Mpst	7.342	0.000	1.435	0.001
Mrm1	5.262	0.002	0.699	0.015
Mrpl1	2.736	0.029	0.918	0.023
Mrpl11	3.383	0.003	0.797	0.009
Mrpl13	5.742	0.003	1.541	0.001
Mrpl14	3.267	0.003	0.603	0.024
Mrpl19	4.355	0.005	1.195	0.004
Mrpl21	3.554	0.003	1.271	0.004

Mrpl22	3.642	0.005	1.335	0.001
Mrpl23	6.261	0.002	1.270	0.006
Mrpl24	3.933	0.003	1.256	0.002
Mrpl28	4.092	0.006	1.045	0.008
Mrpl3	4.030	0.007	1.188	0.006
Mrpl30	2.499	0.012	0.893	0.004
Mrpl37	5.162	0.005	0.767	0.025
Mrpl38	3.386	0.023	1.109	0.001
Mrpl39	4.724	0.011	1.189	0.003
Mrpl4	5.507	0.006	1.081	0.007
Mrpl43	3.087	0.013	0.688	0.029
Mrpl44	3.621	0.004	0.821	0.027
Mrpl45	2.961	0.012	1.128	0.002
Mrpl46	4.425	0.004	1.356	0.001
Mrpl47	3.688	0.003	1.331	0.004
Mrpl48	3.402	0.006	1.108	0.004
Mrpl49	4.867	0.008	0.822	0.039
Mrpl51	4.179	0.000	2.449	0.002
Mrpl55	3.801	0.006	1.613	0.001
Mrpl9	4.944	0.012	0.990	0.006
Mrps10	4.940	0.011	1.655	0.001
Mrps11	3.411	0.006	0.815	0.011
Mrps14	5.389	0.000	1.663	0.001
Mrps21	4.355	0.006	1.363	0.004
Mrps22	4.344	0.049	1.398	0.004
Mrps23	5.330	0.002	1.160	0.008
Mrps25	6.667	0.000	0.878	0.039
Mrps26	2.063	0.039	1.424	0.001
Mrps27	4.451	0.008	0.904	0.016
Mrps28	5.318	0.002	1.251	0.001
Mrps30	3.560	0.005	0.787	0.008
Mrps34	5.501	0.005	1.113	0.010
Mrps35	2.310	0.021	0.813	0.008
Mrps5	1.577	0.008	1.067	0.013
Mrps6	5.947	0.003	0.726	0.010
Mrps7	3.787	0.002	0.977	0.008
Mrps9	3.931	0.005	1.319	0.003
Mtg1	6.441	0.000	0.621	0.005
Mtif3	4.277	0.003	0.790	0.008
Mtrf1	6.583	0.000	1.154	0.001

Mtrf1l	6.728	0.001	1.155	0.001
Ndufa10	2.946	0.005	0.857	0.022
Ndufaf6	5.984	0.000	0.611	0.010
Ndufaf7	7.096	0.001	0.812	0.010
Ndufb9	5.273	0.030	1.251	0.003
Nipsnap3b	7.786	0.000	0.837	0.016
Nme4	5.734	0.000	1.498	0.001
Nsun4	8.150	0.000	1.020	0.005
Nudt13	5.271	0.000	0.656	0.008
Osgepl1	5.507	0.000	0.780	0.008
Pdk4	7.324	0.001	1.003	0.006
Pdss2	6.432	0.000	1.214	0.002
Pgam5	3.612	0.013	0.625	0.039
Pnkd	3.203	0.003	1.893	0.012
Poldip2	6.792	0.003	1.298	0.003
Polrmt	4.208	0.001	1.069	0.042
Ppm1k	4.859	0.005	1.347	0.001
Prepl	3.565	0.000	1.409	0.001
Ptcd2	7.182	0.000	0.962	0.004
Ptcd3	5.013	0.005	1.052	0.008
Pus1	5.690	0.000	0.873	0.017
Pycr1	8.259	0.000	1.058	0.001
Pycr2	7.975	0.000	0.634	0.010
Rbfa	5.502	0.001	0.969	0.011
Taco1	5.984	0.002	0.703	0.013
TCAIM	5.562	0.000	0.938	0.019
Tfb2m	7.000	0.000	1.352	0.004
Tmlhe	6.219	0.002	1.206	0.004
Trmt2b	6.509	0.000	1.178	0.004
Trub2	5.881	0.000	1.037	0.006
Uqcc2	7.437	0.002	1.592	0.001
Yme1l1	4.676	0.000	0.749	0.026

Table 6.4 | Supplementary table for the Figure 3.31

Mitocarta names	Whole heart proteome		KOpellet vs. WTpellet	KOpellet vs. KOinput
	log fold change	q-value	log fold change	log fold change
Mrpl30	0.945	0.003	2.499	0.893
Mrpl1	1.335	0.000	2.736	0.918
Mrpl43	0.606	0.005	3.087	0.688
Mrpl11	1.331	0.003	3.383	0.797
Mrpl48	1.408	0.001	3.402	1.108
Mrpl21	2.453	0.000	3.554	1.271
Mrps30	1.719	0.002	3.560	0.787
Mrpl44	1.133	0.003	3.621	0.821
Mrpl22	1.936	0.000	3.642	1.335
Fastkd5	2.936	0.002	3.784	1.558
Mrps7	1.516	0.001	3.787	0.977
Mrpl55	1.288	0.002	3.801	1.613
Mrps9	2.249	0.000	3.931	1.319
Mrpl3	2.355	0.001	4.030	1.188
Mrpl51	3.626	0.001	4.179	2.449
Polrmt	0.946	0.011	4.208	1.069
Coa8	2.884	0.002	4.249	2.115
Mrpl46	1.816	0.000	4.425	1.356
Mrps27	0.794	0.017	4.451	0.904
Dap3	1.052	0.004	4.614	0.990
Mrpl39	1.715	0.001	4.724	1.189
Mrpl49	0.900	0.037	4.867	0.822
Mrpl9	2.074	0.000	4.944	0.990
Ptcd3	1.249	0.003	5.013	1.052
Ddx28	1.536	0.007	5.052	1.062
Mrpl37	1.143	0.000	5.162	0.767
Mrm1	0.741	0.036	5.262	0.699
Nudt13	1.765	0.024	5.271	0.656
Mrps28	1.874	0.000	5.318	1.251
Mrps14	0.966	0.011	5.389	1.663
Rbfa	2.265	0.000	5.502	0.969
Lactb2	0.604	0.037	5.509	1.109
Clpx	1.525	0.001	5.606	0.835
Grsf1	1.623	0.001	5.691	0.990
Mrpl13	2.820	0.000	5.742	1.541

Trub2	1.602	0.000	5.881	1.037
Mrps6	0.718	0.046	5.947	0.726
Ndufaf6	2.943	0.001	5.984	0.611
Cdk5rap1	4.667	0.000	6.110	1.512
Pdss2	4.473	0.000	6.432	1.214
Mtg1	2.703	0.000	6.441	0.621
Metap1d	3.876	0.001	6.443	1.328
Trmt2b	3.716	0.000	6.509	1.178
Mrps25	0.930	0.006	6.667	0.878
Mtrf1l	1.165	0.023	6.728	1.155
Poldip2	1.171	0.000	6.792	1.298
Mipep	1.817	0.001	6.932	0.655
Tfb2m	3.078	0.000	7.000	1.352
Ndufaf7	0.883	0.018	7.096	0.812
Ptcd2	2.386	0.014	7.182	0.962
Uqcc2	0.889	0.008	7.437	1.592
Pycr2	2.255	0.001	7.975	0.634
Nsun4	4.053	0.002	8.150	1.020
Mmadhc	5.349	0.000	8.780	1.584

Acknowledgements

First, my biggest gratitude belongs to **Prof. Aleksandra Trifunovic**, who gave this immigrant girl an opportunity to join this lab and to witness science on the top-notch level. Sandra, thank you for your mentoring, your guidance, your deep understanding, and your kindness. Your endless effort to make people feel welcome in your lab is more than inspiring and I am very happy I had this opportunity to be part of this scientific family. I have received support from you also on the personal level where I wouldn't have ever expected it and for that, I will be eternally grateful. I have managed to get this far mostly thanks to you.

I would also like to thank **Prof. Thomas Langer** and **Prof. Jan Riemer** for being in my thesis advisory committee. I am grateful for your insights and comments. They helped advance this project. I also want to thank **Prof. Matteo Bergami** for his time and effort to evaluate this thesis, and Jan again to chair my defence committee.

I must also express my gratitude towards **MSCA**, **ITN REMIX**, and **Heike Brucherseifer** to give me opportunities to visit different scientific institutes and conferences. The funding also allowed me to spend a month in the Oroboros company, all of which contributed to my success and my personal growth. I am grateful for every comment, idea, or advice on my project that I received from the REMIX professors, this was a privileged position to be in. I am also grateful that REMIX allowed me to meet **Yvonne, Magda, Alisa, Vanessa**, and **Direnis**, because they are all exceptional young women, and I am happy to call them my friends.

Next, I must thank the members of the Trifunovic lab and the young students, past and present, for allowing me to learn from you and share with you the time I spent in the lab. Thank you for sometimes laughs, sometimes tears, but mostly laughs that we could share together. Thank you, **Linda and Katha**, for keeping the lab organized and for helping us students navigate the lab life. Thank you, **Karolina**, for your time and guidance through some of the difficult experiments of this project. Thank you, **Marijana,** for sharing your slavicness and the secret club with me. And for being a supportive neighbour. Thank you, **Aca**, for all the cats, and birds, and walks for lunch, and listening to me when I needed it. Thank you, **Lea and Franziska**, for your young energy you bring to this ageing lab, and for your support of my project too. **Lance**, thank you for your kindness and your character, stay yourself, your presence is energizing. **Sarah**, you were my first friend ever in this lab. You brought kindness, cuteness, and pastel colours into the lab, thank you for breaking my loneliness. **Harshita**, thank you for the long deep talks we sometimes share, thank you for your friendship and your loyalty, you are in many ways a very inspiring person and you deserve to have your big dreams fulfilled.

Now comes a special thanking part to my lab squad, **Alex, Matthijs, and Milica**. You guys have been there for me and showed me compassion when I needed it the most. I love you all very much. **Alex**, thank you for all the therapeutic sessions and thank you for trusting me and believing in me, your validation and your friendship means a lot to me. **Matthijs**, thank you for being a great colleague and most of all a great friend, you have changed the lab and me for the better. I always feel very adult and smart with you :D Efteling and Disney forever. **Milice**, my substitute life partner, I can't be more grateful to have met you and to have you in my life. I would have not survived this if it wasn't for you and for your deep understanding of the things we go through. I can't thank you enough for not judging me when I was judging myself the most.

I do hope I will be able to keep you guys in my life also in the future. But I will for sure never forget how great you all are and how you have made my lab life great during the happy times, and much more bearable, when I was not doing fine.

And finally, I must thank my family the most. First, I need to start with my dear fathen-in-law Pavel Rozsíval who corrected the grammar of most of my thesis. As challenging as it must have been, I admire your tenacity with which you crunched through the text full of weird words and helped this thesis to look better. Con phải cảm ơn ba và mama đã yêu thương và ủng hộ con suốt cuộc đời. Nếu không có hai ba và ma, thì con đã không đi xa đến thế này. Musím poděkovat i svojí druhé rodině, Lukášovi, Štěpánovi, Andě, mamince Evě, taťkovi Pavlovi a i Aničce s babičkou, protože jste mi vždycky hrozně moc fandili, a já jsem vám za to moc vděčná, mám vás ráda. Tome, my baby brother, děkuju, že seš moje rodinná opora a že se na tebe můžu vždycky spolehnout, když potřebuju. Děkuju, žes zvládnul vyrůst v obstojnýho člověka, i když jsme k tomu s rodiči moc nezvládli přispět. :D Děkuju, že seš můj brácha, miluju tě. A Šimonku, kdyby nebylo tvojí podpory a trpělivosti, tak bych tuhle práci v životě nedodělala. Děkuju, že při mně stojíš a že jsi moje opora, i když to pro tebe taky vůbec nebylo jednoduchý. Moc se těšim na to, co nás spolu čeká.

Erklärung zur Dissertation

gemäß der Promotionsordnung vom 12. März 2020

Diese Erklärung muss in der Dissertation enthalten sein.
(*This version must be included in the doctoral thesis*)

„Hiermit versichere ich an Eides statt, dass ich die vorliegende Dissertation selbstständig und ohne die Benutzung anderer als der angegebenen Hilfsmittel und Literatur angefertigt habe. Alle Stellen, die wörtlich oder sinngemäß aus veröffentlichten und nicht veröffentlichten Werken dem Wortlaut oder dem Sinn nach entnommen wurden, sind als solche kenntlich gemacht. Ich versichere an Eides statt, dass diese Dissertation noch keiner anderen Fakultät oder Universität zur Prüfung vorgelegen hat; dass sie - abgesehen von unten angegebenen Teilpublikationen und eingebundenen Artikeln und Manuskripten - noch nicht veröffentlicht worden ist sowie, dass ich eine Veröffentlichung der Dissertation vor Abschluss der Promotion nicht ohne Genehmigung des Promotionsausschusses vornehmen werde. Die Bestimmungen dieser Ordnung sind mir bekannt. Darüber hinaus erkläre ich hiermit, dass ich die Ordnung zur Sicherung guter wissenschaftlicher Praxis und zum Umgang mit wissenschaftlichem Fehlverhalten der Universität zu Köln gelesen und sie bei der Durchführung der Dissertation zugrundeliegenden Arbeiten und der schriftlich verfassten Dissertation beachtet habe und verpflichte mich hiermit, die dort genannten Vorgaben bei allen wissenschaftlichen Tätigkeiten zu beachten und umzusetzen. Ich versichere, dass die eingereichte elektronische Fassung der eingereichten Druckfassung vollständig entspricht."

Teilpublikationen:

DNA polymerase gamma mutations that impair holoenzyme stability cause catalytic subunit depletion.
PMID: 33956154
Figure 6 I + J

Datum, Name und Unterschrift

17.3.2023, Diem Hien Rozsivalova